DESIGN OF METALLIC FOAMS AS INSULATION IN THERMAL PROTECTION SYSTEMS

By

HUADONG ZHU

A DISSERTATION PRESENTED TO THE GRADUATE SCHOOL
OF THE UNIVERSITY OF FLORIDA IN PARTIAL FULFILLMENT
OF THE REQUIREMENTS FOR THE DEGREE OF
DOCTOR OF PHILOSOPHY

UNIVERSITY OF FLORIDA

2004

To my parents and to my wife Qingxin Meng.

ACKNOWLEDGMENTS

First I would like to express my sincere gratitude to my advisor, Dr. Bhavani Sankar, who is a key influence in my graduate studies. I thank him for accepting me as one of his doctoral students. His unwavering support and feedback guided me through my whole Ph. D research. I would also like to give my sincere appreciation to my advisory committee cochair, Dr. Raphael Haftka, for his guidance and support, without which it would never have been possible to complete this work.

I am blessed with a doctoral committee of compassionate and supportive scholars. I would like to express my gratitude to Dr William Hager, and Dr. Malisa Sarntinoranont for serving on my supervisory committee and for their valuable comments and suggestions. Thanks also go to Dr. Max Blosser from NASA Langley research center, Dr. Jacob Chung and Dr. Andrew J. Rapoff from MAE, Dr. Satchi Venkataraman from San Diego State University, who provide many constructive questions and suggestions on my research work.

Also, I appreciate the friendship and encouragement of all the colleagues at the Center of Advanced Composites (CAC) while working and studying together in the lab.

I owe great love to my parents who have always supported and cared for me. Last, but not least, I would like to thank my wife, Qingxin Meng, for her love and patience throughout my doctorate program.

TABLE OF CONTENTS

LIST OF TABLES

LIST OF FIGURES

NOMENCLATURE

Symbol	Description
a	foam cell size
b	displacement coefficient
C	constitutive matrix
C_p	specific heat
c	displacement coefficient
d_s	foam sell size
d_g	gas collision diameter
E_f	Young's modulus of foam material
h	insulation thickness
k	thermal conductivity
K_b	Boltzman constant
k_g	gas conduction in foam
k_m	thermal conductivity by solid conduction in foam
k_r	thermal conductivity by radiation in foam
L	TPS panel length
l_c	the characteristic length of the metal foam
p	TPS panel surface traction
P_r	Prandtl number

Q_0	applied heat flux
q_r	heat flux radiated out by TPS
S	single layer stiff matrix
t	surface traction
V_f	volume fraction or solidity of foam
ϕ	Galerkin base function
ρ	foam solidity
θ	temperature field
γ	C_p ratio
σ	Stephan-Boltzman constant
ε	emittance
λ_m	mean free path length

Abstract of Dissertation Presented to the Graduate School
of the University of Florida in Partial Fulfillment of the
Requirements for the Degree of Doctor of Philosophy

DESIGN OF METALLIC FOAMS AS INSULATION IN THERMAL PROTECTION SYSTEMS

By

Huadong Zhu

December 2004

Chair: Bhavani V. Sankar
Cochair: Raphael T. Haftka
Major Department: Mechanical and Aerospace Engineering

Metallic foams are novel materials that can be used as thermal insulation in many applications. The low volume fraction of solid, the small cell size and the low conductivity of enclosed gases limit the heat flow in foams. Varying the density, geometry and or material composition from point to point within the foam, one can produce functionally graded foams that may insulate more efficiently. The goal of this research is to investigate the use of functionally graded metal foam in thermal protection systems (TPS) for reusable launch vehicles.

First, the effective thermal conductivity of the foam is derived based on a simple cubic unit cell model. Then two problems under steady state of heat transfer have been considered. The first one is the optimization of functionally graded foam insulation for minimum heat transmitted to the structure and the second is minimizing the mass of the functionally graded foam insulation for a given aerodynamic heating. In both cases optimality conditions are derived in closed-form, and numerical methods are used to

solve the resulting differential equations to determine the optimal grading of the foam. In order to simplify the analysis the insulation was approximated by finite layers of uniform foams when studying the transient heat transfer case. The maximum structure temperature was minimized by varying the solidity profile for a given total thickness and mass. The principles that govern the design of TPS for transient conditions were identified.

To take advantage of the load bearing ability of metallic foams, an integrated sandwich TPS/structure with metallic foam core is proposed. Such an integrated TPS will insulate the vehicle interior from aerodynamic heating as well as carry the primary vehicle loads. Thermal-structural analysis of integrated sandwich TPS panel subjected to transient heat conduction is developed to evaluate their performances. The integrated TPS design is compared with a conventional fibrous Safill TPS design. The weights of both designs are minimized subject to temperature constraints, stress constraints or both. Global buckling, shear crimping and face wrinkling are investigated for the integrated sandwich structure during the launch. It is found that for designs with variable insulation thickness, structure thickness and subjected to structure temperature constraint only, an integrated sandwich design tends to require as thick insulation as possible, while a Safill design requires thin structure. Shear crimping is most critical among all the three failure modes we studied in the integrated sandwich design.

CHAPTER 1
INTRODUCTION

The National Aeronautics and Space Administration (NASA) cooperated with the aerospace industry to develop a space transportation system, which will offer reliable access to space at a much lower cost than today's launch vehicles. This led to an Access-to-Space study (e.g., Powell *et al.*, 1998). The objective of the study was to identify the best space transportation architecture that would provide the significant cost reduction, while increasing safety and reliability. Three major transportation architecture options were evaluated, including upgrading the current Shuttle and current expendable launch vehicle, developing new expendable launch vehicle by using conventional technologies, and developing new reusable vehicles by using advanced technology. The Access-to-Space study concluded that the architecture option that provides the greatest potential for meeting the cost, operability, and reliability goals was a rocket-powered single-stage-to-orbit fully reusable launch vehicle (RLV) fleet designed with advanced technology (e.g., Powell *et al.*, 1998).

Reusable Launch Vehicles

The implementation of the Access-to-Space plan is known as the reusable launch vehicle (RLV). The RLV is to lead to a commercialization of space access with more airplane-like operations, so the cost of delivering payload to orbit is significantly reduced.

The X-33 program has demonstrated the key design and operational aspects of a single-stage-to-orbit (SSTO) reusable launch vehicle (RLV) rocket system.

Several advanced technologies that are not at required maturity levels are identified (Stanley and Piland, 1993), such as graphite-composite reusable primary structure, aluminum-lithium and graphite-composite reusable cryogenic propellant tanks, advanced propulsion systems designed for robustness and operability, low-maintenance thermal protection system (TPS) and advanced avionics that include vehicle health monitoring and autonomous flight control. These advanced technologies can result in RLV with a structural and substructure weight reduction of 20 percent below the current Space Shuttle (Stanley and Piland, 1993).

One of the major differences between RLV and the current shuttle orbiter is integral fuel tank, which is incorporated into the vehicles (Blosser, 2000). Unlike the space shuttle orbiter, most orbiters being proposed for fully reusable launch vehicle systems include integral fuel tanks. The integral fuel tanks will result in larger, lower density vehicles with much larger surface areas than the space shuttle orbiter. This larger surface area must be protected from aerodynamic heating. Powell *et al.* (1998) showed that there is one percent weight reduction by simply replacing the equivalent space shuttle TPS with the advanced TPS only and seven percent weight reduction from vehicle resizing. So the improvement of TPS design for reusable vehicle seems very important.

Thermal Protection Systems

The primary function of the thermal protection system is to regulate the heat flow to and from the vehicle to maintain the underlying structure within acceptable temperature limits (Blosser, 2000). In addition to performing its thermal function, the

TPS must maintain its structural integrity during its life cycle. For example, TPS should withstand the handling damage and low speed impaction during fabrication and assembling; even some coatings can be used to improve its impact resistance (Findley and Johnson, 2003). It should also withstand dynamic loading from the propulsion system and maintain an acceptable shape under dynamic shearing and pressure load during launching. There are several other desirable features in addition to thermal and structural requirements, such as low mass and low cost.

The TPS used on current reusable launch vehicle (Hughes *et al.*, 1985) – shuttle orbiter- includes the reusable surface insulation ceramic tiles, felt fibrous reusable surface insulation and advanced fibrous reusable surface insulation ceramic blanket. Reinforced carbon-carbon (RCC) is also used as hot structure on the current shuttle orbiter. These materials are sufficient in temperature capability for future RLVs, which have a lower heating load because of their lighter plane form loading during atmospheric reentry. However, the durability and maintainability of such materials or designs should be improved to provide more efficient operations.

Metallic thermal protection systems may be a key technology that may help achieve the goal of reducing the cost of space access (Dorsey *et al.*, 2002). The inherent ductility and design flexibility of metallic TPS offer the potential for a more robust system with lower maintenance costs than competing systems. The foil-gage construction of current metallic TPS concepts (Blosser *et al.*, 2002) used on the X-33 vehicle, which is a technology demonstrator for NASA's "next-generation" of space launch vehicle. These concepts make it simple to improve durability by increasing the thickness of the outer face sheet to meet robustness requirements.

The concept of metallic TPS depends largely on the properties of available materials. Metallic foam seems to be a good candidate even though it has a higher thermal conductivity (Ashby *et al.*, 2000) than its non-metallic counterparts. But it has the ability to bear part of the structural load, which may be used to simplify the design of current TPS.

Functionally Graded Metallic Foam Material

More foam is used for thermal insulation than for any other purpose (Gibson and Ashby, 1997). The low volume fraction of solid materials, the small cell size and the poor conductivity of enclosed gases (Ashby *et al.*, 2000) limit the heat flow in foams. The thermal conductivity of foams can be thought of as having four contributions: conduction through solid, conduction through gas, convection within the cells and radiation through the cell walls and across the cell void. These four components compete with one another in total effective thermal conductivity when the density of insulation changes. Usually there will be temperature gradient in foam insulation, so varying the density, geometry and or material composition from point to point within the foam can produce functionally graded materials (FGM) that may insulate more efficiently. Cho and Ha (2002) address a two-dimensional volume-fraction optimization procedure for relaxing the effective thermal stress distribution in Ni–Al_2O_3 FGMs. Their work demonstrated that the determination of volume-fraction distribution of FGM is a crucial step in tailoring optimal heat-resisting FGMs. Venkataraman *et al.* (2001) studied the optimum density distribution of a thermal insulation for steady state heat conduction for open and closed cell foams. For open cell foams, they found that functional grading of the foam density can reduce the heat transfer through the foam for given thickness.

Goal of Dissertation Research

The goal of this research is to investigate the use of functionally graded metal foam in thermal protection systems for reusable launch vehicles. The problem encountered includes understanding the heat transfer in metallic foams, developing optimum TPS designs under steady state and transient heat transfer condition, and identifying and quantifying key issues in the design of metallic foam insulation in TPS design.

Objectives

The objectives of this study are to explore the potential of functionally graded metal foams as insulation materials in TPS design and to develop the understanding of the effect of foam solidity profile, and insulation thickness on the optimal TPS design.

Scope

This dissertation consists of several parts. Chapter 2 reviews the history of metallic TPS design, and current TPS materials and approaches. Chapter 3 contains the model of heat transfer in metallic foams. Chapters 4 and 5 present the optimal design of insulation made of metal foams under steady and transient heat transfer conditions, respectively. Chapter 6 describes the response of functionally graded beams to transverse mechanical loads. In Chapter 7 we develop a thermal-structural analysis of a sandwich TPS panel subjected to transient heat conduction during reentry. Chapter 8 presents some concluding remarks. The temperature dependent material properties and thermal-mechanical load histories are listed in Appendices A and B, respectively.

CHAPTER 2
THERMAL PROTECTION SYSTEMS FOR REUSABLE LAUNCH VEHICLES

The primary function of TPS is to keep the underlying structure of the vehicle within allowable temperature limits. The approach of thermal protection depends largely on the magnitude and duration of the aerodynamic heating, insulation materials' limitation, cost and reliability considerations. Several different types of TPS may be used on the same vehicle, because the aerodynamic heating varies over the surface of vehicle. This chapter presents a review of the approaches to thermal protection system and thermal-structural analysis of sandwich structure.

During the take off and reentry of RLV, the vehicle encounters hypersonic flow. The kinetic energy associated with the hypervelocity flight is converted into heat energy increasing the temperature of the air near the surface of the vehicle (Purse *et al.*, 1964). The rate of such heat transfer depends on many factors, including the vehicle reentry trajectories, the free stream conditions (gas density, pressure, etc), the vehicle geometry and its orientation to flow. For example, inflatable braking devices (IBD) (Alifanov *et al.*, 2003) made of elastic materials can reduce the spacecraft's ballistic parameters to reduce the aerodynamic heating of the vehicle. There are some engineering codes used for hypersonic flow analysis including options for thermal chemical equilibrium and non-equilibrium, such as LAURA (Roe, 1981), GIANT (Olynick and Henline, 1995), DPLUR (Candler *et al.*, 1994).

Thermal Protection Approaches

Hypersonic flight vehicles require thermal protection systems to withstand sustained aerothermal loads. The design of a thermal protection system is based on the principle that the energy transmitted by the hot boundary-layer flow must be absorbed or rejected by the thermal protection system. Different TPSs are used for vehicles with different missions. Two kinds of classification of TPS are presented in Blosser (2000) and NASA (1968). In NASA (1968), the external thermal protection systems are divided into two types, absorptive and radiative, depending on the primary method used to dissipate the incoming energy. The absorptive systems are further sub-classified as heat sink, film and transpiration cooling, ablative and convective cooling system. The radiative systems are normally passive and most of the aerodynamic heat is radiated back out by TPS. Only a small fraction of heat is absorbed by TPS and transmitted to the underlying vehicle structure. The amount of heat that can be absorbed by a vehicle structure is determined by the mass, specific heat capacity, initial and maximum allowable temperature of the structural materials. The radiative system is limited to a maximum heat rate by its operating temperature limit, whereas the absorptive systems are limited to a total heat input.

We follow the classification of TPS given by Blosser (2000), where the TPS is divided by with or without additional external system. TPS concepts are divided into three concepts, passive, semi-passive and active, according to different heat removing methods.

Passive TPS concepts have no working fluid to remove heat. So heat is either radiated out or absorbed by the TPS system. They are the simplest TPS concepts but have

the lowest heat load capacity. There are three passive TPS concepts, heat sink, hot structure and insulated structure (Blosser, 2000).

Heat sink design absorbs almost all the incident heat and stores it in the structure and/or TPS of the vehicle. Usually additional mass may be needed to increase the heat storage capacity. A hot structure design allows the structure temperature to rise until the heat being radiated from the surface is equal to the incident heating. This concept is limited by the allowable temperature limit of the structure materials. Insulated structures have features of both a heat sink and a hot structure design. The outer surface of insulated structure approach is hot, almost at the radiation equilibrium temperature, and it radiates out most of the incident heat. Therefore only a small fraction of heat reaches and is stored in the underlying structure. Insulated structure concept is the choice for most of existing and proposed RLV.

There are two semi-passive TPS concepts. One concept uses heat pipe to transfer the heat of the local high heating area to adjacent areas of low heating. A working fluid absorbs heat from high heating areas by vaporization and flows to cooler and low heating areas where it condenses and releases heat. Another concept is the ablator design using an ablator that undergoes chemical reaction to generate gasses to block much of the aerodynamic heating to the vehicle surface. It can accommodate severe but short heating.

There are three active cooling concepts, transpiration, film and convective cooling. They can accommodate a large heat flux. External pumps are used to bring the coolant to the outer surface. For transpiration cooling, coolant is ejected through a porous surface, while for film cooling, the coolant is ejected parallel to the flow from discrete slots. Convective cooling is accomplished by circulating coolant through passages in the

structure to remove the absorbed heat due to aerodynamic heating. Almost all incident heating is transferred through the outer skin into the coolant. The convective cooling cannot accommodate heat flux as large as transpiration and film cooling. Convectively cooled engine nozzles were used on X-33. A review of actively cooled structure is given in Kelly and Blosser (1994).

Current Passive Thermal Protection Designs

Most of the current TPS effort (Blosser, 2002; Dorsey *et al.*, 2002) is focused on passive systems. Hot structures are being considered for control surfaces and insulated structures are being considered to cover the majority of current RLV, the shuttle orbiter, surface. Different TPS concepts are used under different temperature ranges. Reinforced carbon-carbon (RCC) is used on a surface where maximum temperature is higher than 2300 F. For temperatures below 2300 F, there are two types of concepts in use, flexible blankets and rigid ceramic tiles, and one type proposed for future use, metallic TPS panels.

Reinforced Carbon-Carbon TPS

Reinforced carbon-carbon fabrication begins with a rayon cloth graphitized and impregnated with a phenolic resin (Hughes *et al.*, 1985). This impregnated cloth is layed up as a laminate and cured in an autoclave. After being cured, the laminate is pyrolized to convert the resin to carbon. To provide oxidation resistance for reuse capability, the outer layers of the RCC are converted to silicon carbide. The operating range of RCC is from minus 250 F to about 3,000 F. Reinforced carbon-carbon is used on the wing leading edges, the nose cap including an area immediately aft of the nose cap on the lower

surface (chine panel) and the immediate area around the forward orbiter/external tank structural attachment. Some other carbon or silicon-carbide composites are also considered as the primary or candidates for RLV TPS, such as carbon fiber reinforced silicon-carbide matrix composite, silicon-carbide/ silicon-carbide and advanced carbon/carbon composite.

Flexible Blanket TPS

Felt reusable surface insulation (FRSI) (Cooper and Holloway, 1981) is made from Nomex material, consisting of sheets 3 to 4 square feet. The FRSI varies in thickness from 0.160 to 0.40 inch depending on the heat load encountered during entry. The FRSI is bonded directly to the orbiter by room temperature vulcanizing silicon adhesive. The FRSI blankets protect areas where temperatures are below 700 F. It is used on the upper payload bay doors, portions of the mid-fuselage and aft fuselage sides, portions of the upper wing surface.

Advanced flexible reusable surface insulation (AFRSI) was developed as a partial replacement for FRSI and low temperature reusable surface insulation (LRSI). AFRSI consists of a low-density fibrous silica batting that is made up of high-purity silica and 99.8% amorphous silica fibers. This batting is sandwiched between an outer woven silica high-temperature fabric and an inner woven glass lower temperature fabric. After the composites are sewn with silica thread, it has a quilt-like appearance. The AFRSI blankets are coated with a ceramic collodial silica and high-purity silica fibers (referred to as C-9) that provide endurance.

Some other advanced TPS blanket types are also proposed. Tailorable advanced blanket insulation (TABI) was developed by the NASA Ames Research Center as an

improvement to the AFRSI. Integrally woven corrugations provide higher strength and a higher operational temperature (2200 F) (Chiu and Pitts, 1991) than AFRSI, and TABI is being proposed for use on the windward side of reentry vehicles. Composite flexible blanket insulation (CFBI) is made of AFRSI with added multilayer insulation and provides improved insulation properties. DurAFRSI, which is modified by adding metallic foil brazed to the wire mesh top surface, makes the material more robust.

Rigid Ceramic Tiles TPS

High temperature reusable surface insulation (HRSI) system is composed of a ceramic tile, such as LI-900 or LI-2200, a Nomex (nylon) felt strain isolation mounting pad, and room temperature vulcanizing adhesive. LI-900 and LI-2200 tiles (Myers *et al.*, 2000) are an all-silica, rigid, fibrous insulation systems with a maximum operational temperature of 1200 F and 2300 F, respectively. The LI-900 (9 lb/ft^3) and LI-2200 (22 lb/ft^3) tiles are coated on five sides to improve the surface emissivity and toughness and reduce catalycity. Due to the brittle nature and low strength of tiles, ceramic tile TPS must be isolated from the thermal and mechanical strains of the underlying structure. This is accomplished by the felt strain isolation pad. Strain isolation and thermal shock requirements limit the orbiter tiles to approximately six inch by six inch square footprints. The tiles have been susceptible to impact damage, and require waterproofing after each flight.

The Fibrous Refractory Composite Insulation (FRCI) tile manufacturing process is essentially the same as that for the 99.8-percent-pure silica HRSI tiles, the only change being in the wet-end prebinding of the slurry before it is cast. It is used to replace the HRSI 22 lb/ft^3 tiles.

New tile TPS concepts are also proposed in NASA Ames Research Center (Smeltzer and Waters, 2003). The Alumina Enhanced Thermal Barrier Tiles (AETB) with toughened uni-piece fibrous insulation (TUFI) coating was also developed as an improvement to the LI-900 tile. The AETB tiles demonstrate higher strength, added durability, and have a maximum operational temperature of 2500 F. The system is composed of an eight inch by eight inch AETB ceramic tile that is coated with toughened unipiece fibrous insulation (TUFI) and mounted on a strain isolation pad (SIP). The other concept is silicone impregnated reusable ceramic ablator which is a silica tile impregnated with an ablative silicone that has potential for multiuse capability at RLV leading edge and nosecap condition.

Metallic TPS Panels

The concepts of metallic TPS progressed from early radiative metallic TPS (Bohon *et al.*, 1977) to multi-wall concepts (Shideler *et al.*, 1982) to prepackaged superalloy honeycomb sandwich panel (Blosser, 1996).

The radiative metallic TPS consists of a radiative surface panel, supports, and an insulation package (Bohon *et al.*, 1977). The radiative panel was typically corrugated to provide relatively free thermal expansion transverse to the corrugation and to provide stiffness to resist panel flutter. Flexible supports were designed to accommodate longitudinal thermal expansion while retaining sufficient stiffness to transmit surface pressure loads to the primary structure. The insulation consists of flexible thermal blankets often encapsulated in foil material to prevent moisture absorption. Several radiative metallic TPS designs are shown in Figure 2-1. The aerothermal tests for Rene 41 and L-605 panel were conducted in NASA Langley research center (LaRC) (Devisikis

et al., 1975; Bohon *et al.*, 1975). It was found that panel showed no thermal and structural degradation after multiple mission cycles. The TD Ni-20Cr panel was tested statically for 100 cycles of ascent pressure and combined entry thermal and pressure load (Eidenoff and Rose, 1974). The acoustic and thermal tests were conducted for coated columbium panel (Rummler and Black, 1975). Through the test series, no significant structural damage was observed but some oxidization damages. All radiative metallic TPS designs indicated good durability and reusability. A thermal structural design optimization was undertaken in (Bohon *et al.*, 1977). It was shown that unit mass of radiated metallic TPS is still high compared with later metallic TPS concepts.

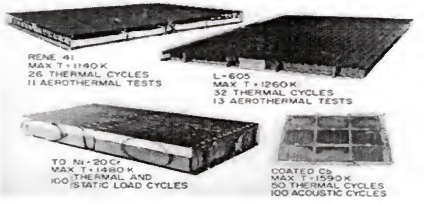

Figure 2-1 Radiative metallic TPS panel (Bohon *et al.*, 1977)

Titanium multiwall tiles were proposed as another promising metallic TPS system, which consist of multilayer of super plastically formed dimpled sheets and flat sheets of titanium foil as shown in Figure 2-2 (Shideler *et al.*, 1982). The sheets are bonded into discrete tiles using liquid interface diffusion (LID) bonding process. The multi-wall TPS panels are mechanically attached to the primary structure by bayonet-type tabs that are bonded to the tile bottom surface. Nomex felt strips under the perimeter of the tile are compressed slightly when each tile is attached. The purpose of strip is to block hot gas,

which might flow under the tile. The beaded closeout edges also accommodate differential thermal expansion due to a temperature gradient through tile thickness. The multiwall concept impedes all three modes of heat transfer, conduction, radiation, and convection. The small contact area of the dimples and the tends to minimize the metal conduction; the multiple foil radiation shields impedes heat transfer by radiation; and the small individual volumes formed by dimpled layer suppress air convection but permit air conduction. The effective thermal conductivity of multiwall TPS was tested (Shideler *et al.*, 1982). It was shown that the conductivity of multiwall TPS was about twice the average conductivity of the basic shuttle reusable surface insulation. However the multiwall tile system can be made mass competitive with the shuttle tile system because the effective density of the multiwall is lower. For comparable thermal performance the multiwall tiles would be thicker but not necessarily heavier.

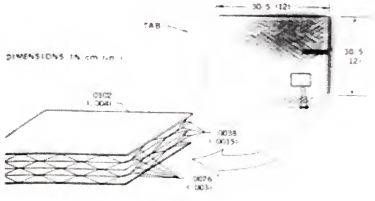

Figure 2-2 Assembled multiwall TPS tile [dimension are in cm (in)] (Shideler *et al.*, 1982)

Some other advanced multiwall TPS concepts were proposed for higher surface temperature. Nickel alloy sandwich concept has fibrous quartz insulation in the center of tile. This concept has an Inconel 617 outer sandwich fabricated as either a multiwall

sandwich or as a honeycomb sandwich. Oxide dispersion strengthened (ODS) materials were also considered for this concept to extend to higher temperature. Designs for even higher surface temperatures using coated refractory alloy and advanced carbon-carbon concepts were also studied (Jackson and Dixon, 1980).

Development of prepackaged superalloy honeycomb panel has been led by the NASA LaRC (Blosser, 1996). Instead of using multiwall concept, the prepackaged superalloy honeycomb concepts consist of a foil-gage metallic box encapsulating lightweight, fibrous ceramic insulation, Cerrachrome or Q-felt quartz fibrous insulation, as shown in Figure 2-3. Both the outer honeycomb sandwich and side walls are made from Inconel 617, which enables the TPS to operate at a maximum temperature between 1800 F and 1900 F. The inner surface is made of a titanium honeycomb sandwich. On two adjacent edges of the panel, the outer facesheet and a flange from the beaded side extend to form a gap cover. This gap cover is designed to inhibit the gas flow in the panel-to-panel gaps. A corresponding under-hanging lip on the opposite two edges of the panel seals the bottom of panel-to-panel gap. The prepackaged superalloy TPS is designed to be mechanically attached to the vehicle structure. Fastener access tubes provide the access from the outer surface of panel to inner surface of panel. The tubes are filled with fibrous insulation. The box rests upon an RTV and Nomex felt edge support system to prevent flow from beneath the panels. The weight of the metallic box is offset to some extent by the low density, efficient fibrous insulations. The inherent ductility of the metallic materials used offers the potential for a more robust TPS and the design can be easily modified to improve durability by making the face sheets thicker. In addition, the encapsulated designs are inherently waterproof, and the mechanical fasteners allow

for easy removal and reattachment. The spacecraft structure may require special design features to accommodate the mechanical fasteners.

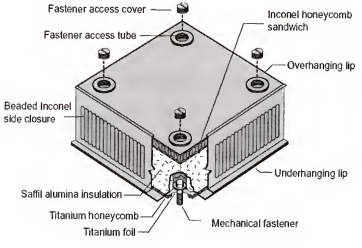

Figure 2-3 Prepackaged superalloy honeycomb sandwich metallic TPS panel (Blosser, 1996)

A new Adaptable, Robust, Metallic, Operable, Reusable (ARMOR) metallic thermal protection system (TPS) concept (Blosser *et al.*, 2002) has been designed, analyzed and fabricated at the NASA LaRC as an improvement to the prepackaged superalloy honeycomb metallic system as shown in Figure 2-4. Same foil-gage, Inconel 617 metallic honeycomb sandwich panel was chosen for the outer surface because it can efficiently carry the aerodynamic pressures at elevated temperatures and is resistant to oxidation. The exterior face sheet of the honeycomb panel extends to overlap the panel-to-panel gap and inhibit ingress of hot gases during reentry and under-hanging lips are removed. A thin-gage titanium box beam frame defines the edges of the panel's inner surface. This frame can be used to compress the felt seal between panel and underlying structure. The outer honeycomb sandwich is structurally connected to the inner box beam

frame by thin Inconel 718 metal support bracket at each corner of the panel. A vent covered by fine mesh is in the bottom metal foil, which can maintain the inter pressure at local atmospheric pressure. Bulged, compliant sides, made of thin gauge metal foil, enclose the sides of the TPS panel and block the radiative heat transfer path in the panel-to-panel gaps. The interior of an ARMOR panel is filled with low-density Saffil alumina insulation. Mass could be reduced by using high temperature multilayer insulation. An oxidation protection coating was applied to the external face skin of the TPS panels. The selected coating consisted of an alumina base layer and a two-phase glass outer layer. A good summary of proposed thermal protection system was given in Table 2-1 reference (Reusable Launch Vehicle: Technology Development and Test Program, 1995). From the table we can see that metallic TPS is most robust and damage tolerant.

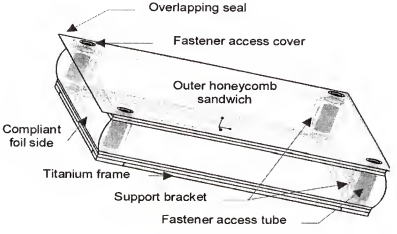

Figure 2-4 Schematic representation of ARMOR metallic TPS panel (Blosser *et al.*, 2002)

For all of the metallic TPS concepts discussed before, they take thermal load of the vehicle only and the structural load is taken by the underlying structure. So TPS and the

structures can be designed separately. Usually TPS support structures (TPSS) are need to install metallic TPS panels. Dorsey (Dorsey *et al.*, 1999) investigated three kinds of TPSS for X-33 vehicle, Stand-off design, Lattice work concept and Carrier Panel concept. He found that for highly integrated Single-Stage-to-Orbit reusable launch vehicles, the total vehicle empty weight can be reduced by efficiently integrating the TPS, TPS support structure and tank system such that the distance between the tank and vehicle outer mold lines (OMLs) is minimized. Since it increases the vehicle packaging efficiency, and decreases in the amount of TPS support structure required. Metallic foams are a new class of materials with low density and novel mechanical and thermal properties. We will take advantage of the load bearing ability of metallic foams and study the performance of the integrated sandwich TPS concept with metallic foam core. In this concept, the top titanium facesheet and the bottom alumina structure are separated by titanium foam core, which also serves as insulation. The design of this concept will be discussed in detail in next several chapters.

Table 2-1 TPS concepts for reusable launch vehicle (RLV) (Reusable Launch Vehicle: Technology Development and Test Program, 1995)

Concepts	Attributes	Concerns
Nose Con and Leading Edges		
Advanced Carbon/Carbon	High strength than reinforced carbon-carbon; used on orbiter	Oxidization-effects data required. High thermal conductivity may require complex heavy attachment mechanism. Rain-erosion resistance data required.
Carbon/SiC or SiC/SiC	Good potential. No coatings required (oxidization resistant)	High thermal conductivity. Rain-erosion resistance data required. Development tests required.

SIRCA	Easy to produced in appropriate size. Low thermal conductivity. Allows backface attachment	Reusability and rain-erosion resistance data required.
AETB tiles with TUFI coating	Easy to produced in appropriate size. Low thermal conductivity. Allows backface attachment. Low fabrication cost	Data required on temperature resistance. Requires waterproofing. Lack of appropriate thermal cycling data. Data required on rain erosion resistance of coating.
AETB/TUFI	Best reusable surface insulation tile material/coating system. Attachment by bonding. Fabrication analogous to shuttle tile	Requires waterproofing. Requires gap fillers.
C/Sic or SiC/Sic standoff panels	Potential low weight. Thermally stable.	High cost. Standoff design for thermal expansion. Development tests required.
Metallic (superalloy)	Robust and damage tolerant. Protected insulation. Panel-to-panel overlap minimizes gap seal problems. Design refined over many years.	Attachment must allow for thermal expansion. Heat transfer through attachment
TABI	Best blanket insulation. Attachment by bonding, no heat shorts. Potential 2000 F reuse. Large size than tile insulation	Requires waterproofing. Protective coating performance data required.
Upper (Leeward) Surfaces		
NEXTEL/AFRSI	Low cost than TABI. Better insulation than TABI. Flight experience on orbiter.	Requires waterproofing. Coating performance data required. Stitching needs more development
Titanium Honeycomb	Robust and damage tolerant. Lightweight. Large panel sizes. Panel-to-panel overlap minimizes gap seal problems.	1000 °F limit
Polybenzimidazole (polymer) Felt	High temperature polymer (800 °F). Low density. Low thermal conductivity. Attached by bonding.	Higher cost than Nomex. Lack of test data. No data on waterproofing.

Thermal and Structural Analysis of Sandwich Structure

Heat Transfer in Insulation Materials

The thermal analysis of TPS is complicated by the temperature and/or pressure dependent thermal material properties, especially thermal conductivity, so it is hard to solve analytically. Usually the thermal analysis is completed by numerical methods such as, finite element method (FEM) or finite difference method (FDM). The effective thermal conductivity of insulation should be evaluated before thermal analysis. Different models are developed to study the heat transfer in different insulation materials, such as fibrous insulation, multilayer insulation (MLI) and foam insulation.

Fibrous materials are very effective thermal insulations for high-temperature applications because they can suppress radiative heat transfer by absorption and scattering and can reduce conduction by the tortuous paths. Lee and Cunnington (1998) used semi-empirical model to calculate the fiber-matrix conduction. Radiative thermal conductivity of an optically thick medium is modeled by a diffusion approximation. The results from this heat transfer model show excellent agreement between experimental data. Daryabeigi (1999) developed an analytical model to model the heat transfer through high-temperature fibrous insulation. The optically thick approximation (i.e., the optical depth is large) was used to simulate radiation heat transfer through the insulation. He assumed that the formulation is applicable over the entire insulation domain. The gas thermal conductivity was derived by using the temperature jump theory for heat transfer in rarefied gas flow. It was found that the use of the optically thick approximation for modeling the radiation heat transfer through the insulation provided agreement within experimental accuracy over most temperatures and pressures. The agreement was not as

good for the lowest density insulation sample studied. The models for gas and solid conduction and their coupling produced agreement within experimental accuracy.

Keller *et al.* (1988, 1992) neglected solid conduction and used either the optically thick or the modified diffusion approximation for modeling the radiation transfer in multilayer insulation (MLI). Krishnaprakas *et al.* (2000) evaluated four heat transfer models including conductance model, elective emittance model, conduction-radiation model, Cunnington and Tien (CT) model taking into consideration the effect of temperature dependence of properties (Cunnington and Tien, 1970). The experimentally observed thermal performance data of MLI have been correlated with these four models. It has been found that the Cunnington and Tien model estimates heat flux sufficiently accurate for spacecraft MLI design purposes. Spinnler *et al.* (2002) studied on the determination of the effective thermal conductivities of multilayer insulation systems with specially designed shields for application in high temperature fuel cells both experimentally and theoretically. They found that a combination of low emissivity screens and optically thin spacers yield optimal reduction of the effective thermal conductivity. Daryabeigi (2002) developed a numerical model for modeling combined radiation and conduction heat transfer in high-temperature multilayer insulations. Radiant heat flux is modeled by two-flux approximation. A parallel thermal network model was used for modeling the combined solid and gas conduction in insulation. The numerical model was validated by comparison with steady-state effective thermal conductivity measurements and by transient thermal tests simulating reentry aerodynamic heating conditions.

The effective thermal conductivity of titanium open cell foams used in our research will be discussed in next chapter. The foams are modeled by the simple unit cell with slender cylinder struts. Three heat transfer modes are considered, solid conduction through foam struts, gas conduction through the air enclosed in foams and radiation in foams.

Structural and Thermal Analysis of Sandwich Structure

The sandwich structure can be analyzed by classic laminate plate theory (CLPT), shear deformation plate theory (SDPT) or other higher order theory. CLPT (Reddy, 1996; Kollar and Springer, 2002; Vinson and Sierakowski, 1986; Reddy, 1999) is an extension of the Kirchhoff plate theory to the laminate composite plates. In this theory, a straight line along the normal to the mid-surface remains straight and normal to the deflected mid-surface after loading, that is, there is no transverse shear deformation. The transverse normal effects are neglected too. This theory can be used for thin laminate palate with ratio of its thickness to representative lateral dimension less than 1/20 (Zenkour, 2003).

First-order shear deformation (FSDT) (Reissner, 1975, 1985; Yang *et al.*, 1966) can yield more accurate results. It relaxes the assumption of CLPT and includes a gross transverse shear-deformation in its kinematics assumptions, i.e., the transverse shear strain is assumed to be constant with respect to the thickness coordinate. The transverse shear stresses are constants because of constant shear strains. While in composite laminate plates, the transverse shear stresses vary at least quadratically through thickness direction, so shear correction factors (Whitney, 1973; Bert, 1973; Chow, 1971; Wittrick, 1987) are introduced to correct for the discrepancy between the actual transverse shear force distributions and those computed using the kinematics relations of the FSDT.

Higher order theories (Lo *et al.*, 1977a, 1977b; Reddy, 1984a, 1984b) can represent the kinematics better, may disregard shear correction factors and yield more accurate transverse shear stresses. To avoid the need of shear correction coefficient used in FSDT, the displacement in the thickness coordinate should be expanded at least in cubic term to have quadratic variation of transverse shear strains and shear stresses.

Thin sandwich panels can analyzed as laminate plates by FSDT with the shear deformation in facesheet being neglected. There are two approaches that can capture the 3-D effects due to through-thickness displacement and stress variation. They are the equivalent single-layer approach and the discrete-layer approach. In first approach (Savoia and Reddy, 1992), high order terms are considered in the expansion of the displacement components in thickness direction. So the non-linear variations of strain and stress in thickness direction are permitted with approximate transverse normal and shear deformation. The other approach (Pai and Nayfeh, 1995) is layer-wise theory in which a unique displacement field is assumed in each layer. Hsueh and Lee (2003) analyzed the distribution of elastic thermal stresses in two dissimilar materials joined by a graded layer and derived an exact closed-form solution. They used Hsueh and Evans' model to decompose the strain distribution in the bilayer into a uniform component and a bending component, such that the strain continuity condition at the interface is automatically satisfied. In this model, linear strain distribution in thickness direction is assumed.

Venkataraman and Sankar (2001) analyzed sandwich beams subjected to a transverse half-sinusoid pressure distribution. The exponential variation of elastic stiffness coefficients allows exact elasticity solution. The solution of displacements and stresses are obtained by enforcing the compatibility of the tractions and displacements at

the interface. This method can be used for the structural analysis of functionally graded sandwich structure with the analytical solution of thermal stresses for functionally graded beams discussed in (Sankar and Tzeng, 2001). Yang and Shen (2002) have presented a free and forced vibration analysis of initially stressed functionally graded plates in a thermal environment based on a higher order shear deformation plate theory. Cheng and Batra (2003) have used the asymptotic expansion method to study the 3D thermo-elastic deformations of a functionally graded elliptic plate. Tarn and Wang (1995) have also given an asymptotic solution for non-homogeneous plates. Recently Vel and Batra (2002, 2003a) presented a three-dimensional exact solution for the mechanical vibrations and the steady state thermal stresses in a simply supported functionally graded rectangular plate. Vel and Batra (2003b) have also given an exact solution for static thermo-elastic cylindrical bending deformations of a functionally graded plate. Vel and Batra (2003c) analyzed 3D transient heat conduction problem for a rectangular simply supported functionally graded plate with the uniform temperature prescribed at the edges and subjected to either time-dependent temperature or heat flux on the top and the bottom surfaces. The material properties are taken to be analytical functions of the thickness coordinate and are uniform in the other two directions. Transient stresses developed by the resulting temperature gradients have been evaluated for a simply supported FG plate. It is found that for the case of rapid time-dependent prescribed surface temperature, the transient longitudinal stress is nearly eight times its steady state value. Ootao and Tanigawa (1999) have approximated an FG plate as a laminated plate consisting of a series of laminate, with each lamina assigned slightly different material properties. Kim

and Noda (2001) adopted a laminate theory and obtained Green's function solution for analyzing the 3D transient temperature distribution.

In order to compute the temperature and the overall strain/stress distributions in FGMs, one needs the appropriate estimates for properties of the graded layer, such as the thermal conductivity, the coefficient of thermal expansion, Young's modulus and Poisson's ratio. The thermal-mechanical response by the theoretical approach can be modeled at microscopic levels, predicted upon the interaction between matrix and inclusions, and continuum levels, by accounting for only the volume fraction and individual properties of the constituent phases. The prediction methods of the overall thermal-mechanical properties within the framework of single continuum mechanics are generally classified into three categories: direct, variational and approximation approaches (Wakashima and Tsukamoto, 1991). The direct approach seeks the closed-form analytic solutions to the overall properties of ideal composites. The variational approach provides the upper and lower bounds for the overall properties expressed in terms of the phase volume fraction (Hashin and Shtrikman, 1963). In the approximation approaches, the models by Hill (1965), Walpole (1966) and Budiansky (1965), the mean-field micromechanics models by Mori and Tanaka (1973) and Wakashima and Tsukamoto (1991, 1992), the modified rule of mixtures by Tomota *et al.* (1976) and the unit cell model by Ravichandran (1994) are representative homogenized (or averaging) estimates for the overall material properties. Owing to the assumed simplifications, the validity of each model should be checked for specific materials. Cho and Ha (2001, 2002) gave a good review for different methods.

Design Optimization of Sandwich Structure

The TPS design should satisfy both mechanical and thermal design requirements for the insulation and the underlying structure. Mechanical requirements must be satisfied to ensure structure integrity, such as stress limits, displacement limits and other constraints. Thermal requirements must be satisfied to avoid material property degradation of the structure, which usually places upper temperature limits for the structure. Usually the problem can be formulated as:

$$\begin{aligned} &\text{Min } f(X,t) \\ &\text{S.T. } T_i/T_a - 1 \le 0 \\ &\quad U_i/U_a - 1 \le 0 \\ &\quad \sigma_i/\sigma_a - 1 \le 0 \\ &\quad X_L \le X \le X_U \end{aligned} \tag{2-1}$$

where $f(X)$ is the object function, and X is the design variable vector. T_i, U_i, σ_i are temperature, displacement and stress at given area of structure respectively. T_a, U_a, σ_a are allowable temperature, displacement and stress respectively. X_L and X_U are the lower and upper bound of the design variable vector. Usually the solution procedure can be divided into two interactive parts. One part is the thermal-structural analysis, in which finite element method and/or finite different method are used to solve for temperature, displacement and stress at the given part of structure or insulation. A second optimization part will search the best design. There are many optimization methods, such as gradient projection method (Haftka *et al*., 1990), penalty function method (Fox, 1971), feasible direction method (Fox, 1971) and sequential quadratic programming (Haftka *et al*., 1990). In our study, the two latter methods are used.

The easible direction method is a step by step iteration method in the form:

$$X_{q+1} = X_q + \alpha S_q \tag{2-2}$$

Vector S is usable feasible direction, which is defined as a small step can be taken along it without immediately leaving the feasible domain from the point X and reducing the objective function. This method produces an improving succession of feasible X_q vectors by moving in a succession of usable feasible direction. There are two general parts for this method. First, a usable feasible vector must be determined for each step of iteration and second, the step size must be determined. Among all possible choices of usable feasible directions we seek the direction which is best in some sense (Haftka *et al.*, 1990). One criterion is to reduce the objective function as much a possible, the other is to keep away from the constrained boundary a much as possible. So a sub-optimization problem is formulated to find the best search direction, it is easy to solve. Once a usable feasible direction has been found, selecting step is still challenging. If at the end of the step no constraints are active, we continue in the same direction as long as the objective function can be reduced. When we reach the constraint boundaries, we will start a new iteration.

When the evaluation of objective function and/or constraints needs much computation, iterative approximate method can be used (Haftka *et al.*, 1990). The idea of this method is reducing the exact structure analysis in optimization part. The structure analysis is applied first to generate necessary information of object function and constraints at several points in design space and then construct polynomial approximation of response in this space. Then the optimization search is carried on this approximation problem. There are several kinds of approximation, such as linear approximation based on first order derivative. We use sequential quadratic programming (SQP) method in our later study. This method is based on the theorem that optimum is a minimum of the Lagrangian function in the sub space of vectors orthogonal to the gradient of the active

constraints. First, we create a quadratic approximation to the Lagrangian and linear approximate constraint functions. We use the linearized constraints with quadratic objective function to create a direction finding sub-optimization problem. Solve the sub-problem to get search direction and approximate Lagrange multipliers. Then another sub-problem is formulated to find optimal step size.

CHAPTER 3
HEAT TRANSFER IN FUNCTIONALLY GRADED METALLIC FOAMS

Functionally Graded Material (FGM) is a new generation of materials in which composition and structure of the material gradually change over volume, resulting in corresponding changes in the properties of the material. In the simplest FGMs, two different material ingredients change gradually from one to the other. Discontinuous changes such as a stepwise gradation of the material ingredients can also be considered as a FGM. Most of current research focus on FGM compositionally graded from a refractory ceramic to a metal. It can incorporate incompatible functions such as the heat, wear, and oxidation resistance of ceramics and the high toughness, high strength, machinability and bonding capability of metals without severe internal thermal stresses. Foams are also important material ingredients for FGMs. The gradual change of foam distribution from the interior to the surface can impart it many properties such as mechanical shock resistance, thermal insulation (Ford *et al.*, 1999).

Metallic foams are a class of materials with low density and novel mechanical and thermal properties. They have a dispersion of gas bubbles in a metallic bulk material. These extremely lightweight materials have some very promising properties including high specific stiffness, very good energy-absorption, low thermal conductivity and outstanding absorption of electromagnetic waves. Because of these interesting properties, metallic foams have a number of potential applications in aerospace engineering, such as thermal protection system materials.

Metal foam is characterized by its cell topology (open cell, closed cells), relative density, cell size, cell shape and anisotropy. The relative density or solidity or volume fraction is defined as the ratio of the density of foam over that of the solid which it is made of. Each cell of closed cell foam is sealed off from its neighbors by membrane-like face, while cells of open cell foam are interconnected. Several factors combine to limit the heat flow in foams: the low volume fraction of the solid phase; the small cell size which virtually suppresses convection and reduces radiation by repeated absorption and reflection at the cell wells; and the poor conductivity of the enclosed gas (Gibson and Ashby, 1997). The thermal conductivity k is an important material property which characterizes heat conduction in solids. It is defined by Fourier's law: the heat flux q (the amount of heat flowing across a unit area) induced by a temperature gradient, ∇T, is

$$q = -k\nabla T \tag{3-1}$$

The effective thermal conductivity of a foam, which characterizes all kinds of heat transfer in foams, can be thought of as having four contributions: conduction through the solid, k_s, conduction through the gas k_g, convection within the cells k_c and radiation through the cell walls and across the cell voids, k_r. The relative contribution for each component to thermal conductivity of closed-cell rigid polyurethane foams is discussed in Gibson and Ashby, (1997). It shows that there is a minimum k at a relative density, at which point the conductivity is only a little larger than that of air contained in cells. At lower densities, the conductivity increases, partly because of the increasing transparency of cell walls to radiation and partly because at very low density the cell walls may rupture. As the relative densities of the foams increases, the contribution from conduction increases while that from radiation decreases. Heat transfer increases with the cell size.

This is partly because radiation is reflected less often in a foam with large cells and partly because the cell convection starts to contribute. Temperature changes the conductivity in a complex way. Usually conduction decreases with decreasing temperature. Radiation, too, becomes less effective at low temperature. The result is that heat transfer through most foams falls steeply with decreasing temperature.

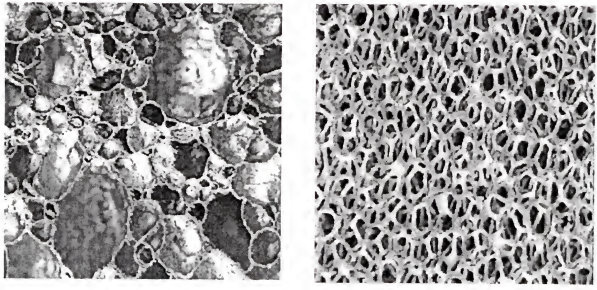

Figure 3-1 Photographs of close cell and open cell aluminum foams (Andrews *et al.*, 1999)

There has been extensive work in both experimental and analytical modeling of heat transfer in foams. Gibson (1997) discussed thermal properties of foams. Calmidi *et al.* (1999) studied conduction of high porosity aluminum foams experimentally. The experiment was conducted using air and water. They also derived an analytical expression of conduction based on the hexagonal structural model of metal foams. One dimension heat transfer was assumed. The unit cell is divided in three layers and the conductivity for each layer is derived by applying parallel law of thermal resistance.

Phanikumar *et al.* (2002) examined the flow and heat transfer characteristics of metal foam samples. By using a two-equation model, which assumes no local thermal equilibrium between the fluid and the solid phases, for the temperature and by integrating the porous medium and the clear fluid domains using the single-domain approach, they could successfully predict heat transfer in aluminum foams for a wide range of Rayleigh numbers and pore sizes. The predictions based on the non-equilibrium model for temperature are in better agreement with experimental data compared to those based on the local thermal equilibrium assumption Phanikumar *et al.* (2002). Lee *et al.* (2000) gave a good review on radiation in high porosity fibrous media. They model radiation heat-transfer based on the diffusion approximation using a modified Rosseland mean coefficient that corrects for the effect of scattering by fibers and absorption of the matrix medium. They found that radiation is the primary mode of heat transfer in high-porosity fiber thermal insulations even at temperatures above a few hundred Kelvin. Sullins and Daryabeigi (2001) studied the effective thermal conductivity, which include conduction through solid strut and gas and radiation, of metallic nickel foam for a temperature range from 100 to 1000 K. An analytical model was developed to predict the effective conductivity at different temperature and pressure. They found a conduction coupling term for gas/solid conduction is needed to correlate prediction and experimental values. Blosser (2000) studied heat transfer in honeycomb and fibrous insulation. A semi-empirical equation was used to calculate heat transfer in a foam core.

Model of Metallic Foams

An analytical model of the heat transfer through the foam is required to investigate the optimum design of functionally graded metallic foam insulations. The insulation

material is an open cell foam cell with spatial variation in its cell size and thickness. For preliminary investigations the foam was idealized as having rectangular cells of uniform size (Venkataraman *et al.*, 2001). Heat transfer through porous metal foams involves a number of heat transfer modes. Equations are developed for gas conduction, metal conduction and radiation. Convection is neglected for simplicity.

The heat transfer equations presented here are based on an idealized model of metal foams, where the repeating volume element is a rectangular array as shown in Figure 3-2. The dimensions of the cell are given by a in the plane transverse to the direction of heat transfer and b in the direction of heat transfer. The diameter of the struts of open-cell foam is given by d_s .The volume fraction (V_f) of metal in the open-cell foam, referred to as solidity, is given by the expression:

$$V_f = \frac{\text{Volume in struts}}{\text{Total volume}} = \frac{(8a+4b)(\pi d_s^2/4)/4}{a^2 b} = \frac{\pi}{4}\left(2\frac{a}{b}+1\right)\left(\frac{d_s}{a}\right)^2 \qquad (3\text{-}2)$$

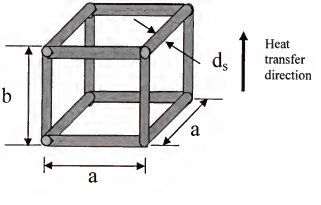

Figure 3-2 Rectangular representative volume element used for heat transfer model in open-cell foam with fixed strut diameter d_s

For a cubic cell, the expression for solidity reduces to the following equation,

$$V_f = \frac{3}{4}\pi\left(\frac{d_s}{a}\right)^2 \qquad (3\text{-}3)$$

A comparable expression for the solidity of a closed-cell foam with walls of thickness t is given by,

$$V_f = \frac{\text{Volume in walls}}{\text{Total volume}} = \frac{\left(2a^2 + 4ab\right)\left(\frac{t}{2}\right)}{a^2 b} = \frac{t}{a}\left(\frac{a}{b} + 2\right) \qquad (3\text{-}4)$$

The effective heat transfer coefficient is assumed to be a linear combination of three components: gas conduction, metal conduction and radiation. The convection in foam is neglected. The expressions used for the different heat transfer modes are described as follows.

Effective Thermal Conductivity

Heat transfer through metal foams involves combined modes of heat transfer, solid conduction through foam materials, gas conduction through air in foams and radiation through the foam cell. The relative contributions of the different heat transfer modes vary with the relative density, temperature and pressure change. Radiation becomes more dominant at high temperatures and with large temperature gradients through the insulation, while gas conduction are minimal at low pressures and become more significant with increasing pressure. The complex coupling of the heat transfer modes makes the analysis and design of metal foam difficult. Convection effects, which are much smaller than the aforementioned modes, are neglected for simplicity.

Gas Conduction

Gas conduction is modeled in the voids in the metallic foam. Away from any solid boundaries, the thermal conductivity of a gas is independent of pressure (Burmeister,

1983). However, gas molecules interact with solid surfaces in such a way that the thermal conductivity of a gas enclosed in a small cavity does vary with pressure. The pressure dependent thermal conductivity for air is calculated using the following equation (Daryabeigi, 1999):

$$k_g = \frac{k_g^*}{1 + 4\frac{(2-\alpha)}{\alpha}\frac{\gamma}{(\gamma+1)}\frac{1}{\Pr}\frac{\lambda_m}{l_c}} \tag{3-5}$$

where,

$k_g^* = 3.954\text{x}10^{-03} + 7.7207\text{x}10^{-05}T - 1.6082\text{x}10^{-08}T^2$ is the temperature dependant air conductivity [W/(m-K)] at one atmosphere;

α is the accommodation coefficient (a measure of the average efficiency of the energy exchange between gas molecules and solid surfaces, assumed = 1.0);

γ is the specific heat ratio (assume1.4 for air);

$\lambda_m = \frac{K_B T}{\sqrt{2}\pi d_g^2 P}$ is the mean free path length (the mean distance traveled by gas molecules between collisions with other molecules);

T is the temperature (K);

$K_B = 1.38062\text{x}10^{-23}$ is the Boltzman constant (J/molecule K);

$d_g = 3.65009\text{x}10^{-10}$ is the gas collision diameter (m);

P is the gas pressure (Pa);

$P_r = 0.7086 - 3.7245\text{x}10^{-06}T + 2.2556\text{x}10^{-08}T^2$ is the Prandtl number expressed as a function of temperature;

l_c is the characteristic length of the metal foam (m);

All of the above quantities are readily apparent, except for the characteristic length. For closed-cell foams, an obvious choice for characteristic length is the cell size in the direction of heat transfer. However, for open-cell foam the choice of characteristic length is not as straightforward. For this study the characteristic length for open-cell foams was calculated using the following equation (Bankvall, 1973) derived for fibrous insulation.

$$l_c = \frac{\pi}{4} \frac{d_s}{V_f} \tag{3-6}$$

Solid Conduction

Solid conduction through a foam can be complicated due to the geometry of the foam. A comprehensive study of heat transfer through polymeric foams was published by Glicksman (1994). The following expressions, derived by Glicksman (1994), are more applicable to realistic foam geometries than expressions that could be derived directly from the simplified geometry in Figure 3-2.

For open-cell foams,

$$k_m = \tfrac{1}{3} k_m^* V_f \sqrt{\frac{a}{b}} \tag{3-7}$$

where k_m^* is the metal conductivity.

For titanium metal used in our calculations the conductivity as a function of temperature is given by

$k_m^* = 2.7379 + 1.3462\text{x}10^{-02} T - 1.7207\text{x}10^{-07} T^2$ $\quad [\text{W/(m°K)}]$.

Radiation

Radiation through foams is also complicated by foam geometry. Glicksman (1994) has addressed the more complex problem of translucent polymeric foams, but also developed expressions for opaque open and closed cell foams. When Glickman's equations are converted to the notation in the current study the expressions become: for open-cell foams,

$$k_r = \frac{16}{3}\left(\frac{\sigma T^3}{4.1\frac{\sqrt{V_f}}{b}}\right) \tag{3-8}$$

where,

$\sigma = 5.6697\text{x}10^{-08}$ is the Stephan-Boltzman constant, W/(m^{2}K^4)

ε is the emittance.

The overall effective thermal conductivity consists of the contributions of all modes of heat transfer. For this study it is assumed that the contributions of the three modes of heat transfer can be linearly combined as follows:

$$k_e = (1 - V_f)k_g + k_m + k_r \tag{3-9}$$

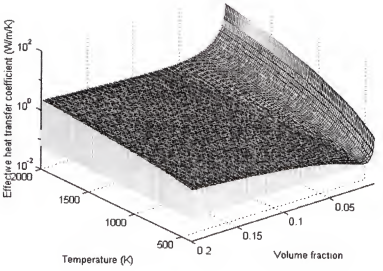

Figure 3-3 Dependence of the effective thermal conductivity on the temperature and volume fraction for a fixed strut diameter of 0.05 mm (Venkataraman *et al.*, 2001)

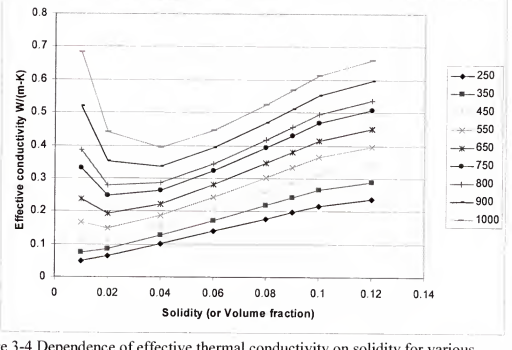

Figure 3-4 Dependence of effective thermal conductivity on solidity for various temperatures ranging from 250 K to 1000 K. The strut diameter is fixed at 0.05 mm (Venkataraman *et al.*, 2001)

Figure 3-2 and 3-3 show the effective thermal conductivity in the titanium open cell foams for varying temperatures and density and a constant pressure (one atmospheric pressure, 101325 Pa). The variations in density were achieved by tailoring the cell size while keeping the strut diameter fixed at 0.05 mm (0.002 inch). The limit on the strut diameter forces larger cell sizes for low densities. For dense foams, when heat transfer is dominated by conduction, this is of little consequence, so the effective conductivity is monotonic function of solidity. For higher temperatures or low-density foams, radiation is more important, and larger cell sizes increase the radiative heat transfer so that there is an optimum value of the solidity. This indicates that there may be merit in tailoring a solidity distribution to minimize heat transfer.

Fabrication of Metallic Foams

There are several distinct process-routes developed to make metal foams. They fall into four classes (Ashby *et al.*, 2000): foams are formed from vapor phase; foams are electrodeposited from an aqueous solution; those depend on liquid-state processing; and foams created in solid state. Titanium foams can be made from vapor phase deposition or electrodeposition of titanium onto a polymer foam precursor which is subsequently burned out leaving cell edges with hollow cores.

Open cell polymer foams with low relative densities and a wide range of cell sizes of great uniformity are available from numerous sources. They can be used a templates to create investment-casting molds into which a variety of metals and their alloys can be cast. An open cell polymer foam mold template with the desired cell size and relative density is first selected. This can be coated with a mold casting slurry which is then dried

embedded in casting sand. The mold is then baked both to harden the casting materials and to decompose (and vapor) the polymer template, leaving behind a negative image of the foam. This mold is subsequently filled with a metal alloy and allowed to cool. After directional solidification and cooling, the mold materials are removed leaving behind the metal equivalent of the original polymer foam. This method gives open cell foams with pore size of 1-5 mm and relative density as low as 0.05.

An analytical model of the heat transfer through the open cell foam is developed in this chapter. The effective thermal conductivity is assumed to be a linear combination of three components: gas conduction, solid conduction and radiation. Equations are developed for these three heat transfer modes. Convection is neglected for simplicity. We found that for dense foams the effective conductivity is monotonic function of solidity because heat transfer is dominated by conduction. For higher temperatures or low-density foams, radiation is more important, and larger cell sizes increase the radiative heat transfer so that there is an optimum value of the solidity.

CHAPTER 4
OPTIMUM DESIGN OF METALLIC FOAM INSULATION UNDER STEADY STATE HEAT TRANSFER CONDITION

In this chapter an optimality criterion is developed for minimizing heat transfer through open cell titanium foam insulation with variable cell size through its thickness. We want to find solidity profiles that may yield large improvements in weight efficiency based on currently available models for effective thermal conductivity of metallic foams. The resulting effective thermal conductivity of the foam is a function of temperature, pressure, properties of the foam material, and the foam geometry. The optimization problem is to determine the solidity distribution that minimizes the one dimensional steady state heat conduction through the thickness of titanium foam insulation. For a fixed inner wall temperature and foam insulation thickness the outside wall temperature is maximized. Maximizing the outside wall temperature maximizes the heat radiated out from the hot surface of the insulation and therefore corresponds to minimizing the transmitted heat. The optimality condition is developed and used to obtain the optimum solidity profile. The maximum temperature obtained using a functionally graded foam and uniform density foam are compared to illustrate performance payoffs provided by optimization of functionally graded foam properties.

Temperature Optimization

Optimality Criteria for Minimum Heat Transfer

We consider an insulation panel of thickness h with a given heat flux Q_0 on its hot side ($x=h$) and a given temperature T_0 on its cool side ($x=0$). The insulation panel is made from functional graded titanium foam. The variations in solidity were achieved by tailoring the cell size while keeping the strut diameter d_s fixed at 0.05 mm (0.002 inch). We assume that there is very little heat transfer in the plane of panel, so that the problem can be treated as one-dimensional. Furthermore, we assume that transient effects can be neglected.

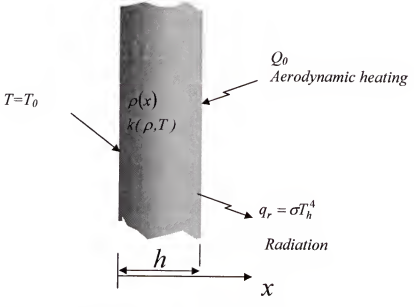

Figure 4-1 Schematic representation of one-dimensional heat transfer problem

The steady state heat transfer equation and boundary conditions are:

$$\begin{aligned} &kT' = Q_0 - \sigma T_h^4 \qquad 0 \le x \le h \\ &T(0) = T_0 \end{aligned} \tag{4-1}$$

where prime denotes differentiation with respect to x. The conductivity is given as function of solidity and temperature $k = k(\rho, T)$. We want to maximize the temperature T_h=$T(h)$ at hot side of insulation to maximize its radiation, subject to Equation (4-1) as a constraint, so we form the Lagrangian

$$L = T(h) - \int_0^h \lambda(x)\left[kT' - Q_0 + \sigma T^4(h)\right]dx \tag{4-2}$$

and take the variation

$$\delta L = \delta T(h) - \int_0^h \lambda(x)\left[\delta k T' + k\delta T' dx + 4\sigma T^3(h)\delta T(h)\right]dx \tag{4-3}$$

In order to evaluate this integral we use

$$\delta k = \frac{\partial k}{\partial \rho}\delta\rho + \frac{\partial k}{\partial T}\delta T$$

and

$$\int_0^h \lambda k \delta T' dx = \lambda k \delta T\Big|_0^h - \int_0^h (\lambda k)' \delta T dx$$

Hence we obtain

$$\begin{aligned}\delta L = &\left[1 - 4\sigma T^3(h)\int_0^h \lambda dx - \lambda(h)k(h)\right]\delta T(h) \\ &- \int_0^h T'\lambda\frac{\partial k}{\partial \rho}\delta\rho dx + \int_0^h (\lambda k)'\delta T dx - \int_0^h \lambda\frac{\partial k}{\partial T}T'\delta T dx\end{aligned} \tag{4-4}$$

This gives us the following optimality conditions

$$T'\lambda\frac{\partial k}{\partial \rho} = 0 \qquad \textit{and} \qquad (\lambda k)' - \lambda T'\frac{\partial k}{\partial T} = 0 \tag{4-5}$$

In the first condition, $T' = 0$ implies uniform temperature that corresponds to no heat transfer. Therefore, the optimality condition becomes,

$$\frac{\partial k}{\partial \rho} = 0 \tag{4-6}$$

Physically this implies that in order to minimize heat transmitted through the insulation we should use the solidity that minimizes the conductivity. On expanding the terms of the second condition we have

$$\lambda' k + \lambda \left(\frac{\partial k}{\partial \rho} \rho' + \frac{\partial k}{\partial T} T' \right) - \lambda T' \frac{\partial k}{\partial T} = 0 \tag{4-7}$$

On substituting Equation (4-6) in (4-7) and simplifying we obtain

$$\lambda' k = 0 \qquad \text{or} \qquad \lambda = c \,(\text{constant}) \tag{4-8}$$

Numerical Evaluation of Designs

From the derivation of effective thermal conductivity presented in a previous section one can note that for a fixed value of the strut diameter, the effective conductivity (heat transfer coefficient) is a function of temperature (T) and volume fraction or solidity (V_f), i.e.

$$k = k(T, V_f) \tag{4-9}$$

The optimality condition for minimizing heat transmitted is given by

$$\frac{\partial k}{\partial \rho} = 0 \tag{4-10}$$

Since, the density is obtained as a scalar multiple of the volume fraction ($\rho = \rho_m^* V_f$), the optimality condition can be stated as,

$$\frac{\partial k}{\partial V_f} = 0 \tag{4-11}$$

Substituting the expression for effective conductivity in the optimality condition provides us the values of optimum solidity (or volume fraction, V_f^*) and heat transfer coefficient (k^*) as a function of temperature.

The dependence of the effective conductivity or heat transfer coefficient as a function of temperature and solidity is shown in Figure 4-2. The solidity is varied by changing the cell size only. The strut diameter is kept constant at 0.05 mm (0.002 inches). It can be noticed that for each temperature there is a unique value of the heat transfer coefficient or solidity at which the optimality condition is satisfied. The values of the conductivity (k^*) and solidity that satisfy the optimality condition were obtained numerically and were fit as quadratic polynomials on the temperature and plotted in Figure 4-3. The optimum heat transfer coefficient (k^*) and solidity (V_f^*) are then approximated by a polynomial expression obtained by a least squares fit.

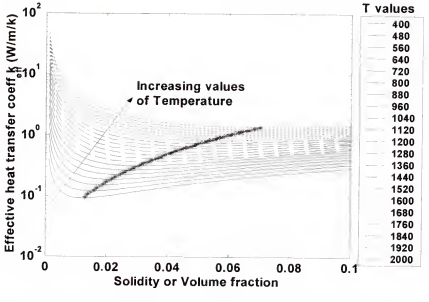

Figure 4-2 Optimal conductivity depending on solidity for minimum heat design

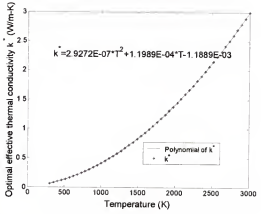

Figure 4-3 Optimum effective conductivity and solidity as function of temperature for minimum heat design. Quadratic polynomials fitted to data are also given

Optimum Temperature and Density Distribution

The 1-D heat conduction with radiation boundary condition is governed by

$$kT' = Q_0 - \sigma T_h^4 \tag{4-12}$$

where, σ is the Stephan-Boltzman constant and $T_h = T(h)$. The optimal thermal conductivity k^* is now expressed only as a function of temperature T using the optimality condition:

$$k^* = a_0 + a_1 T + a_2 T^2 \tag{4-13}$$

where a_is are fitting coefficient. Substituting k in the governing differential equation above and integrating results in,

$$\int_{T_0}^{T} (a_0 + a_1 T + a_2 T^2) dT = \int_0^x (Q_0 - \sigma T_h^4) dx \tag{4-14}$$

or

$$(a_0 T + \frac{a_1}{2} T^2 + \frac{a_2}{3} T^3) = (Q_0 - \sigma T_h^4) x + (a_0 T_0 + \frac{a_1}{2} T_0^2 + \frac{a_2}{3} T_0^3) \tag{4-15}$$

evaluating the above expression at $x=h$, provides us a polynomial expression that can be solved to obtain T_h

$$(a_0 T_h + \frac{a_1}{2} T_h^2 + \frac{a_2}{3} T_h^3) + h\sigma T_h^4 = Q_0 h + (a_0 T_0 + \frac{a_1}{2} T_0^2 + \frac{a_2}{3} T_0^3) \qquad (4\text{-}16)$$

once T_h is known we can solve Equation (4-15) to obtain the temperature distribution.

The temperature distribution in the insulation of fixed thickness (h=0.01 m) inside temperature (T_0=400 K) and different values of incident heat flux (from 0.1 to 1.0 MW/m^2) are calculated using the Equations (4-12) and (4-16) and plotted in Figure 4-4. The plots are as expected, i.e., when the thickness (h) and inside wall temperature (T_0) are kept constant and heat flux at surface is increased the outside temperature increases. The plots in Figure 4-4 are the temperature distribution that satisfies the optimality condition for maximum temperature at $x=h$. Once the optimum temperature profile is determined, the distribution of cell size or solidity can be calculated using the polynomial expressions for solidity shown in Figure 4-3.

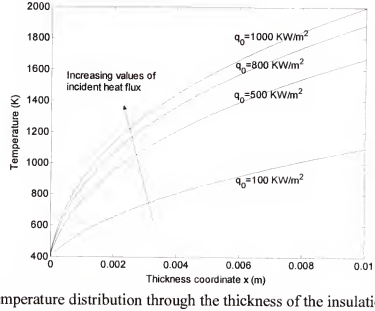

Figure 4-4 Temperature distribution through the thickness of the insulation for different values of incident heat flux that satisfy optimality conditions for maximum outside temperature

The hot surface temperature for uniform design which maximizes the hot surface temperature is also calculated in the same way described before. The comparison of maximum temperatures attained by graded and uniform insulation is plotted in Figure 4-5. From the plot we can see that differences in temperature for both designs are small and functionally graded insulation had marginally higher temperature (0.13- 0.15%). The improvement decreases as temperature (incident heat flux) increases.

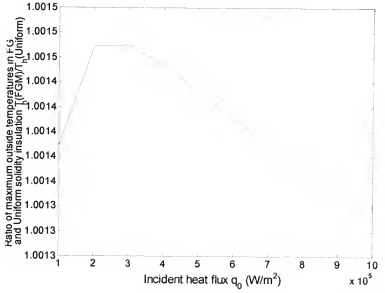

Figure 4-5 Ratio of maximum temperatures attained by functionally graded and uniform insulation

We can only improve the hot surface temperature a little; however, the heat transmitted through insulation is reduced quite a lot. The comparison of heat transmitted through the graded and uniform insulation is plotted in Figure 4-6. From the plot we can see that heat transmitted through FGM insulation was 2.5% to 4.7% lower than uniform density insulation and the difference increases with the temperature.

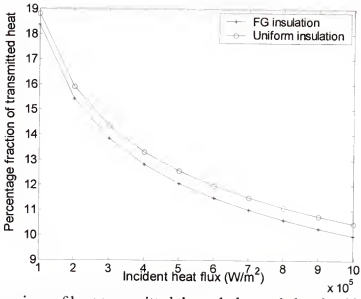

Figure 4-6 Comparison of heat transmitted through the graded and uniform insulation of minimum heat design

The cell size distribution that satisfies optimality criterion for maximizing the outside wall temperature is shown in Figure 4-7. In the same plot the density for maximizing the temperature in uniform density foam is also indicated.

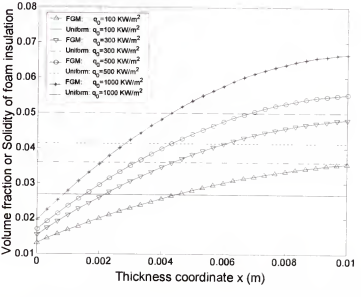

Figure 4-7 Optimal cell size distribution for graded and uniform insulations of minimum heat design

Mass Optimization

In this section we will identify density profiles that may yield improvements in weight efficiency compared to materials with uniform density. The objective of the optimization problem is to determine the solidity distribution that minimizes the mass of the titanium foam of given thickness for a fixed inner and outer wall temperatures. The optimality condition is developed and used to obtain the optimum solidity profile. The minimum mass obtained using the functionally graded foam and that of uniform density foam are compared to illustrate the performance payoffs provided by the optimization of graded foam properties. We used the same foam model as that used in temperature optimization.

Criterion for Minimum Mass Design

We consider an insulation panel of thickness h with a given heat flux Q_0 and temperature T_m on its hot side (x=h) and a given temperature T_0 on its cool side (x=0), as shown in Figure 4-8. For the purpose of illustration, the temperatures T_0 and T_m are assumed as 400 K and 1500 K, respectively. These temperatures, respectively, are the maximum temperatures the insulation can withstand. We assume that there is very little heat transfer in the plane of panel, so that the problem can be treated as one-dimensional.

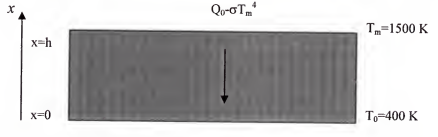

Figure 4-8 Schematic of heat transfer in insulation. Q_0 is the applied aerodynamic heating, and σT_m^4 represents the heat radiated back into space.

The steady state heat transfer equation and boundary conditions are:

$$kT' = Q_0 - \sigma T_m^{\ 4}$$
$$T(0) = T_0 = 400K \qquad T(h) = T_m = 1500K \tag{4-17}$$

where σ is the Stephan-Boltzman constant and a prime denotes differentiation with respect to x. We have assumed the emittance of the surface as unity. The thermal conductivity variation shown in Figure 3-4 can be represented as a function of volume fraction V_f and temperature T:

$$k = k(T, V_f) \tag{4-18}$$

The density of the foam ρ is given by $\rho = \rho_m^* V_f$, where ρ_m^* is the mass density of the strut material and V_f is the solidity or volume fraction of the foam. The mass per unit area of the foam insulation, m, is given by

$$m = \rho_m^* \int_0^h V_f(x)dx \tag{4-19}$$

Our objective is to minimize m subject to the constraints given by Equation (4-17). Using a Lagrange multiplier $\lambda(x)$ for the constraint, the problem becomes equivalent to minimizing the integral:

$$L = \int_0^h F(x, T, V_f, T')dx \tag{4-20}$$

where,

$$F = V_f + \lambda(x)(kT' - Q_0 + \sigma T_m^{\ 4}) \tag{4-21}$$

The Euler-Lagrange Equations corresponding to Equation (4-20) are:

$$\frac{\partial F}{\partial V_f} - \frac{d}{dx}\left(\frac{\partial F}{\partial V_f'}\right) = 0$$
$$\frac{\partial F}{\partial T} - \frac{d}{dx}\left(\frac{\partial F}{\partial T'}\right) = 0 \tag{4-22}$$

substituting for F in Equation(4-22) we obtain:

$$1 + \lambda T' \frac{\partial k}{\partial V_f} = 0$$
$$\lambda T' \frac{\partial k}{\partial T} - (\lambda k)' = 0 \tag{4-23}$$

Eliminating $\lambda(x)$ from Equation (4-23) and also using the governing equation (4-17), we obtain the optimality condition as

$$V_f' = -\left(\frac{k}{\partial k / \partial V_f}\right)' \tag{4-24}$$

Integrating the above equation, we derive the optimum density profile as

$$V_f(x) = V_{fc} - \frac{k}{\partial k / \partial V_f} \tag{4-25}$$

where V_{fc} is a constant that will be determined by the condition $T(h)=T_m$. For a given temperature T and the integration constant V_{fc}, Equations (4-18) and (4-25) determine the optimum volume fraction V_f^* and the optimal k^* independently of the position x.

Numerical Evaluation of Designs That Satisfy the Optimality Criterion

Equations (4-18) and (4-25) are solved for the optimal k^* and V_f^* for a range of values of V_{fc} and T, and the results are shown in Figure 4-9. The range of V_{fc} was chosen such that the values of T_m obtained would be in the useful range for the example problem.

Figure 4-9 indicates that there may be two values of V_f for a given k, but for minimum mass design we obviously select the lower value, that is, values of V_f where $dk/dV_f \leq 0$ on the k-V_f plot.

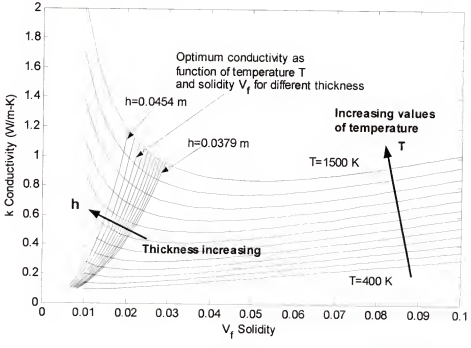

Figure 4-9 Loci of optimum solidity values of minimum mass design with various values of thickness

The values of the optimal conductivity k^* shown in Figure 4-9 were fitted as quadratic polynomials of the temperature for a range of values of V_{fc} (hence thickness). The quadratic function is written:

$$k^* = k^*(T) = aT^2 + bT + c \tag{4-26}$$

This quadratic approximation allows analytical solution of the heat conduction Equation (4-17). Substituting the optimum $k^*=k^*(T)$ from Equation (4-26) into (4-17)

$$\frac{dT}{dx} = \frac{Q_0 - \sigma T_m^{\ 4}}{aT^2 + bT + c} \tag{4-27}$$

Equation (4-27) can be integrated to obtain

$$\frac{a}{3}T^3 + \frac{b}{2}T^2 + cT - (Q_0 - \sigma T_m^4)x + c_0 = 0 \tag{4-28}$$

where,

$$c_0 = -\frac{a}{3}T_0^3 - \frac{b}{2}T_0^2 - cT_0 \tag{4-29}$$

Solving Equation (4-28) provides us with the distribution of temperature across the thickness of the panel. Choosing different V_{fc}s and repeating the previous procedure, we can identify the specific V_{fc} that satisfies boundary condition $T(h)=T_m$ for a given thickness h. With the optimal temperature profile $T(x)$ shown and using Equation (4-28), we can find the optimal solidity profile $V_f^*(x)$ by solving Equation (4-18). After we obtain $V_f^*=V_f^*(x)$, we substitute it into Equation (4-19) to find the mass per unit area of insulation. Figure 4-10 shows the temperature distribution in a FGM for different thicknesses of insulation for the case $T(h)=T_m$=1500 K and Q_0=300,000 W/m. The values of V_{fc} corresponding to the different thicknesses are shown in Table 4-1. The thicknesses of insulation are chosen such that they are in useful range. The corresponding solidity profiles are shown in Figure 4-11 and the corresponding distribution of cell size calculated by Equation (3-3) is shown in Figure 4-12. From Figure 4-11, we can see that the optimal functionally graded insulation requires high solidity at hot side and low solidity at cool side.

Table 4-1 Different V_{fc} corresponds to different insulation thickness for minimum mass design under steady state heat transfer condition

V_{fc}	-0.3	-0.275	-0.25	-0.225	-0.2	-0.175	-0.15	-0.125	-0.1	-0.075	-0.05
h (m)	0.0378	0.0379	0.0381	0.0383	0.0386	0.0389	0.0394	0.04	0.041	0.0426	0.0457

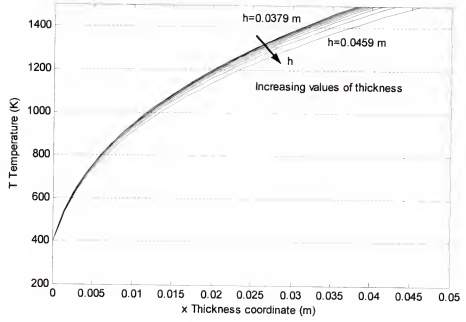

Figure 4-10 Candidate temperature distributions through the thickness of the insulation for different thickness to minimize mass, Q_0=300,000 W/m

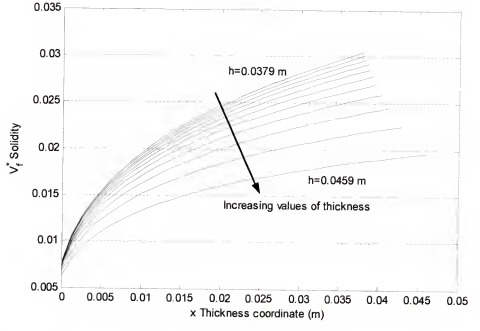

Figure 4-11 Optimum solidity profile of minimum mass design for various thickness of the insulation

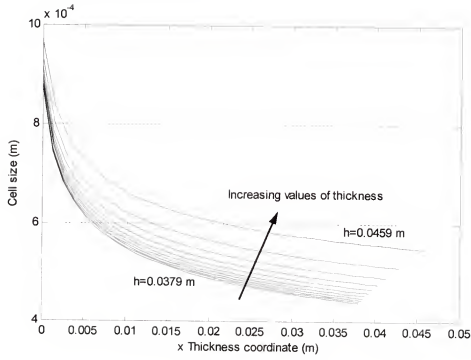

Figure 4-12 Optimum cell size distributions of minimum mass design for various thicknesses of the insulation

For the purpose of comparison, the problem of an optimum (minimum mass) foam insulation having a uniform solidity that satisfies Equation (4-17) was also solved. The procedures are described in Venkataraman *et al.* (2001). The areal density (mass per unit area) of the insulation is obtained as the product of thickness and solidity. Figure 4-13 compares the relative areal density for uniform and optimal grade foam insulation for various insulation thicknesses. It can be seen that the mass savings are high for thin insulation with about 8.5% less mass for 37.9 mm thick insulation and only about 4% savings for 45.9 mm.

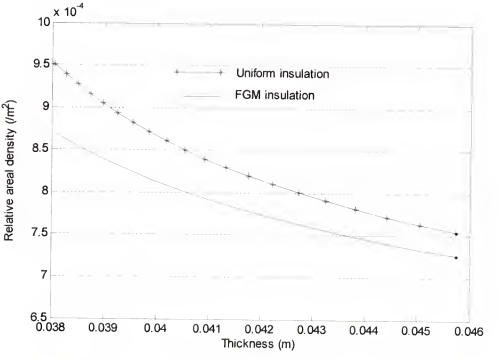

Figure 4-13 Comparison of mass per unit area for functionally graded and uniform density insulations

Since we used a quadratic approximation to the optimum conductivity, we should check the accuracy of our calculations by verifying the temperature at the outside wall of the insulation panel. Using the results of $T^*(x)$ and $V_f^*(x)$, which are plotted in Figures 4-11 and 4-12, we can calculate the conductivity $k(x)$ from Equation (4-18). Integrating Equation (4-17), we obtain the temperature at the outside wall as

$$T_h = T_0 + (Q_0 - \sigma T_m^4) \int_0^h \frac{1}{k(x)} dx \tag{4-30}$$

Substituting for $k(x)$ in Equation (4-30), and using numerical integration, we find T_h for insulations of various thicknesses. The results are shown in Figure 4-14. It can be noted that the error on outside wall temperature is less than half degree.

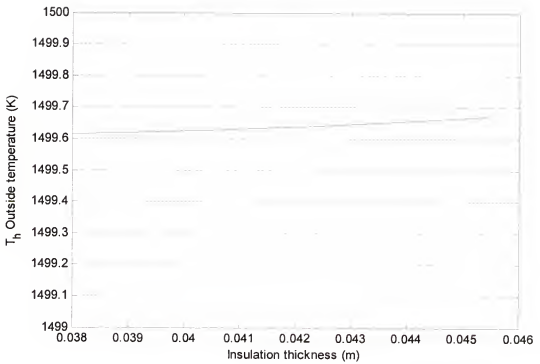

Figure 4-14 Temperature at the outside wall for various designs studied

The problem of steady state heat conduction in functionally graded open-cell metal foam insulation is studied in this chapter. The heat transmitted through insulation (minimum heat design) or the insulation mass (minimum mass design) are minimized by varying the insulation solidity profile. Optimality conditions are derived for these two optimization problems, which are reduced to that of ordinary, nonlinear differential equations and are solved numerically. The results include optimum cell size variation through the thickness of the insulation for both designs. It is shown that using functionally graded insulation can reduce the heat transmitted through the insulation 2.5-4.7 percent or reduce insulation mass 4-8 percent compared with uniform foam insulation.

CHAPTER 5
OPTIMUM DESIGN OF METALLIC FOAM INSULATION UNDER TRANSIENT HEAT TRANSFER CONDITION

In the last chapter we showed that functionally graded foams can improve the performance of the insulation under steady state heat flow. The solidity profile or variation of solidity through the thickness of the insulation can be optimized in order to minimize the transmitted heat for given mass or, minimize the mass for specified heat transfer. Unlike steady state conditions, mass plays an important role on the temperature history under transient heating conditions due to the effect of heat capacity of materials. The objective of this chapter is to develop a methodology for optimizing functionally graded foam insulations taking into consideration the transient heat transfer conditions that arise during reentry. We simplify the design task to a point design. We choose a point on the area of the surface that has the most critical heat influx and investigate the one-dimensional heat transfer problem at that point. Some simplification of this problem is made, including the heat load.

Analysis

In this section we identify the necessary information and modeling details required to perform transient thermal analysis of TPS insulation. Figure 5-1 shows a schematic of the simplified problem. The foam insulation is subjected to a transient heat flux $q_i(t)$ incident on the outside surface. The foam insulation is attached to the structural mass that

makes the wall of the RLV tank. We assume that the amount of heat q_c that can be removed from the structure internally is negligibly small. The objective of the optimization is to ensure that the maximum temperature in the structural mass T_s is below a specified limit $T_{s_{lim}}$ for all times during reentry and after landing. A similar constraint has to be imposed for the maximum temperature in the insulation $T_{max}(x)$ to ensure that it does not exceed the maximum limiting temperature of the insulation material. However, we want the temperature at the outside wall to be as high as it can be so that most of the incident heat can be rejected by radiation at this surface.

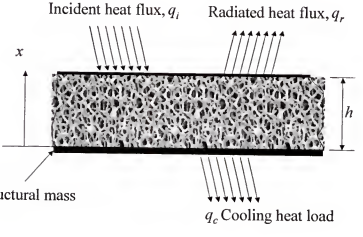

Figure 5-1 Schematic of the heat transfer in the insulation on a reusable launch vehicle structure

Blosser *et al.* (2002) gives a typical heat flux into the vehicle during reentry. The heat flux varies significantly over the surface. The leading edge of the wings and the nose of the vehicle, which are the stagnation points for the flow, have the highest heating rate. For our study we choose a location on the lower surface referred to as station 413 (STA 413) as a representative point for the point design. The heat flux (Blosser *et al.*, 2002) for

that location is reproduced here in Figure 5-2. The details of the assumptions and calculations used to obtain the heat flux are discussed by Blosser *et al.* (2002).

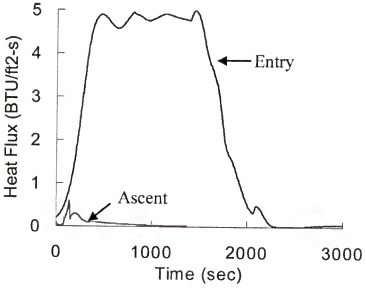

Figure 5-2 Heat flux at a chosen point on the windward side during ascent and reentry

For the preliminary phase of this study, we will simplify the heat flux history functions as constant heat load:

$$q(t) = \begin{cases} q_{\max} & 0 < t < t_0 \\ 0 & t_0 < t < t_f \end{cases} \tag{5-1}$$

where q_{max}=5.0 BTU/ft^2-s (5.6745 × 10^4 W/m^2) is the maximum intensity of the heat flux, t_f is the final time of the reentry (when the vehicle has landed). In our current study t_0 is 2000 seconds and t_f is 5000 seconds. The pressure differences are ignored, as they appear to be small in value.

The heat transfer in the TPS is assumed to be one-dimensional. The finite width effects of the TPS insulation and the heat shorts resulting from the support structure around the perimeter of the TPS tiles are ignored. The structural mass on the inside will

correspond to the mass of the stiffened panel shell used for the RLV tank construction. The insulation itself is made of titanium open cell foam material. The foam is idealized as having rectangular cells of uniform size. The diameter of the struts of foam is given by d_s. The volume fraction (V_f) of metal in the foam, referred to as solidity, varies from 0.01 to 0.11. The variation in solidity is achieved by tailoring the cell size while keeping the strut diameter fixed d_s at 0.05 mm (0.002 inch). We assume titanium has a temperature independent constant heat capacity Cp equal to 0.1 Btu/lb$_m$/^{o}R.

The governing equation for this one dimensional heat conduction problem is given by:

$$\frac{\partial}{\partial x}\left(k\frac{\partial T}{\partial x}\right) = \rho_d C_p \frac{\partial T}{\partial t} \tag{5-2}$$

where C_p is the specific heat of insulation material and ρ_d is the insulation density. We use explicit finite difference method to discretize Equation (5-2).

Optimal Two-Layer Design to Minimize the Maximum Structural Temperature

Numerical Discretization

For two-layer design we can descretized Equation (5-2) as:

$$\rho_{di} C_p \frac{T_i^{n+1} - T_i^n}{\Delta t} = \frac{k_{i+1/2}\left(T_{i+1}^n - T_i^n\right)}{(\Delta x)^2} - \frac{k_{i-1/2}\left(T_i^n - T_{i-1}^n\right)}{(\Delta x)^2} \tag{5-3}$$

The subscript i denotes the node of spatial discretization and the superscript n denotes the time step. The conductivity at the middle of two nodes (i, $i+1$) is given by

$$k_{i+1/2} = \frac{2k_i k_{i+1}}{k_i + k_{i+1}} \tag{5-4}$$

The structural mass m_s attached to the cool-side of the insulation is thermally insulated on the inside. The scheme of finite difference becomes

$$q_c + m_s C_{ps} \frac{T_1^{n+1} - T_1^n}{\Delta t} + A \frac{\Delta x}{2} C_p \rho_{d1} \frac{T_1^{n+1} - T_1^n}{\Delta t} = A k_{1+1/2} \frac{T_2^n - T_1^n}{\Delta x} \tag{5-5}$$

$$T_1^{n+1} = T_1^n + \frac{\Delta t}{m_s C_{ps} + \frac{A \rho_{d1} C_p \Delta x}{2}} \cdot \left(A k_{1+1/2} \frac{T_2^n - T_1^n}{\Delta x} - q_c \right) \tag{5-6}$$

where A is the cross section of insulation. C_{ps} is the heat capacity of structural mass and T_1 is the cool side temperature. The heat flow from the cool side, q_c, is assumed to be zero in our study. Only radiation is included at the hot side of insulation. The emittance is assumed to be one. We neglect the convection between the insulation and outer air. The radiation boundary condition at the hot side of the TPS can be expressed as:

$$T_{hot}^{n+1} = T_{hot}^n + \frac{2}{\rho_{di} C_p \Delta x} \cdot \left[\Delta t (Q - \varepsilon \sigma T_{hot}^n) - k_{hot-1/2}^n (T_{hot}^n - T_{hot-1}^n) \frac{\Delta t}{\Delta x} \right] \tag{5-7}$$

where T_{hot} is the temperature of the outmost node at hot side. At the interface between layer 1 and layer 2, we have,

$$T_i^{n+1} = T_i^n + \frac{2\Delta t}{(\Delta x_1 \rho_{d1} + \Delta x_2 \rho_{d2}) C_p} \cdot \left[\frac{k_{i+1/2} \left(T_{i+1}^n - T_i^n \right)}{\Delta x_2} - \frac{k_{i-1/2} \left(T_i^n - T_{i-1}^n \right)}{\Delta x_1} \right] \tag{5-8}$$

where Δx_1 and Δx_2 are the layer 1 and layer 2 discretization, respectively. The finite difference scheme for the solution used 21 nodes to calculate the heat transfer and temperature distribution in the insulation and at least two elements are used to model each layer. For explicit scheme requires that the maximum time step should satisfy the following condition:

$$\Delta t \le \frac{(\Delta x_1)^2}{2k_1/\rho_1 C_p}$$
$$\Delta t \le \frac{(\Delta x_2)^2}{2k_2/\rho_2 C_p} \qquad (5\text{-}9)$$

where k_1 and k_2 are the conductivity in layer 1 and layer 2 respectively. The maximum diffusivity ($k/\rho C_p$) in both layer 1 and 2 is less than 1.25×10^4 m^2/s. The smallest space discretization is 0.005 m because of our side constraints in Equation (5-10). So the maximum time step we can take is 0.3125 second. In our numerical evaluation we take 0.25 second as our time step.

Performance of Steady State Optimal Design

We start by assessing the performance of functionally graded insulation designed for steady-state conditions by comparing them with uniform solidity insulation. The solidity profile of the functionally graded insulation is designed to maximize the hot side temperature of insulation, and it is subjected to a constant heat flux q_{max} under steady-state condition. Maximizing the outside temperature is equivalent to minimizing the heat flux into the insulation, which, as described in Venkataraman *et al.* (2001), requires minimizing the effective conductivity at every point for the given temperature at that point. The solidity of the uniform TPS is chosen such that it has the same thickness and mass as the graded insulation. In this chapter the insulation thickness is chosen as 0.2 m, which is greater than the designs in chapter 4 in order to keep the temperatures of the insulation and the structure in a reasonable range. And the graded insulation areal density (m_p) is obtained as 20.9 kg/m^2 (4.29 lb/ft^2). The solidity of corresponding uniform

insulation is 0.0236, as shown in Figure 5-3. The initial temperature of the structure and insulation panel is 300 K. Aluminum is selected as the structure at the cool side with a thickness of 2.2 mm (0.0866 inch) (Blosser *et al.*, 2002). It has an areal density (m_s) of 6.1 kg/m^2 (1.25 lb/ft^2). The heat capacity C_{ps} of structural mass is assumed to be temperature independent and equal to 494.16 J/kg/K (0.118 Btu/lb$_m$/^{o}R). The structural mass is insulated at the cool side (x=0) so that there is no heat transfer out of the structure. The ambient temperature for $t \geq 2000$ seconds, when the aerodynamic heating stops, is assumed to be 300 K. Both minimum heat design and minimum mass design under steady state heat transfer condition require high solidity at hot side and low solidity at cool side of insulation.

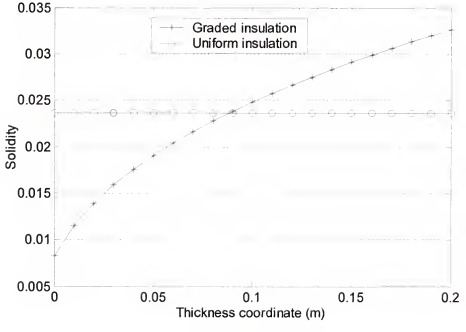

Figure 5-3 Solidity profiles for graded insulation designed for the steady-state conditions and uniform insulation of same mass

The maximum structural temperature of the uniform insulation is lower than that in graded insulation, as shown in Figure 5-4. That is to say, the optimal solidity profile we obtained under steady-state conditions is far from optimal to protect the inner structure in the transient case. Figure 5-5 gives the temperature profiles for both graded insulation and uniform insulation at different times. It explains why the steady-state optimum is not useful for transient conditions. It can be seen from Figures 5-4 through 5-6 that for the early times the graded insulation provides better protection. However, later, and especially once the applied heat is removed, the uniform insulation becomes superior. The functionally graded insulation has much more material on the hot side and that material continues to send heat to the structure after the external heating ends.

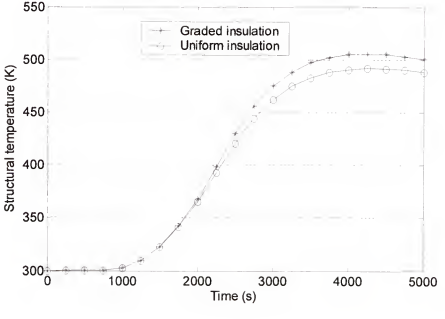

Figure 5-4 Structural temperature histories for graded insulation designed for steady-state conditions and uniform insulation of a given mass

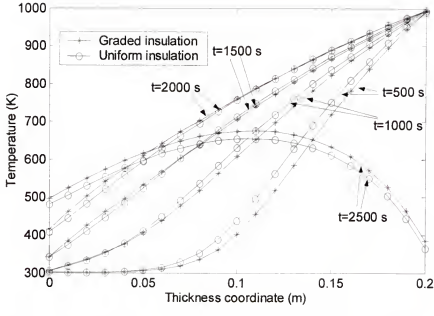

Figure 5-5 Temperature profiles in a graded insulation designed for steady-state conditions and a uniform insulation of same mass at different times

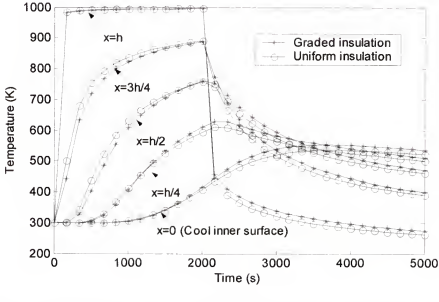

Figure 5-6 Temperature histories of a graded insulation designed for the steady-state conditions and a uniform insulation of equal mass at different locations

Two-layer Design with Transient Analysis

Our ultimate goal is to design a functionally graded insulation for a given critical condition at the chosen point. However, we first solve the simpler problem, insulation with two uniform layers, to gain understanding of the effects of using functionally graded insulations. We consider an insulation panel with fixed thickness h=0.2 m and fixed areal mass density m_p=22.15 kg/m^2 (4.54 lb/ft^2), which is slightly higher than the mass used in the previous section. The mass is chosen such that the average solidity of insulation is 0.025. As before, the mass of the structure is m_s=6.1 kg/m^2 (1.25 lb/ft^2). The foam insulation is made of two uniform layers, layer-1 (cool side) and layer-2 (hot side), with thickness and solidity h_1, ρ_1, h_2, ρ_2, respectively.

The division of mass and thickness between the two layers is optimized numerically for minimizing the maximum temperature of the structure. We add the constraints that the solidities $\rho_1$and ρ_2 should be between 0.01 and 0.11. The problem is formulated as:

$$\underset{h_1,\rho_1}{Minimize}\left\{\max_t\left[T_{str}\left(h_1,\rho_1,t\right)\right]\right\}$$

such that

$$\begin{aligned} & h_1\rho_1 + h_2\rho_2 = m_p \Big/ \rho_{Ti} \\ & 0.01 \le h_1 \le 0.19 \\ & 0.01 \le h_2 \le 0.19 \\ & 0.01 \le \rho_1 \le 0.11 \\ & 0.01 \le \rho_2 \le 0.11 \end{aligned} \qquad (5\text{-}10)$$

where T_{str} is the temperature of structure and ρ_{Ti} is the density of titanium (4431.8 kg/m^3). We use the Matlab™ function (*fmincon*) for constrained nonlinear optimization to solve the optimization problem. A Sequential Quadratic Programming (SQP) method is used in

this function. The optimization search starts from a uniform design, which has ρ_1= ρ_2=0.025 and h_1=h_2=$h/2$. Surprisingly, for the present transient problem the optimum cooler inner layer had high solidity, while the hotter outer layer had low solidity, which is the opposite of what we would expect on the basis of conductivity. In order to clarify the results we also analyzed an extreme design, which had the minimum allowable solidity in the outer layer (0.01), the maximum allowable solidity (0.11) in the inner layer, and a uniform design, which had uniform solidity (0.025) through the whole insulation. These three designs are compared in Table 5-1.

Table 5-1 Two-layer designs for minimizing the maximum temperature of structure under transient conditions

	Optimal Two-layer design	Extreme Two-layer design	Uniform design
Cool side h_1 (m)	0.0162	0.0300	N.A.
Cool side solidity ρ_1	0.1100	0.1100	0.0250
Hot side h_2 (m)	0.1838	0.1700	N.A.
Hot side solidity ρ_2	0.0175	0.0100	0.0250
T_{str}^{max} (K)*	471.1	498.8	488.6
Time at which T_{str}^{max} is reached (s)	4203.7	3115.0	4572.0

* T_{str}^{max} is the maximum temperature of structure.

Figure 5-7 shows the temperature history of the structure for these three designs. It can be seen that with uniform insulation the structure heats up more slowly, but it continues to heat much longer. For the extreme design the structure heats up fast, but peaks much earlier than the two other designs.

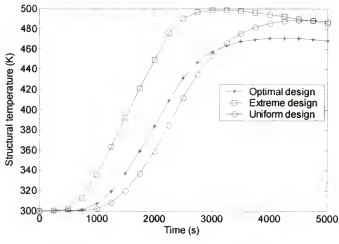

Figure 5-7 Structural temperature history for various two-layer designs

Close inspection of the history of heat absorbed by the various insulations explains the behavior. Figure 5-8 shows that during the heating period the uniform design absorbs more heat, but it also loses more heat during the cooling period. Figure 5-9 shows that in terms of total heat captured from the outside, the uniform design exceeds than the optimum design through out the entire history, even though the difference lessens during the cooling period.

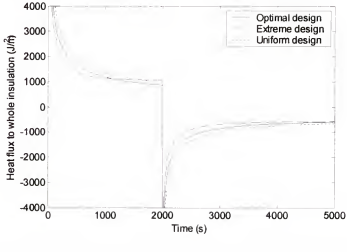

Figure 5-8 History of heat flux to insulation in various two-layer designs

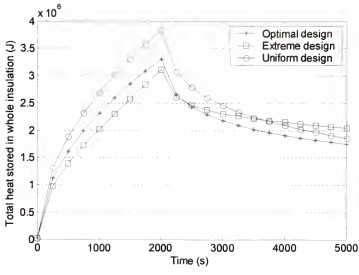

Figure 5-9 History of heat stored in the whole insulation in the two-layer designs

As can be seen from these figures, it is useful to deal separately with the heating period and the cooling period of the outer surface. During the heating period, the optimum and extreme designs with low thermal mass on the outside can heat up more rapidly, as shown in Figure 5-10, and radiate out more heat than the uniform design. The extreme design rejects heat more efficiently than the other two designs, and it lets in only 2.73% of the applied heat. The optimum design lets in only 2.91% of the applied heat, while the uniform design allows in 3.37%. Figure 5-10 shows that the extreme design outer surface heats up more rapidly than the optimum design, however the optimum design eventually surpasses it. This is because the high conductivity of the low-solidity hot outer layer of the extreme design allows more of the heat to flow through the insulation instead of being stored in its outer layer. Even though the optimum and extreme insulations can reduce the heat absorbed by the whole insulation, they conduct more heat to structure during the heating period. One reason is that their outer layers have higher conductivity, as shown in Figure 5-11, and low solidity, which does not allow

them to absorb much heat, and hence facilitates the heat flow to structure. The structural temperatures of the optimal and extreme design are 65 K and 90 K higher respectively than the uniform design at 2000 seconds, as shown in Figure 5-7.

While during the cooling period the uniform insulation allows more heat to escape out than the optimal design, the difference is small, as shown in Figure 5-8. The extreme design, on the other hand, has low conductivity in the outer layer, once that layer cools. Thus it is more difficult for it to let out the heat stored in the inner layer (Figure 5-8).

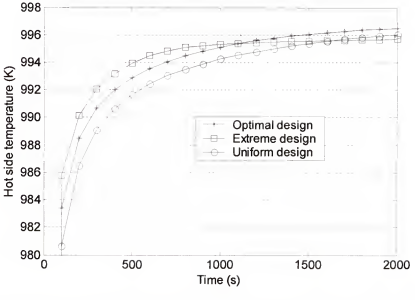

Figure 5-10 History of hot side temperatures in various two-layer designs during the heating phase

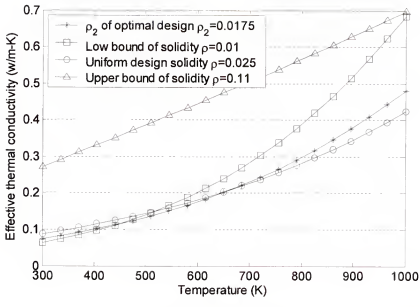

Figure 5-11 Effective conductivity of foam as a function of temperature for different designs

Finally we check the benefits of refining the design by increasing the number of layers to three. The total mass and total thickness remains fixed. The results for the optimal three-layer design are given in Table 5-2. It can be seen form Table 5-2 that the difference in maximum structural temperature is less than 1 K. So we can conclude that the optimal two-layer design can lower the maximum structure temperature by about 17 K compared to the uniform design, while optimal three-layer design can only achieve marginal improvement compared with the two-layer design which indicates that the optimal two-layer design captures most of the benefits of using a functionally graded foam insulation. The possible reason is that the outer layer is less important than inner layer as far as structural temperature is concerned. It should be noted that all of above calculation is based on model with 21 nodes, and there is about 1 K difference of structure temperature between 41- node model and 21-node model for the same design.

Based on the above reasoning, we can simplify our optimization problem to a two layer optimization problem with a little error in structure temperature but much simplification in calculation.

Table 5-2 Comparison between optimal three-layer design and two-layer design for minimizing maximum structural temperature

	Two-layer design	Three-layer design
Cool layer h_1 (m)	0.0162	0.0166
Cool layer ρ_1	0.1100	0.1100
Middle layer h_2 (m)	N.A.	0.0260
Middle layer ρ_2	N.A.	0.0141
Hot layer h_3 (m)	0.1838	0.1574
Hot layer ρ_3	0.0175	0.0178
T_{str}^{max} (K)*	471.1	470.8

* T_{str}^{max} is the maximum temperature of structure.

Optimal Two-layer Design to Minimize the Maximum Structural Temperature with Thickness Penalty

The lightweight TPS may not necessarily result in the lightest weight vehicle. A thinner but heavier TPS may results in a vehicle that is smaller and lighter because it requires less volume to contain the required fuel. A smaller vehicle has less surface area and less aerodynamic drag and therefore requires less fuel to accelerate to orbit. So there is a penalty for using thicker TPS.

Without Thickness Penalty

First, we will not consider the weight penalty from increasing thickness. So, the problem of mass optimization for given maximum structure temperature is formulated as minimize the mass of two flexible layer insulation which prevent the inner structure reach its temperature limits. To satisfy the maximum structure temperature limit is not trivial in this optimization problem. So we use our previous results to calculate the best design which minimizes the maximum structure temperature for a given mass and thickness. Repeating the previous procedure for a set of mass and thickness combinations we can find the optimal thickness and density combination. In our study the insulation thickness varies from 0.1 m to 0.3 m and insulation volume varies from 0.0025 m^3 to 0.0075 m^3. The lower and upper bounds of solidity for each layer are, respectively, 0.01 and 0.11. The lower and upper bound of thickness of each layer are 0.01m and 0.3 m, respectively. Sequential Quadratic Programming (SQP) is used in our calculation and model with 21 nodes is used in current calculation. The results are shown in Figure 5-12. Figure 5-13 indicates that for a given mass, increasing the total thickness of insulation can lower the maximum structure temperature. Checking the density of inner layer, we found that for most design their inner layer density is 0.11 or slightly lower than 0.11. For designs with same thickness, when we decrease the total mass of insulation, the thickness of inner layer decreases too, until it reaches its lower limit.

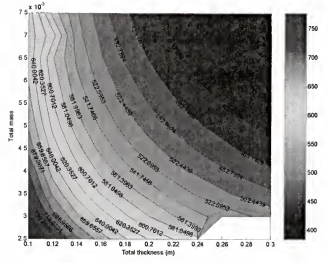

Figure 5-12 Maximum structure temperature contours for optimal design

Maximum structure temperature contour for uniform design is plotted in Figure 5-13. Comparing Figure 5-13 with Figure 5-12, we can find that when the average density of insulation is much higher than minimum density, i.e. 0.01, our optimal design can lower maximum structure temperature much. We found that for a given maximum structure temperature limits, if we want to minimize the mass of insulation, we should always choose uniform design with minimum allowable density.

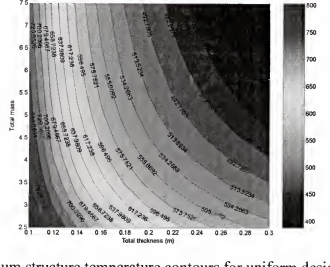

Figure 5-13 Maximum structure temperature contours for uniform design

Effect of Thickness Penalty

Now we will take penalty for a thicker insulation into account. Geometry of liquid oxygen (LOX) and liquid hydrogen (LH2) tank of X-33 is used in our current study. X-33 has a dual-lobe LOX tank and two quad-lobe LH2 tank (Dorsey *et al.*, 1999). We assume whole LOX tank is covered by TPS and LH2 tank 61% covered. The surface area of LOX and LH2 tank is approximated to 3000 ft^2 and 6,146 ft^2 respectively. So the total surface area covered by TPS is 10,498 ft^2. The penalty is assumed that 6,000 lb weight increase for one inch increase of insulation thickness. Now we can find the areal penalty is 0.5715 lb/ft^2, *i.e.* 2.793 kg/m^2 for one-inch thickness increase. The optimization problem is formulated as:

$$\begin{aligned} \underset{t}{\text{Minimize}} \quad & f = W_{insulation}(h_1, \rho_1) - 2.793(h - h_{base}) \\ \text{S. T.} \quad & \\ & 0.01 \le \rho_1 \le 0.11 \\ & 0.01 \le \rho_2 \le 0.11 \\ & T_{max\_structure} = 450K \end{aligned} \tag{5-10}$$

We choose our baseline design as 0.2 m thick insulation with areal density 22.14 kg/m^2 (4.53 lb/ft^2, 0.005 m^3 in volume). Repeating previous work for a set of mass and thickness combinations we can find the different thickness and density combination for given maximum structure temperature limit. It should be noted that a hot surface structural mass is added to our model. It is super alloy sandwich panel made of Inconel 617 with thickness 0.253 inch. The C_p of Inconel 617 is 0.1 $Btu/lb/^oR$. The thermal mass of hot surface structure is lumped to the outer surface node. In our study the total

thickness varies from 0.2 m to 0.3 m and density varies from 5.12 b/ft^2 to 7.16 lb/ft^2 (25 kg/m^2 to 35 kg/m^2). The results are shown in Figure 5-14. It indicates that for a given temperature limits, we can find a critical thickness, which minimize the weight of insulation with penalty. It can be noted that for a 450 K temperature limit, the optimal thickness of the insulation is about 9.5 inch and the minimum density is about 6.1 lb/ft^2. The cases when we neglect the gas conduction component in total effective conductivity are also studied to account for the rare air in the reentry of vehicle. The results are shown in Figure 5-15. It can be seen that there is about 20 K drop for structure temperature if we neglect gas conduction.

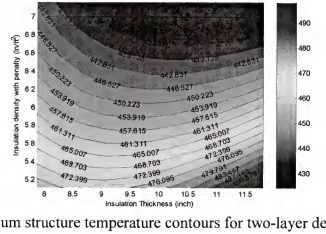

Figure 5-14 Maximum structure temperature contours for two-layer design

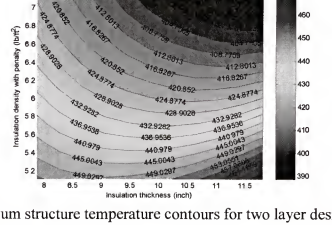

Figure 5-15 Maximum structure temperature contours for two layer design (without gas conduction)

In this chapter the problem of minimizing maximum structure temperature of a functionally graded metal foam insulation under transient heat conduction is studied. The performance of functionally graded insulation designed for steady state conditions is compared with uniform density insulation. It indicates that the optimal volume fraction profile we obtained under steady state conditions is not optimum for the transient case. The maximum structure temperature of two-layer insulation with constant density for each layer is minimized by varying the solidity profile for a given thickness and mass. It is shown that the cooler inner layer has high density, while the hotter outer layer has low density, which is the reverse of the optimum design for steady state condition. We also consider the penalty for insulation thickness. For a given maximum structure temperature limits, we should always choose uniform design with minimum allowable density to minimize the mass of insulation if insulation thickness penalty is neglected. While with insulation thickness penalty, we can find a critical thickness, which minimize the weight of insulation. But it does not change the nature of design, i.e. hot layer with low solidity and cool layer with high solidity.

CHAPTER 6
RESPONSE OF FUNCTIONALLY GRADED METALLIC FOAMS TO MECHANICAL LOADS

As the use of metallic foams increases, new methodologies have to be developed to characterize the foams, and also to design and analyze structural components made of these materials. The methods should be such that they can be incorporated into available methods with least amount of modifications, if any. One of such problem is that of response of metal foams to thermo-mechanical loads. Although foams are highly heterogeneous, it will be useful to idealize them as continua wherein the properties change smoothly with respect to the spatial coordinates. This will enable solutions to some fundamental solid mechanics problems, and also will help in developing finite element models of the structures made of foams.

Analysis of Functionally Graded Beams

In a series of papers Sankar and his coworkers (Sankar, 2001; Sankar and Tzeng, 2002; Venkataraman and Sankar, 2001; Apetre *et al.*, 2002) reported analytical methods for the thermal-mechanical and contact analysis of functionally graded beams and also sandwich beams with functionally graded cores.

In their studies the thermo-mechanical properties of the FGM were assumed to vary through the thickness in an exponential fashion, e.g., $E(z)=E_0e^{\lambda z}$. The material was assumed to be isotropic at every point and the Poisson's ratio was assumed to be constant

everywhere. This assumption enabled them to obtain analytical solutions using Fourier transform methods. However, in practice the properties of FGM will vary in an arbitrary fashion and the aforementioned solution technique may not be useful. In the present study we assume that the property variation through the thickness can be expressed in the form of a polynomial in the z coordinate. Then we demonstrate the application of both Fourier transform and Galerkin methods in order to obtain an approximate solution for displacements and stresses in a functionally graded beam. The solutions are compared with available exact solutions and the agreement is found to be very good.

Analysis

Consider a functionally graded beam of height h and length L as shown in Figure 6-1. The beam and the loading are symmetric about the centerline $x=L/2$. The beam is assumed to be in a state of plane strain normal to the x-z plane.

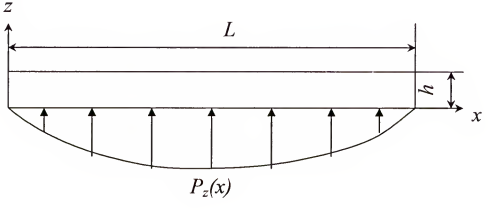

Figure 6-1 A FGM beam subjected to symmetric transverse loading.

The lower surface of the beam is subjected to normal traction such that

$$\sigma_{zz}(x,0) = -p_z(x) = -p_n \sin\xi x \tag{6-1}$$

where $\xi = n\pi / L$, $n = 1, 3, 5$. Since n is odd, the load is also symmetric about the centerline. The boundary conditions are similar to that of a simply supported beam, but the actual boundary conditions will become clear later.

We assume that the FGM is isotropic at every point and the Poisson's ratio ν is a constant through the thickness. The variation of Young's modulus E in the thickness direction is given by a polynomial in z as:

$$E(z) = E_0\left(a_1 + a_2\left(\frac{z}{h}\right) + a_3\left(\frac{z}{h}\right)^2 + a_4\left(\frac{z}{h}\right)^3\right) \tag{6-2}$$

where E_0 is the Young's modulus at z=0, and a_1, a_2, a_3 and a_4 are material constants.

The differential equations of equilibrium are:

$$\begin{aligned} \frac{\partial \sigma_{xx}}{\partial x} + \frac{\partial \tau_{xz}}{\partial z} &= 0 \\ \frac{\partial \tau_{xz}}{\partial x} + \frac{\partial \sigma_{zz}}{\partial z} &= 0 \end{aligned} \tag{6-3}$$

Assuming that the principal material directions coincide with the x and z axes, the constitutive equations are:

$$\begin{Bmatrix} \sigma_{xx} \\ \sigma_{zz} \\ \tau_{xz} \end{Bmatrix} = \begin{bmatrix} c_{11} & c_{13} & 0 \\ c_{13} & c_{33} & 0 \\ 0 & 0 & c_{55} \end{bmatrix} \begin{Bmatrix} \varepsilon_{xx} \\ \varepsilon_{zz} \\ \gamma_{xz} \end{Bmatrix} \tag{6-4}$$

or

$$\sigma = C\varepsilon$$

The elasticity matrix $[C]$ is related to material constants by:

$$C = \frac{E}{(1+\nu)(1-2\nu)} \begin{pmatrix} 1-\nu & \nu & 0 \\ \nu & 1-\nu & 0 \\ 0 & 0 & \frac{1-2\nu}{2} \end{pmatrix} \tag{6-5}$$

We assume the solution for displacements as:

$$\begin{aligned} u(x,z) &= U(z)\cos\xi x \\ w(x,z) &= W(z)\sin\xi x \end{aligned} \tag{6-6}$$

Substituting Equation (6-6) into (6-4), we obtain,

$$\begin{pmatrix} \sigma_{xx} \\ \sigma_{zz} \\ \tau_{xz} \end{pmatrix} = \begin{pmatrix} c_{11} & c_{13} & 0 \\ c_{13} & c_{33} & 0 \\ 0 & 0 & G \end{pmatrix} \begin{pmatrix} -\xi U \sin\xi x \\ W' \sin\xi x \\ U' + \xi W \cos\xi x \end{pmatrix} \tag{6-7}$$

the prime (′) after a variable denotes differentiation with respect to z. From Equations (6-6) and (6-7), one can note that the boundary conditions of the beam at $x=0$ and $x=L$ are $w(0,z)=w(L,z)=0$ and $\sigma_{xx}(0,z) = \sigma_{xx}(L,z) = 0$, which corresponds to simply support conditions in the context of beam theory. Equation (6-7) can be rewritten as:

$$\begin{aligned} \begin{pmatrix} \sigma_{xx} \\ \sigma_{zz} \end{pmatrix} &= \begin{pmatrix} S_x \\ S_z \end{pmatrix} \sin\xi x \\ \tau_{xz} &= T_z \cos\xi x \end{aligned} \tag{6-8}$$

where

$$\begin{aligned} \begin{pmatrix} S_x \\ S_z \end{pmatrix} &= \begin{pmatrix} c_{11} & c_{13} \\ c_{13} & c_{33} \end{pmatrix} \begin{pmatrix} -\xi U \\ W' \end{pmatrix} \\ T_z &= G(U' + \xi W) \end{aligned} \tag{6-9}$$

Substituting for $\sigma_{xx}, \sigma_{zz}, \tau_{xz}$ from Equation (6-7) into equilibrium Equation (6-3), we obtain a set of ordinary differential equations in $U(z)$ and $W(z)$:

$$\begin{aligned} \xi S_x + T_z' &= 0 \\ S_z' - T_z \xi &= 0 \end{aligned} \tag{6-10}$$

In order to solve Equation (6-10) we employ the Galerkin method. We assume solutions of the form:

$$\begin{aligned} U(z) &= c_1\phi_1(z) + c_2\phi_2(z) + c_3\phi_3(z) + c_4\phi_4(z) \\ W(z) &= b_1\phi_1(z) + b_2\phi_2(z) + b_3\phi_3(z) + b_4\phi_4(z) \end{aligned} \tag{6-11}$$

where ϕ_is are basis functions, and b_is and c_is are coefficients to be determined. For simplicity we choose 1, z, z^2, z^3 as basis functions. That is,

$$\phi_1(z) = 1; \qquad \phi_2(z) = z; \quad \phi_3(z) = z^2; \qquad \phi_4(z) = z^3 \tag{6-12}$$

Substituting the approximate solution in the governing differential equations, we obtain the residuals. Equating their weighted averages to zero minimizes the residuals:

$$\begin{aligned} \int_0^h \left(\xi S_x + T_z'\right)\phi_i(z)dz = 0, \qquad i = 1,4 \\ \int_0^h \left(S_z' - T_z\xi\right)\phi_i(z)dz = 0, \qquad i = 1,4 \end{aligned} \tag{6-13}$$

Using integration by parts we can rewrite Equation (6-13) as:

$$\begin{aligned} \int_0^h \phi_i \xi S_x dz + T_z(h)\phi_i(h) - T_z(0)\phi_i(0) - \int_0^h T_z \phi_i' dz = 0 \qquad i = 1,4 \\ \int_0^h S_z \phi_i' dz + \int_0^h T_z \xi \phi_i dz - \left(S_z(h)\phi_i(h) - S_z(0)\phi_i(0)\right) = 0 \qquad i = 1,4 \end{aligned} \tag{6-14}$$

Substituting for $S_x(z)$, $S_z(z)$ and $T_z(z)$ from Equation (6-9) into (6-14) and using the approximate solution for $U(z)$ and $W(z)$ in Equation (6-11) we obtain:

$$\begin{pmatrix} K_{ij}^{(1)} & K_{ij}^{(2)} \\ K_{ij}^{(3)} & K_{ij}^{(4)} \end{pmatrix} \begin{pmatrix} b \\ c \end{pmatrix} = \begin{pmatrix} f_i^{(1)} \\ f_i^{(2)} \end{pmatrix} \tag{6-15}$$

where,

$$
\begin{aligned}
K_{ij}^{(1)} &= \xi \int_0^h c_{13}\phi_i\phi_j' dz - \xi \int_0^h G\phi_i'\phi_j dz \\
K_{ij}^{(2)} &= -\int_0^h G\phi_i'\phi_j' dz - \xi^2 \int_0^h c_{11}\phi_i\phi_j dz \\
K_{ij}^{(3)} &= -\xi^2 \int_0^h G\phi_i\phi_j dz - \int_0^h c_{33}\phi_i'\phi_j' dz \\
K_{ij}^{(4)} &= \xi \int_0^h c_{13}\phi_i'\phi_j dz - \xi \int_0^h G\phi_i\phi_j' dz \\
f_i^{(1)} &= \phi_i(0)T_z(0) - \phi_i(h)T_z(h) \\
f_i^{(2)} &= \phi_i(0)S_z(0) - \phi_i(h)S_z(h)
\end{aligned}
\tag{6-16}
$$

$$
\begin{pmatrix} b \\ c \end{pmatrix}^T = (b_1 \quad b_2 \quad b_3 \quad b_4 \quad c_1 \quad c_2 \quad c_3 \quad c_4)
$$

Traction boundary conditions on the top and bottom surfaces of beam are:

$$
\begin{aligned}
&\tau_{xz}(x,0) = 0 \\
&\tau_{xz}(x,h) = 0 \\
&\sigma_{zz}(x,0) = -p_n \sin \xi x \\
&\sigma_{zz}(x,h) = 0
\end{aligned}
\tag{6-17}
$$

In terms of S_z and T_z, the boundary conditions take the form,

$$
\begin{aligned}
&T_z(0) = T_z(h) = 0 \\
&S_z(0) = -p_n \\
&S_z(h) = 0
\end{aligned}
\tag{6-18}
$$

Equation (6-18) can be used to evaluate $f_i^{(1)}$ and $f_i^{(2)}$ in Equation (6-16) which are the right hand side of Equation (6-15). Solving Equation (6-15), we obtain the solutions for the coefficients b_i and c_i, which yield the approximate solutions for $U(z)$ and $W(z)$ in Equation (6-11). Once $U(z)$ and $W(z)$ are determined, stress at any point can be computed using Equations (6-8) and (6-9).

Results and Discussion

In order to verify the present method, examples from Sankar (2001) are used. In these examples the variation of Young's modulus is assumed to be of the form $E = E_0 e^{4z/h}$. The same variaton can be approximated by the polynomial form given in Equation (6-2). The coefficients of the polynomial, a_1, a_2, a_3 and a_4 were determined by using the least squares curve fitting. Two types of beams were considered, and the varitaion of Young's modulus in these beams are given by $E_h / E_0 = 10$ and $E_h / E_0 = 0.1$, respectively. In the first beam the load is applied on the softer face of the beam and in the second on the harder side. In both cases E_0 was taken as 1 GPa and ν=0.25. The thickness of the beam is h=10 mm. The coeffiecients of the cubic polynomial for $E(z)$ are given in Table 6-1.

Table 6-1 The coefficients of the cubic polynomial for $E(z)$. E_0=10 GPa and beam thickness h=10 mm

E_h/E_0	a_1	a_2	a_3	a_4
10	1	2.9577	-0.7889	6.7982
0.1	1	-2.1845	1.9844	-0.6996

The results for the normalized bending stress for various values of $\xi h = n\pi/L$ are presented in Figures 6-2 and 6-3. It should be noted that smaller values of ξh represent slender beams or beams subjected to more uniformly distributed loads, whereas larger values of ξh indicate short stubby beams or beams subjected to concentrated loads. From Figures 6-2 and 6-3, it can be noted that the results of the Galerkin method agree well

with the exact solution (Sankar, 2001). The normalized stresses are less than unity when the loads are applied to the softer face (Figure 6-2, $E_h / E_0 = 10$). On the other hand the normalized stresses are much greater than unity when the loads are applied to the harder face (Figure 6-3, $E_h / E_0 = 0.1$). One can also note the approximate location of the neutral axis for the two beams in these figures.

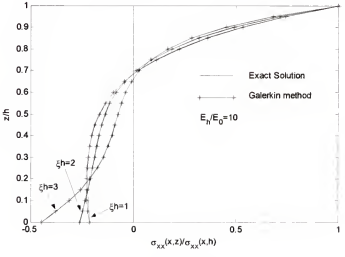

Figure 6-2 Normalized axial stress σ_{xx} through the thickness of FGM beam ($E_h=10E_0$)

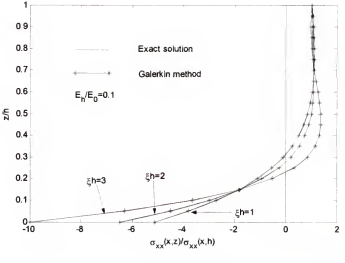

Figure 6-3 Normalized axial stress σ_{xx} through the thickness of FGM beam ($E_h=0.1E_0$)

The transverse shear stresses are plotted in Figures 6-4 and 6-5. The approximate solution deviates from the exact solution, but still within engineering accuracy. The shear stresses attain the maximum value at the neutral axis. The normalized maximum shear stress values are above the conventional 1.5, when the loads are applied on the harder surface of the beam (Figure 6-5), but fall below 1.5, in some cases when the loads are applied to the soft side (Figure 6-4).

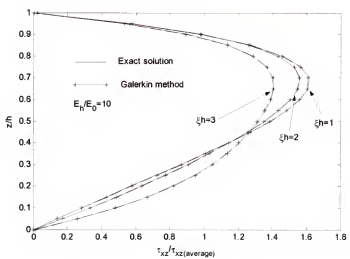

Figure 6-4 Transverse shear stresses through the thickness of FGM beam ($E_h=10E_0$)

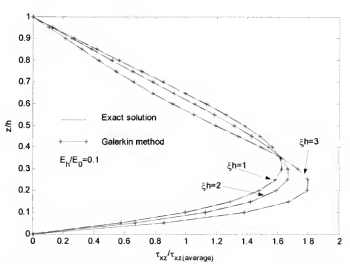

Figure 6-5 Transverse shear stresses through the thickness of FGM beam ($E_h=0.1E_0$)

In this chapter we developed a combined Fourier series-Galerkin method for the analysis of functionally graded 1-D plate. The present analysis agrees very well with the exact solution and can be applied to functionally graded structures with arbitrary variation of properties and also can be extended to plate like structures and sandwich construction wherein the core material and or the face sheets are functionally graded, as discussed in detail in next chapter.

CHAPTER 7
ANALYSIS OF SANDWICH TPS PANELS WITH FOAM CORE UNDER THERMAL LOAD

In this chapter, we develop a thermal-structural analysis of a sandwich TPS panel subjected to transient heat conduction during reentry. The material properties such as Young's modulus, yield strength, thermal conductivity and coefficient of thermal expansion are assumed to be temperature dependent. Hence approximate methods such as finite difference method for heat conduction and Galerkin method for structural analysis have to be used. The sandwich panel is divided into four elements (two face sheets and two core layers with different solidities). The solution for strains and stresses in the entire sandwich panel is obtained by enforcing the compatibility of tractions and displacements at the interfaces between each element. The Fourier series method is used to reduce the partial differential equations to a pair of ordinary differential equations, which are solved using the Galerkin method. For the purpose of comparison, the panel is also analyzed by one dimensional plate theory.

First we identify the necessary information and modeling details required to perform structural analysis of the TPS insulation. The heat transfer in the TPS is assumed to be one-dimensional. The finite width effects of the TPS insulation and the heat shorts resulting from the support structure around the perimeter of the TPS tile are ignored. The structural mass on the inside will correspond to the mass of the stiffened panel shell used

for the RLV tank construction. The insulation itself is made of a titanium open cell foam material.

The heat transfer in foams proceeds by three modes: conduction through the solid materials, conduction in the gas filling this foam and radiation inside the foam. The model used to calculate the heat transfer coefficient in the foam is discussed in Chapter 3. To minimize radiation, higher density foams (smaller foam pore sizes) are required while to minimize conduction we need low-density foams (large foam pore sizes). Since there is a temperature gradient through the insulation, an optimum insulation requires different densities in different regions. Optimum density profiles of metallic foam insulations that minimize heat transmitted to the inside under transient steady-state heat transfer conditions are presented in Venkataraman *et al.* (2001).

Figure 7-1 shows a schematic of the simplified sandwich TPS panel. The length of the panel is 0.4572 m (18 inch). The top face sheet is made of homogeneous titanium plate with thickness 0.5 mm. The foam core is divided into two layers with total thickness 90 mm (3.54 inch). The solidity in each layer of foam core can vary continuously. The foam is idealized as having rectangular cells of uniform size. The variation in solidity is achieved by tailoring the cell size while keeping the strut diameter (d_s) fixed at 0.05 mm (0.002 inch). The structural mass on the inside will correspond to the mass of the stiffened panel shell used for the RLV tank construction (Blosser, 2000) which is made of aluminum with thickness 2.2 mm (about 0.0866 inch). The areal density of the structure is 6.1 kg/m^2 (1.25 lb/ft^2). The temperature dependent material properties of titanium and aluminum are shown in Appendix A.

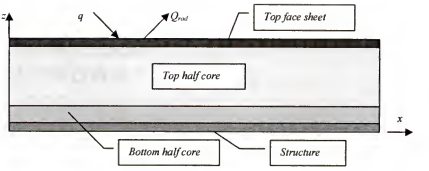

Figure 7-1 Schematic of the heat transfer in the insulation on a RLV structure

Structural Analysis of the TPS Panel

The TPS panel is assumed to be simply supported and in a state of plane strain normal to the *z-x* plane (one dimensional plate). The governing equations are formulated for each layer. The solutions of strains and stresses of entire sandwich are obtained by enforcing the compatibility displacements and continuity of tractions at the interface, which is analogous to assembling element stiffness matrices in FEM analysis. We will derive the elasticity solution for a typical layer first.

Analysis of a Single Layer

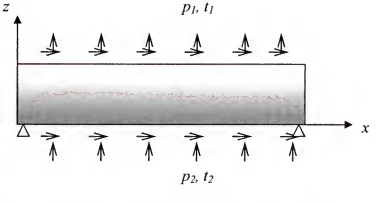

Figure 7-2 Functionally graded plate subjected to symmetric loading

Consider a functionally graded one-dimensional plate of height h and length L as shown in Figure 7-2. The boundary conditions at the two edges of the plate, x=0 and x=L, are similar to that of a simply supported plate. We assume that the Poisson's ratio v is a constant through the thickness. The variation of Young's modulus E in the thickness direction is given by a polynomial in z as:

$$E(z) = E_0\left(a_1 + a_2\left(\frac{z}{h}\right) + a_3\left(\frac{z}{h}\right)^2 + a_4\left(\frac{z}{h}\right)^3\right) \tag{7-1}$$

where E_0 is the Young's modulus at plane z=0 and a_i is constant.

There are normal and shear tractions applied on both top and bottom surfaces. The tractions are assumed to be symmetric about the centerline (x=L/2):

$$\begin{aligned} p_1 &= \sum_n P_{1n} \sin\xi_n x \\ t_1 &= \sum_n T_{1n} \cos\xi_n x \\ p_2 &= \sum_n P_{2n} \sin\xi_n x \\ t_2 &= \sum_n T_{2n} \cos\xi_n x \\ \xi_n &= \frac{n\pi}{L} \qquad n = 1,3,5\ldots \end{aligned} \tag{7-2}$$

The temperature distribution $\theta(x,z)$ at bottom surface is also assumed symmetric about the centerline (x=L/2). The temperature variation in the thickness direction follows same pattern for each x, which can be expressed in polynomial as:

$$\begin{aligned} \theta(x,z) &= \left[\sum_{n=1}^{\infty} T_n \sin\xi_n x\right] \cdot \left[\sum_{\lambda=1}^{\infty} d_\lambda z^{\lambda-1}\right] \\ \xi_n &= \frac{n\pi}{L} \qquad n = 1,3,5\ldots \qquad \lambda = 1,2,3\ldots \end{aligned} \tag{7-3}$$

We will solve the problem for one value of ξ_n. Let

$$\theta_{n\lambda}(x,z) = \sum_{\lambda=1}^{4} d_\lambda T_n z^{\lambda-1} \sin\xi_n x \tag{7-4}$$

Assume the displacements are in the form of:

$$\begin{aligned} u(x,z) &= U(z)\cos\xi_n x \\ w(x,z) &= W(z)\sin\xi_n x \end{aligned} \tag{7-5}$$

The strains are derived as:

$$\begin{aligned} \varepsilon_{xx} &= -U\xi_n \sin\xi_n x \\ \varepsilon_{zz} &= W'\sin\xi_n x \\ \gamma_{xz} &= (U'+W\xi_n)\cos\xi_n x \end{aligned} \tag{7-6}$$

Assuming that the principal material directions coincide with the x and z axes, the constitutive equations are:

$$\begin{Bmatrix} \sigma_{xx} \\ \sigma_{zz} \\ \tau_{xz} \end{Bmatrix} = \begin{bmatrix} c_{11} & c_{13} & 0 \\ c_{13} & c_{33} & 0 \\ 0 & 0 & c_{55} \end{bmatrix} \left\{ \begin{bmatrix} \varepsilon_{xx} \\ \varepsilon_{zz} \\ \gamma_{xz} \end{bmatrix} - \theta(x,z) \begin{bmatrix} \alpha_x(z) \\ \alpha_z(z) \\ 0 \end{bmatrix} \right\} \tag{7-7}$$

where $[C]$ can be expressed as:

$$C^{-1} = \begin{pmatrix} \dfrac{1}{E_{11}} & \dfrac{-\nu_{13}}{E_{11}} & 0 \\ \dfrac{-\nu_{13}}{E_{11}} & \dfrac{1}{E_{33}} & 0 \\ 0 & 0 & \dfrac{1}{G_{13}} \end{pmatrix} \tag{7-8}$$

Equation (7-6) can be rewriten as:

$$\begin{Bmatrix} \sigma_{xx} \\ \sigma_{zz} \\ \tau_{xz} \end{Bmatrix} = \begin{bmatrix} c_{11} & c_{13} & 0 \\ c_{13} & c_{33} & 0 \\ 0 & 0 & c_{55} \end{bmatrix} \begin{bmatrix} \varepsilon_{xx} \\ \varepsilon_{zz} \\ \gamma_{xz} \end{bmatrix} - \begin{bmatrix} \beta_x(z) \\ \beta_z(z) \\ 0 \end{bmatrix} \cdot \sum_{\lambda=1}^{4} d_\lambda T_n z^{\lambda-1} \sin\xi_n x \tag{7-9}$$

where the βs can be expressed as:

$$\begin{Bmatrix} \beta_x \\ \beta_z \\ 0 \end{Bmatrix} = \begin{bmatrix} c_{11} & c_{13} & 0 \\ c_{13} & c_{33} & 0 \\ 0 & 0 & c_{55} \end{bmatrix} \begin{bmatrix} \alpha_x(z) \\ \alpha_z(z) \\ 0 \end{bmatrix} \tag{7-10}$$

Substitute the Equation (7-6) into Eqation (7-9), we have,

$$\begin{aligned} \sigma_{xx} &= S_x(z)\sin\xi_n x \\ \sigma_{zz} &= S_z(z)\sin\xi_n x \\ \tau_{xz} &= T_z(Z)\cos\xi_n x \end{aligned} \tag{7-11}$$

where

$$\begin{aligned} S_x &= \left(-c_{11}U\xi_n + c_{13}W' - d_\lambda T_n z^{\lambda-1}\beta_x(z)\right) \\ S_z &= \left(-c_{13}U\xi_n + c_{33}W' - d_\lambda T_n z^{\lambda-1}\beta_z(z)\right) \\ T_z &= c_{55}\left(U' + W\xi_n\right) \end{aligned} \tag{7-12}$$

The governing equilibrium equations are (body forces are neglected):

$$\begin{aligned} \frac{\partial \sigma_{xx}}{\partial x} + \frac{\partial \tau_{xz}}{\partial z} &= 0 \\ \frac{\partial \tau_{xz}}{\partial x} + \frac{\partial \sigma_{zz}}{\partial z} &= 0 \end{aligned} \tag{7-13}$$

Substituting Equation (7-11) into Equation (7-13), we obtain,

$$\begin{aligned} \xi_n S_x(z) + T_z'(z) &= 0 \\ S_z'(z) - \xi_n T_z(z) &= 0 \end{aligned} \tag{7-14}$$

Equation (7-14) is solved by Galerkin method by assuming:

$$\begin{aligned} U(z) &= c_j \phi_j(z) \\ W(z) &= b_j \phi_j(z) \qquad j = 1,4 \end{aligned} \tag{7-15}$$

where,

$$\phi_1(z) = 1; \qquad \phi_2(z) = z; \quad \phi_3(z) = z^2; \qquad \phi_4(z) = z^3 \tag{7-16}$$

Substituting the approximate solution in the governing differential equations, we obtain the residuals. The residuals are minimized by equating their weighted averages to zero:

$$\begin{aligned}&\int_0^h\left(\xi_n S_x + T_z'\right)\phi_i(z)dz = 0, \qquad i = 1,4\\&\int_0^h\left(S_z' - T_z\xi_n\right)\phi_i(z)dz = 0, \qquad i = 1,4\end{aligned} \tag{7-17}$$

Using integration by parts we can rewrite Equation (7-17) as:

$$\begin{aligned}&\int_0^h \phi_i\xi_n S_x dz + T_z(h)\phi_i(h) - T_z(0)\phi_i(0) - \int_0^h T_z\phi_i' dz = 0 \qquad i = 1,4\\&\int_0^h S_z\phi_i' dz + \int_0^h T_z\xi_n\phi_i dz - \left(S_z(h)\phi_i(h) - S_z(0)\phi_i(0)\right) = 0 \qquad i = 1,4\end{aligned} \tag{7-18}$$

Substituting for $S_x(z)$, $S_z(z)$ and $T_z(z)$ from Equation (7-12) into Equation (7-18) and using the approximate solution for $U(z)$ and $W(z)$ in Equation (7-15) we obtain:

$$\begin{pmatrix} K_{ij}^{(1)} & K_{ij}^{(2)} \\ K_{ij}^{(3)} & K_{ij}^{(4)} \end{pmatrix}\begin{pmatrix} \bar{b} \\ \bar{c} \end{pmatrix} = \begin{pmatrix} f_i^{(1)} \\ f_i^{(2)} \end{pmatrix} \tag{7-19}$$

where,

$$\begin{aligned}K_{ij}^{(1)} &= \xi_n\int_0^h c_{13}\phi_i\phi_j' dz - \xi_n\int_0^h c_{55}\phi_i'\phi_j dz\\K_{ij}^{(2)} &= -\int_0^h c_{55}\phi_i'\phi_j' dz - \xi_n^2\int_0^h c_{11}\phi_i\phi_j dz\\K_{ij}^{(3)} &= -\xi_n^2\int_0^h c_{55}\phi_i\phi_j dz - \int_0^h c_{33}\phi_i'\phi_j' dz\\K_{ij}^{(4)} &= \xi_n\int_0^h c_{13}\phi_i'\phi_j dz - \xi_n\int_0^h c_{55}\phi_i\phi_j' dz\\f_i^{(1)} &= \phi_i(0)T_z(0) - \phi_i(h)T_z(h) + \sum_{\lambda=1}^{4}\xi_n d_\lambda T_n\int_0^h z^{\lambda-1}\beta_x(z)\phi_i dz\\f_i^{(2)} &= \phi_i(0)S_z(0) - \phi_i(h)S_z(h) - \sum_{\lambda=1}^{4} d_\lambda T_n\int_0^h z^{\lambda-1}\beta_z(z)\phi'_i dz\end{aligned} \tag{7-20}$$

$$D = \begin{pmatrix} \bar{b} \\ \bar{c} \end{pmatrix}^T = (b_1 \quad b_2 \quad b_3 \quad b_4 \quad c_1 \quad c_2 \quad c_3 \quad c_4) \tag{7-21}$$

The boundary conditions at both top and bottom surface are shown as following:

At top surface

$$\begin{aligned} t_1 &= T_1 \cos \xi_n x \\ p_1 &= P_1 \sin \xi_n x \end{aligned} \tag{7-22}$$

Hence we have

$$\begin{aligned} S_z(h) &= P_1 \\ T_z(h) &= T_1 \end{aligned} \tag{7-23}$$

At bottom surface

$$\begin{aligned} t_2 &= T_2 \cos \xi_n x \\ p_2 &= P_2 \sin \xi_n x \end{aligned} \tag{7-24}$$

which yields

$$\begin{aligned} S_z(0) &= -P_2 \\ T_z(0) &= -T_2 \end{aligned} \tag{7-25}$$

Substituting Equations (7-23) and (7-25) into Equation (7-20), $[f]$ in Equation (7-20) can be rewritten as:

$$\begin{bmatrix} f_1^{(1)} \\ f_2^{(1)} \\ f_3^{(1)} \\ f_4^{(1)} \\ f_1^{(2)} \\ f_2^{(2)} \\ f_3^{(2)} \\ f_4^{(2)} \end{bmatrix} = -\begin{bmatrix} \phi_1(h) & 0 & \phi_1(0) & 0 \\ \phi_2(h) & 0 & \phi_2(0) & 0 \\ \phi_3(h) & 0 & \phi_3(0) & 0 \\ \phi_4(h) & 0 & \phi_4(0) & 0 \\ 0 & \phi_1(h) & 0 & \phi_1(0) \\ 0 & \phi_2(h) & 0 & \phi_2(0) \\ 0 & \phi_3(h) & 0 & \phi_3(0) \\ 0 & \phi_4(h) & 0 & \phi_4(0) \end{bmatrix} \cdot \begin{bmatrix} T_1 \\ P_1 \\ T_2 \\ P_2 \end{bmatrix} + d_\lambda T_n \begin{bmatrix} \xi_n \int_0^h z^{\lambda-1} \beta_x(z) \phi_1 dz \\ \xi_n \int_0^h z^{\lambda-1} \beta_x(z) \phi_2 dz \\ \xi_n \int_0^h z^{\lambda-1} \beta_x(z) \phi_3 dz \\ \xi_n \int_0^h z^{\lambda-1} \beta_x(z) \phi_4 dz \\ -\int_0^h z^{\lambda-1} \beta_z(z) \phi_1' dz \\ -\int_0^h z^{\lambda-1} \beta_z(z) \phi_2' dz \\ -\int_0^h z^{\lambda-1} \beta_z(z) \phi_3' dz \\ -\int_0^h z^{\lambda-1} \beta_z(z) \phi_4' dz \end{bmatrix} \tag{7-26}$$

or,

$$f = \Phi P + M \tag{7-27}$$

Equation (7-15) can be expanded as:

$$\begin{bmatrix} U_1 \\ W_1 \\ U_2 \\ W_2 \end{bmatrix} = \begin{bmatrix} 0 & 0 & 0 & 0 & 1 & h & h^2 & h^3 \\ 1 & h & h^2 & h^3 & 0 & 0 & 0 & 0 \\ 0 & 0 & 0 & 0 & 1 & 0 & 0 & 0 \\ 1 & 0 & 0 & 0 & 0 & 0 & 0 & 0 \end{bmatrix} \begin{bmatrix} b_1 \\ b_2 \\ b_3 \\ b_4 \\ c_1 \\ c_2 \\ c_3 \\ c_4 \end{bmatrix} \tag{7-28}$$

or,

$$U = HD \tag{7-29}$$

Now we have three Equations (7-19), (7-27) and (7-29). From these three equations, we obtain,

$$U = HK^{-1}\left[\Phi P + M\right] = K^{*}P + M^{*} \tag{7-30}$$

or,

$$P = SU - R \tag{7-31}$$

where

$$\begin{aligned} S &= \left[K^{*}\right]^{-1} \\ R &= \left[K^{*}\right]^{-1} M^{*} \end{aligned} \tag{7-32}$$

Analysis of the Whole Panel

Assume tractions are in the form:

$$\begin{aligned} p_i &= P_i \sin \xi_n x \\ t_i &= T_i \cos \xi_n x \\ \xi_n &= \frac{n\pi}{L} \qquad i = 1,2,3,4,5 \quad L = 1,3,5\ldots \end{aligned} \tag{7-33}$$

For given temperature distribution in each layer:

$$P^{(i)} = S^{(i)}U^{(i)} - R^{(i)} \tag{7-34}$$

In order to satisfy equilibrium, the contribution of the different tractions at each interface should sum to zero. Enforcing the balance of force and displacement at the interface, we obtain the global stiffness matrix S_G:

$$S_G \cdot \begin{bmatrix} U_1 \\ W_1 \\ U_2 \\ W_2 \\ U_3 \\ W_3 \\ U_4 \\ W_4 \\ U_5 \\ W_5 \end{bmatrix} - \begin{bmatrix} R_1^{(1)} \\ R_2^{(1)} \\ R_3^{(1)} \\ R_4^{(1)} \\ 0 \\ 0 \\ 0 \\ 0 \\ 0 \\ 0 \end{bmatrix} - \begin{bmatrix} 0 \\ 0 \\ R_1^{(2)} \\ R_2^{(2)} \\ R_3^{(2)} \\ R_4^{(2)} \\ 0 \\ 0 \\ 0 \\ 0 \end{bmatrix} - \begin{bmatrix} 0 \\ 0 \\ 0 \\ 0 \\ R_1^{(3)} \\ R_2^{(3)} \\ R_3^{(3)} \\ R_4^{(3)} \\ 0 \\ 0 \end{bmatrix} - \begin{bmatrix} 0 \\ 0 \\ 0 \\ 0 \\ 0 \\ 0 \\ R_1^{(4)} \\ R_2^{(4)} \\ R_3^{(4)} \\ R_4^{(4)} \end{bmatrix} = \begin{bmatrix} T_1 \\ P_1 \\ 0 \\ 0 \\ 0 \\ 0 \\ 0 \\ 0 \\ T_5 \\ P_5 \end{bmatrix} \tag{7-35}$$

Solving the above Equation (7-35), we can obtain the displacement field for each layer. The displacement field and the constitutive equations can be used to obtain the stress field in each layer.

Sankar and Tzeng (2002) derived the one dimensional plate theory following the Euler-Bernoulli beam assumption. They also neglected the normal stress σ_{zz} in thickness direction We follow a similar procedure to derive a sandwich beam theory for the composite sandwich panel.

Numerical Results

The analysis procedures described in the preceding section was used to calculate the stresses in a TPS panel during the reentry of the vehicle. Based on our previous work of minimizing the maximum temperature of a structure in Chapter 5, we found that the cooler inner layer of the optimal two-layer design has high solidity, while the hotter outer layer has low solidity. So we vary the solidity of foam linearly from 0.11 at bottom to 0.01 at top surface. It should be noted that the elastic constants of metal foams depend on

the relative density. Choi (2002) derived an expression for the Young's modulus of a cellular solid as:

$$E_f = \frac{1}{3}\rho E_s \tag{7-36}$$

where ρ is the solidity and the subscripts f and s, refer to the homogenized foam and the strut material, respectively. In our study, the heat flux and pressure on the vehicle during reentry are obtained from Blosser (2002). The heat flux varies significantly over the surface. For our study we choose a location on the windward surface referred to as station 1199 (STA 1199) as a representative point for the point design. The heat flux and pressure histories for that location are reproduced in Appendix B.

The stress variations with respect to time at various locations of the TPS are presented in Figs. 7-3 through 7-6. It can be noted that both laminate and Galerkin solutions agree well with each other, which means laminate theory can provide relatively accurate results for slender beam (L/h=4.9). We also compared the two solutions for beam with length L=225 mm (9 *in.)* (L/h=2.46). The results are shown in Figures 7-7 through Figure 7-10. The maximum difference between theses two solutions for stresses in the structure is 18%, which suggests that the laminate theory may not be suitable for the analysis of thick TPS.

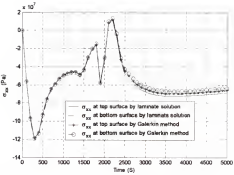

Figure 7-3 History of normal stress (σ_{xx}) distribution in top facesheet (L=18 *inch*)

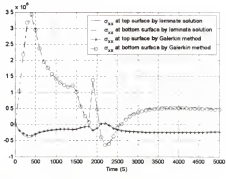

Figure 7-4 History of normal stress (σ_{xx}) distribution in top half core (L=18 *inch*)

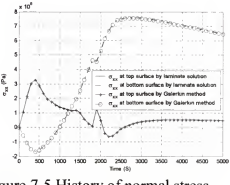

Figure 7-5 History of normal stress (σ_{xx}) distribution in bottom half core (L=18 *inch*)

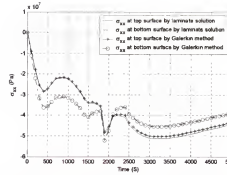

Figure 7-6 History of normal stress (σ_{xx}) distribution in structure (L=18 *inch*)

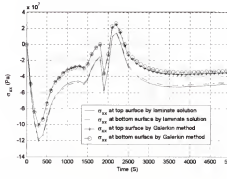

Figure 7-7 History of normal stress (σ_{xx}) distribution in top facesheet (L=9 *inch*)

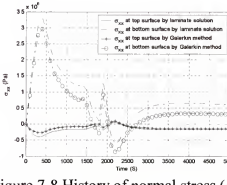

Figure 7-8 History of normal stress (σ_{xx}) distribution in top half core (L=9 *inch*)

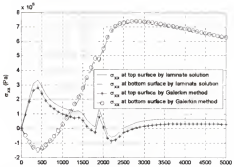

Figure 7-9 History of normal stress (σ_{xx}) distribution in bottom half core (L=9 *inch*)

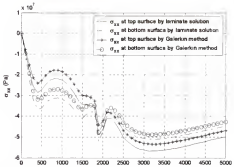

Figure 7-10 History of normal stress (σ_{xx}) distribution in structure (L=9 *inch*)

We also investigated the performance of functionally graded foam insulation for transient heat transfer condition by comparing it with the uniform solidity foam insulation. For the purpose of comparison, the problem of uniform foam with same weight is also solved. Figures 7-11 and 7-12 show the temperature histories at the top face sheet and structure, respectively. It is shown in Figure 7-12 that the maximum structural temperature can be reduced by 30 K by linearly varying the insulation foam solidity. This is achieved by increasing the top face sheet temperature faster for linear design compared with uniform design, as shown in Figure 7-11. The histories of stress ratio, which is defined as the ratio between the stresses in each layer and temperature-dependent yield stress, are also plotted for each layer in Figures 7-13 through 7-16. These four plots indicate that the maximum stress ratio in the base structure and foam core can be reduced 25% or more by linearly varying the foam solidity with only 5% increase in stress ratio in the top face sheet.

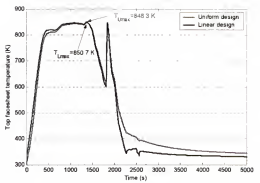

Figure 7-11 Temperature history at top facesheet for both linear and uniform designs

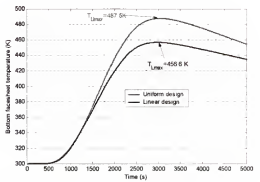

Figure 7-12 Structural temperature history for both linear and uniform designs

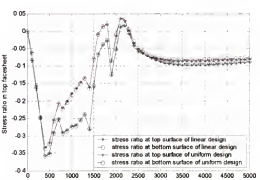

Figure 7-13 History of normal stress (σ_{xx}) distribution in top face sheet (L=18 *inch*)

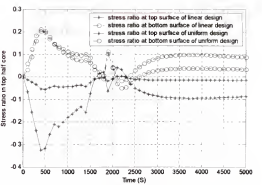

Figure 7-14 History of normal stress (σ_{xx}) distribution in top half core (L=18 *inch*)

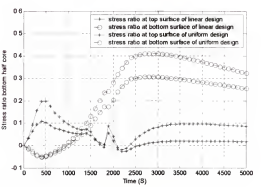

Figure 7-15 History of normal stress (σ_{xx}) distribution in bottom half core (L=18 *inch*)

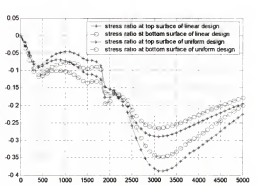

Figure 7-16 History of normal stress (σ_{xx}) distribution in structure (L=18 *inch*)

The analysis procedures developed in this paper will be useful in optimizing the multilayer TPS structure subjected to temperature and stress constraints. The results suggest that classical lamination theory may not be suitable for the analysis of thick TPS panels. More accurate plate theories, e.g., higher order theories or sandwich plate theories, need to be developed. One of the major issues in the TPS for RLV's is that the temperature attains the maximum after the vehicle has landed when the mechanical loads are minimum or almost do not exist. On the other hand during the beginning phase of the reentry the mechanical loads are high but the thermal loads are low. This situation offers an opportunity to optimize the TPS and minimize the mass.

Evaluation of Integrated Sandwich TPS Design with Metal Foam Core for Launch Vehicles

The objective of current work is to evaluate the performance of two kinds of TPS panel design, integrated sandwich TPS design and conventional Safill® TPS design.

Integrated Sandwich TPS Design and Safill Design

Two designs are shown in Figures 7-17 and 7-18, respectively. The square panel for each design is assumed to have a length of 457.2 mm (18 inch). The thickness of the top face sheet is fixed at 0.5 *mm*. The top face sheet of the integrated sandwich TPS baseline design is made of titanium. The foam core is made of titanium foam. For the convenience of analysis, the core is divided into two uniform sub-layers. The underlying structure is made of aluminum. The non-integrated design is a Safill™ TPS design, which uses fibrous Safill (density 3.0 lb/ft^3) as insulation. The Safill insulation is encapsulated by supporting structures, such as side foil, support bracket and outer

honeycomb sandwich. As a preliminary study, these supporting structures are neglected in our analysis. We want to investigate the performance of the two designs during launch and reentry of the RLVs. The temperature dependent material properties (Zhu and Sankar, 2004) are used in this study. The thermal and mechanical loads are extracted from a windward point 1199 of X-33 (Blosser, 2002) and are plotted in Figures 7-19 and Figure 7-21, respectively. Each design is optimized to minimize the total weight of the TPS panel, which includes the insulation, the underlying structure and/or the top facesheet. During the optimization, several side constrains are applied. For integrated design, the thickness of titanium foam sub-layer has a lower bound 5 *mm* and the solidity of titanium foam can vary only from 0.01 to 0.11. For both integrated sandwich and Safill design, the structure thickness has a lower bound 1.0 *mm*. Simply-supported boundary conditions are assumed for the square panel.

The material properties of foam are related to bulk material properties and solidity or volume fraction as in Choi (2002) and Ashby (2000):

$$
\begin{aligned}
E_{foam} &= \frac{1}{3}\rho E_s \\
G_{foam} &= \frac{1}{18}\rho^2 E_s \\
\sigma_{foam\_strength} &= 0.55\rho^{1.5}\sigma_s
\end{aligned}
\tag{7-37}
$$

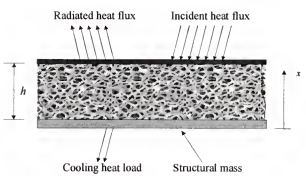

Figure 7-17 Schematic of integrated sandwich TPS

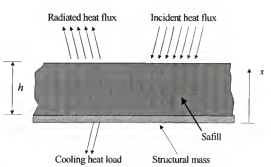

Figure 7-18 Schematic of Safill TPS

Minimum Weight Design during Reentry

The weight of sandwich TPS is minimized by varying the thickness and solidity of the two uniform foam core layers and/or the thickness of the structure. The constraint is that the maximum structure temperature cannot exceed 450 K. We also compare the integrated design with the Safill design, which insulates the structure to be below 450 K. Constant pressure (14.7 psi) is assumed in the calculation of thermal conductivity of Safill insulation. The design variables are insulation thickness, insulation solidity (for integrated sandwich design) and /or structure thickness for different cases we considered. The solidity of titanium foam is defined as the ratio between the foam density and density of the material from which the foam is made. Sometimes the solidity ρ is also referred to as the (solid) volume fraction in Chapter 3 and Chapter 4.

Optimum Design Considering Structural Temperature Constraint

In this case, the metallic foam insulation thickness is allowed to vary from 10 mm to 90 mm and the thickness of structure from 1 mm to 10 mm. Figure 7-19 shows the thermal load at point 1199, which is measured from the beginning of reentry phase. The lower and upper bound of integrated TPS design variables are as follows:

$$Minimize\{[W_{TPS}(h_2, \rho_2, h_3, \rho_3, h_4)]\}$$

such that

$$T_{str} \le 450K$$
$$h2 + h3 \le 90mm$$
$$5mm \le h_2 \le 85mm$$
$$0.01 \le \rho_2 \le 0.11$$
$$5mm \le h_3 \le 85mm$$
$$0.01 \le \rho_3 \le 0.11$$
$$1mm \le h_4 \le 10mm \qquad (7\text{-}38)$$

The initial design is a uniform foam design with a solidity of 0.01. The optimization results are shown in Table 7-1. The results indicate that the total thickness of foam insulation reaches the upper bound of 90 mm in the optimal design while its solidity tends to be close to the lower bound 0.01. For optimal Safill design the structure thickness reaches the lower bound of 1 mm and the optimal Safill thickness is 83 mm. The weight of the Safill design is only 38% of the weight of the sandwich TPS design. The temperature histories at both cool side and hot side of two designs are plotted in Figure 7-20. It takes Safill design more time to reach maximum structural temperature than sandwich design does. From Figure 7-21, we can see the stresses in the bottom foam core layer of sandwich design exceeds the foam strength σ_f= 0.535 MPa.

Table 7-1 Minimum weight design with variable insulation and structural thickness, subject to 450 K maximum temperature constraint

	Top facesheet h_1 (mm)	Top core h_2 (mm)	Top core solidity ρ_2	Bottom core h_3 (mm)	Bottom solidity core ρ_3	Structure thickness (mm)	Total Areal density (lb/ft^2)
Optimal Integrated design I	0.5	45.0	0.0140	45.0	0.0114	3.76	**3.62**
Optimal Safill design I	Thickness of Safill insulation h=83 mm					1.0	**1.38**

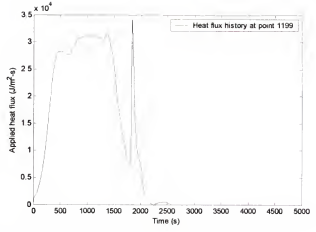

Figure 7-19 Reentry heat flux history at windward point 1199

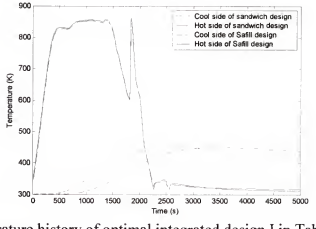

Figure 7-20 Temperature history of optimal integrated design I in Table 7-1

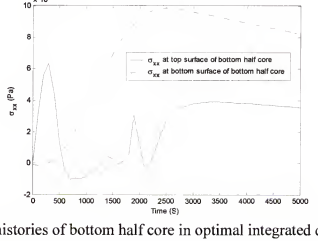

Figure 7-21 Stress histories of bottom half core in optimal integrated design I considering structural temperature and stress constraints

We repeated the optimization performed in the previous section with one more constraint that the stresses in each layer (both face sheets and foam core) should not exceed their strength. The applied pressure history is plotted in Figure 7-22. For Safill design its maximum structural temperature is 393 K only, as shown in Figure 7-23. So the structural temperature constraint is not active at all for Safill design. The optimal designs are shown in Table 7-2 below. Optimal Safill design in Table 7-2 has thick alumina structure as 7.26 mm and the thickness of structure can be reduced by using alumina sandwich structure or other stiffened structures. From Figure 7-23 and 7-24, we can see that for integrated sandwich design, the maximum stresses in both bottom half core and top half core are close to their strength. The weight for both sandwich and Safill design increases compared with the cases subject to structural temperature only.

Table 7-2 Minimum weight design with variable insulation and structural thickness, subject to 450 K maximum temperature constraint and stress constraints

	Top facesheet h_1(mm)	Top core h_2 (mm)	Top core ρ_2	Bottom core h_3 (mm)	Bottom core ρ_3	Structure thickness (mm)	Total Areal density (lb/ft^2)
Optimal Integrated design II	0.5	71.4	0.0207	18.6	0.0458	3.01	**4.28**
Optimal Safill design II	Thickness of Safill insulation h=33.3 mm					7.26	**4.24**

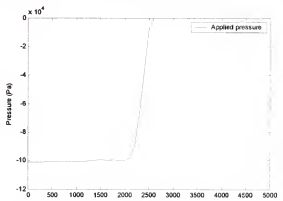

Figure 7-22 Re-entry pressure history at windward spot 1199

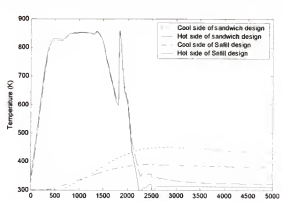

Figure 7-23 Temperature history of optimal integrated design II

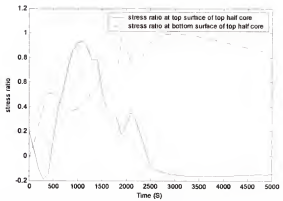

Figure 7-24 Stress ratio histories of top half core in optimal integrated design II

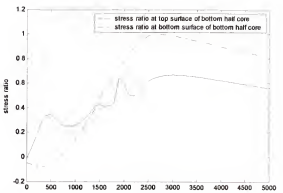

Figure 7-25 Stress ratio histories of bottom half core in optimal integrated design II

Optimum Integrated Sandwich Design for a Given Structure Thickness Considering Temperature Constraint only

Usually the structure thickness of sandwich TPS cannot reach the optimal thickness mentioned in above section because of design restrictions. So we need to investigate the optimal integrated sandwich design to protect the thin structure. In this case the structure thickness is assumed to be 2.2 mm and the foam insulation thickness has an upper bound of 90 mm. The results are shown in Table 7-3. From the results we can see that the total weight of integrated sandwich design increases. This is because the increasing weight of insulation is not as efficient as increasing the weight of structure to reduce the maximum structure temperature. The inner layer foam core has the highest allowable solidity. It should be noted that if we also remove the constraints of total insulation thickness, the optimal design will move closer to the optimal design in previous section, i.e. thick foam insulation with solidity close to the lower bound of 0.01.

Table 7-3 Minimum weight design for integrated sandwich with fixed foam insulation thickness upper bound 90 mm and structure thickness of 2.2 mm.

	Top facesheet h_1(mm)	Top core h_2 (mm)	Top core ρ_2	Bottom core h_3 (mm)	Bottom core ρ_3	Structure thickness (mm)	Total Areal density (lb/ft^2)
Integrated design III	0.5	72.35	0.0208	17.65	0.110	2.2	**4.83**

Failure Analysis of the TPS Structure due to Launch Loads

During the launch, the panel is subjected to a compressive load of N=-2.978×10^5 N/m (1700 lb/in). For Safill design, we assume the compressive load is carried by the structure only. The failure modes for this design could be the buckling of the structure or reaching its compression strength. In the integrated design the whole sandwich panel carries the load. Sandwich panel can fail in several ways depending on the sandwich geometry, load and boundary condition, such as global buckling, core shear failure, shear crimping and face wrinkling.

The buckling load is calculated by the classical laminate theory as in Whitney (1987):

$$N_{buck} = \frac{\pi^2\left[D_{11}m^4 + 2(D_{12}+2D_{66})m^2n^2R^2 + D_{22}n^4R^4\right]}{a^2\left(m^2+kn^2R^2\right)} \tag{7-39}$$

where D is the bending stiffness matrix of laminate plate. The critical buckling load reaches minimum when m=n=1.

The critical load for shear crimping failure mode is given in Zenkert (1997):

$$N_{shear} = \left(G_2h_2 + G_3h_3\right) \tag{7-40}$$

where G_2, G_3 is the shear modulus of top half core and bottom half core, respectively.

We assume the compression load is applied to neutral plane of the sandwich structure. So both the core and the face sheet have the same strain. The critical failure stress in the face sheet for this failure mode is given as in Zenkert (1997):

$$\sigma_{fwrk} = \frac{1}{2}\sqrt[3]{E_f E_c G_c} \tag{7-41}$$

When the core consists of multiple layers (two in the present case) the material properties of the foam core are homogenized as:

$$\begin{aligned} \frac{h_2 + h_3}{E_c} &= \frac{h_2}{E_2} + \frac{h_3}{E_3} \\ \frac{h_2 + h_3}{G_c} &= \frac{h_2}{G_2} + \frac{h_3}{G_3} \end{aligned} \tag{7-42}$$

The minimum weight design for each case is shown in Table 7-4. Most of the design variables reach lower bound for optimal integrated sandwich TPS design. Again, it should be noticed that Safill design may use stiffened structure instead of using alumina plate as structure. The Figure 7-26 indicates that the shear crimping is critical among all the three failure modes we studied for the integrated sandwich design.

Table 7-4 Minimum weight design for both integrated sandwich TPS design and Safill design during launch

	Top facesheet h_1(mm)	Top core h_2 (mm)	Top core ρ_2	Bottom core h_3 (mm)	Bottom core ρ_3	Structure thickness h_4 (mm)	Total Areal density (lb/ft^2)
Integrated	0.5	5.0	0.01	5.0	0.098	1.0	**1.51**
Safill design			N.A.			6.17	**3.50**

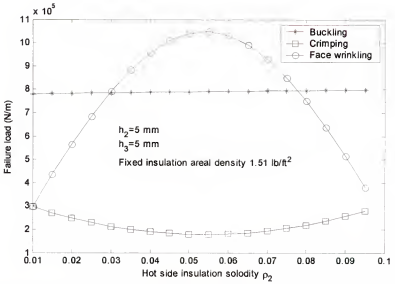

Figure 7-26 Critical load for a two-uniform-insulation integrated sandwich TPS panel with insulation thickness of 5 mm each and fixed insulation areal density 1.51 lb/ft^2.

For both integrated and Safill designs subjected to structure temperature constraints only, the integrated sandwich design tends to require as thick insulation as possible, while the Safill design yields thinner structure. Constraints of stress in both insulation and structure seem to be more critical than structural temperature for both designs. For integrated sandwich design with thin structure, cool side foam insulation calls for higher solidity or higher thermal mass. Shear crimping is critical among all the three failure modes we studied in the integrated sandwich design.

Since titanium face sheet used in this concept can not withstand temperatures more than 1000 K, new face sheet should be considered such as consideration of functionally graded face sheets so that it can withstand higher temperatures.

CHAPTER 8
CONCLUDING REMARKS

The concept of integrated metallic thermal protection systems is investigated under steady state and transient heat transfer condition. Such integrated TPS structures would insulate the vehicle interior from aerodynamic heating as well as carry primary vehicle loads. We take advantage of the load bearing ability of metallic foams and study the performance of integrated sandwich TPS concept with metallic foam core.

First we investigated the use of functionally graded metal foams in thermal protection systems (TPS) and developed an understanding of the effect of varying density profile on the optimal TPS design. The problem of minimum heat design is formulated as to minimize the heat transmitted through the foam insulation by varying density profile under steady state heat transfer condition. The foam thickness, inside wall temperature and aerodynamic heat load were assumed constant. This problem is equivalent to the problem of maximizing the outside temperature and hence maximizing the heat radiated out of the TPS. The optimality condition was obtained analytically.

We also studied the minimum mass design under steady state heat conduction in functionally graded open-cell metal foam insulation. The mass is minimized by varying the solidity profile for a given thickness. An optimality condition is derived and the optimization problem is reduced to that of an ordinary, nonlinear differential equation, which is solved numerically. The results include optimum cell size variation through the

thickness of the insulation for given aerodynamic heating, and the corresponding temperature distribution.

Then the problem of minimizing the maximum temperature of a structure insulated by functionally graded metal foam insulation under transient heat conduction is studied. The performance of insulation designed for steady state conditions is compared with uniform solidity insulation. It is found that the optimum steady state insulation performs poorly under transient conditions. The maximum structural temperature of a two-layer insulation with constant solidity for each layer is minimized by varying the solidity profile for a given total thickness and mass.

The method of Fourier series is combined with the Galerkin method for solving the two-dimensional elasticity equations for a sandwich thermal protection system insulation panel with foam core subjected to transverse loads. The variation of Young's modulus through the thickness is given by a polynomial in the thickness coordinate and Poisson's ratio is assumed to be constant. The Fourier series method is used to reduce the partial differential equations to a pair of ordinary differential equations, which are solved using the Galerkin method. The method will be useful is analyzing functionally graded TPS structures with arbitrary variation in thermo-mechanical properties in the thickness direction. The analysis was also performed using one-dimensional laminated plate theory and the results were compared. Significant differences between Galerkin solutions and laminate solutions suggest that the laminate theory may not be suitable for the analysis of thick integrated TPS.

Two kinds of thermal protection systems (TPS) for launch vehicles are compared during launch and reentry phases of the mission. One is the integrated sandwich structure

with titanium foam core as insulation, and the other is a structural panel with Safill insulation (fibrous alumina insulation) design. The weights of both designs are minimized subject to temperature constraints, stress constraints or both. The sandwich structure is analyzed by the method of Fourier expansion combined with the Galerkin method. Global buckling, shear crimping and face wrinkling are investigated for the integrated sandwich structure during the launch. It is found that for designs with variable insulation thickness, variable structure thickness and subjected to structure temperature constraint only, integrated sandwich design tends to require as thick insulation as possible, while Safill design requires thin structure. Shear crimping is the most critical among all the three failure modes we studied in integrated sandwich design.

The main findings of the design of metal foams as insulation can be summarized as follows:

1. For the design of minimum heat transmitted through insulation under steady state heat transfer condition, the optimal design requires minimum conductivity at each temperature through the thickness of insulation. The results show that using optimally graded insulation can lower heat transmitted to structure by 2.5-4.7 percent compared to uniform insulation with same weight.

2. For minimum weight design under steady state heat transfer condition, it is shown that for a given thickness a functionally graded insulation can be designed such that it is 4-8 percent lighter than the one with uniform solidity.

3. For the problem of minimizing the maximum temperature of a structure insulated by functionally graded metal foam insulation under transient heat conduction, it is shown that the cooler inner layer of the optimal design has high solidity, while the hotter outer layer has low solidity. This is in contrast to the steady state optimum design, where the solidity profile is the reverse.

4. Significant differences between Galerkin solutions and laminate solutions suggest that the laminate theory may not be suitable for the analysis of thick integrated TPS.

5. It is found that for designs with variable insulation thickness, variable structure thickness and subjected to structure temperature constraint only, integrated sandwich design tends to require as thick insulation as possible, while Safill design

requires thin structure. Shear crimping is most critical among all the three failure modes we studied in integrated sandwich design.

The present dissertation demonstrates the use of functionally graded metal foams as insulation in an integrated thermal protection system. Based on the thermal-mechanical analysis of integrated TPS, we found foam core failure is one of the most critical TPS failure modes, which requires us to predict the material properties of foam core more accurately. To achieve this accurate prediction, we need to develop a micro model, which captures the complex geometry of foam and predicts its thermal and mechanical property changes, such as coefficient of thermal expansion (CTE) and modulus in a functionally graded foam core due to the variation of volume fraction. Micro-mechanical models can be used to verify our macro model by finite element method (FEM).

APPENDIX A
TEMPERATURE DEPENDENT MATERIAL PROPERTIES OF TITANIUM AND ALUMNIUM

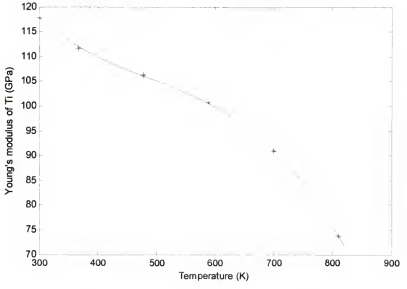

Figure A-1 Temperature dependent Young's modulus of titanium

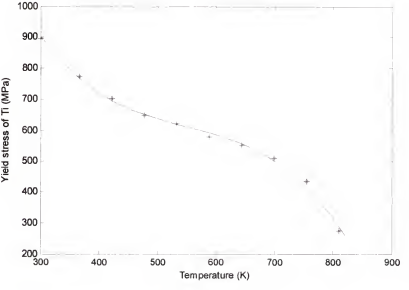

Figure A-2 Temperature dependent yield stress of titanium

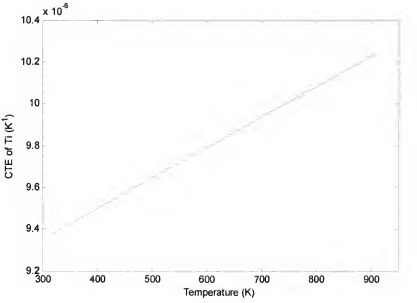

Figure A-3 Temperature dependent CTE of titanium

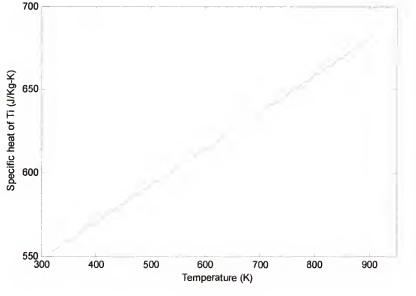

Figure A-4 Temperature dependent specific heat of titanium

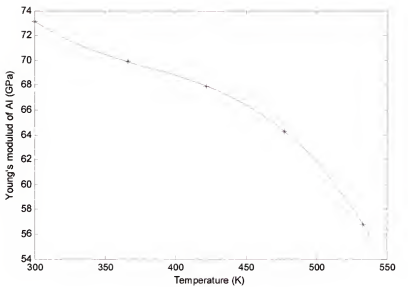

Figure A-5 Temperature dependent Young's modulus of aluminum

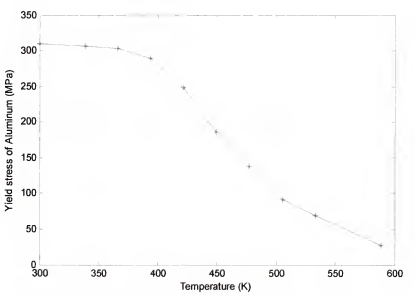

Figure A-6 Temperature dependent yield stress of aluminum

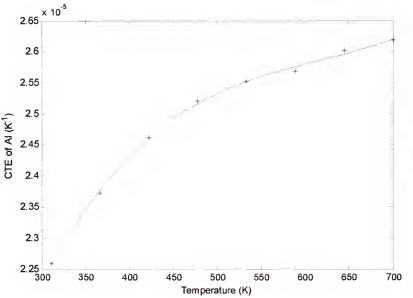

Figure A-7 Temperature dependent CTE of aluminum

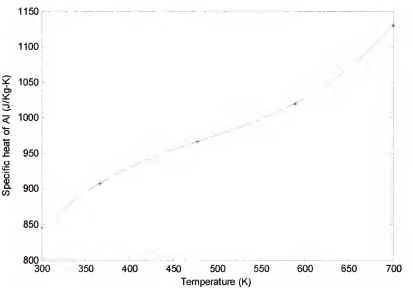

Figure A-8 Temperature dependent specific heat of aluminum

APPENDIX B
REUSABLE LAUNCH VEHICLE HEATING PROFILE

Table B-1 Thermal load and transverse pressure for reentry of reusable launch vehicle

Time (s)	Heat transfer Coefficient (lb_m/ft^2-s)	Pressure (psf)	Radiation Equilibrium temperature (F)	Heat Rate (btu/ft^2-s)
0.00E+00	5.52E-04	2.12E+03	-3.86E+01	1.19E-03
5.00E+00	6.65E-03	2.10E+03	4.22E+01	1.55E-01
1.00E+01	1.16E-02	2.07E+03	4.79E+01	4.32E-02
1.50E+01	1.64E-02	2.01E+03	4.95E+01	3.42E-02
2.00E+01	2.09E-02	1.93E+03	4.96E+01	2.84E-02
2.50E+01	2.50E-02	1.82E+03	4.87E+01	2.25E-02
3.00E+01	2.86E-02	1.69E+03	4.74E+01	1.86E-02
3.50E+01	3.13E-02	1.55E+03	4.58E+01	1.52E-02
4.00E+01	3.33E-02	1.39E+03	4.45E+01	1.65E-02
4.50E+01	3.42E-02	1.23E+03	4.33E+01	1.69E-02
5.00E+01	3.39E-02	1.06E+03	4.21E+01	1.63E-02
5.50E+01	3.25E-02	8.93E+02	4.05E+01	1.41E-02
6.00E+01	3.07E-02	7.38E+02	3.72E+01	-5.67E-04
6.50E+01	2.78E-02	5.98E+02	3.48E+01	7.74E-03
7.00E+01	2.47E-02	4.74E+02	3.66E+01	3.46E-02
7.50E+01	2.14E-02	3.68E+02	6.24E+01	1.63E-01
8.00E+01	1.80E-02	2.83E+02	9.45E+01	1.78E-01
8.50E+01	1.48E-02	2.14E+02	1.36E+02	2.00E-01
9.00E+01	1.19E-02	1.59E+02	1.87E+02	2.19E-01
9.50E+01	9.31E-03	1.16E+02	2.46E+02	2.40E-01
1.00E+02	7.19E-03	8.32E+01	3.08E+02	2.56E-01
1.05E+02	5.51E-03	5.88E+01	3.69E+02	2.80E-01
1.10E+02	4.21E-03	4.10E+01	4.20E+02	3.04E-01
1.15E+02	3.20E-03	2.83E+01	4.60E+02	3.28E-01
1.20E+02	2.43E-03	1.92E+01	4.90E+02	3.54E-01
1.25E+02	1.90E-03	1.31E+01	5.14E+02	3.82E-01
1.30E+02	1.11E-03	8.96E+00	4.66E+02	2.89E-01
1.35E+02	2.22E-04	6.20E+00	2.24E+02	7.61E-02
1.40E+02	1.94E-04	4.33E+00	2.32E+02	9.40E-02
1.45E+02	1.65E-04	3.06E+00	2.34E+02	9.49E-02
1.50E+02	1.41E-04	2.18E+00	2.34E+02	9.47E-02
1.55E+02	1.21E-04	1.57E+00	2.32E+02	9.37E-02
1.60E+02	1.04E-04	1.13E+00	2.29E+02	9.20E-02
1.65E+02	8.88E-05	8.20E-01	2.24E+02	8.91E-02

1.70E+02	7.57E-05	5.91E-01	2.17E+02	8.56E-02
1.75E+02	6.48E-05	4.28E-01	2.10E+02	8.20E-02
1.80E+02	5.54E-05	3.11E-01	2.01E+02	7.81E-02
1.85E+02	4.71E-05	2.24E-01	1.92E+02	7.36E-02
1.90E+02	4.02E-05	1.63E-01	1.82E+02	6.93E-02
1.95E+02	3.43E-05	1.18E-01	1.72E+02	6.50E-02
2.00E+02	2.92E-05	8.55E-02	1.61E+02	6.06E-02
2.05E+02	2.50E-05	6.26E-02	1.51E+02	5.68E-02
2.10E+02	2.15E-05	4.58E-02	1.41E+02	5.31E-02
2.15E+02	1.86E-05	3.35E-02	1.31E+02	4.97E-02
2.20E+02	1.61E-05	2.48E-02	1.21E+02	4.65E-02
2.25E+02	1.41E-05	1.89E-02	1.13E+02	4.40E-02
2.30E+02	1.25E-05	1.47E-02	1.06E+02	4.18E-02
2.35E+02	1.11E-05	1.14E-02	9.86E+01	3.97E-02
2.40E+02	9.84E-06	9.00E-03	9.19E+01	3.79E-02
2.45E+02	8.84E-06	7.16E-03	8.61E+01	3.63E-02
2.50E+02	7.98E-06	5.75E-03	8.08E+01	3.49E-02
2.55E+02	7.24E-06	4.67E-03	7.60E+01	3.37E-02
2.60E+02	6.63E-06	3.88E-03	7.23E+01	3.28E-02
2.65E+02	5.99E-06	3.17E-03	6.69E+01	3.15E-02
2.70E+02	5.42E-06	2.56E-03	6.12E+01	3.01E-02
2.75E+02	4.95E-06	2.12E-03	5.67E+01	2.91E-02
2.80E+02	4.54E-06	1.76E-03	5.25E+01	2.82E-02
2.85E+02	4.21E-06	1.51E-03	4.97E+01	2.76E-02
2.90E+02	3.95E-06	1.31E-03	4.80E+01	2.72E-02
2.95E+02	3.76E-06	1.17E-03	4.80E+01	2.72E-02
3.00E+02	3.59E-06	1.06E-03	4.80E+01	2.72E-02
3.05E+02	3.45E-06	9.82E-04	4.91E+01	2.74E-02
3.10E+02	3.34E-06	9.16E-04	5.09E+01	2.78E-02
3.15E+02	3.26E-06	8.73E-04	5.38E+01	2.85E-02
3.20E+02	3.19E-06	8.31E-04	5.66E+01	2.91E-02
3.25E+02	3.12E-06	7.92E-04	5.94E+01	2.97E-02
3.30E+02	3.08E-06	7.71E-04	6.33E+01	3.06E-02
3.35E+02	3.04E-06	7.51E-04	6.71E+01	3.15E-02
3.40E+02	3.01E-06	7.32E-04	7.11E+01	3.25E-02
3.45E+02	2.98E-06	7.17E-04	7.55E+01	3.36E-02
3.50E+02	2.97E-06	7.07E-04	7.67E+01	3.39E-02
3.55E+02	2.94E-06	6.97E-04	7.58E+01	3.36E-02
3.60E+02	2.92E-06	6.87E-04	7.48E+01	3.34E-02
3.65E+02	2.90E-06	6.76E-04	7.37E+01	3.31E-02
3.70E+02	2.87E-06	6.66E-04	7.26E+01	3.29E-02
3.75E+02	2.85E-06	6.55E-04	7.16E+01	3.26E-02
3.80E+02	2.83E-06	6.45E-04	7.05E+01	3.23E-02
3.85E+02	2.81E-06	6.35E-04	6.94E+01	3.21E-02
3.90E+02	2.78E-06	6.25E-04	6.84E+01	3.18E-02
3.95E+02	2.76E-06	6.15E-04	6.73E+01	3.16E-02
4.00E+02	2.74E-06	6.06E-04	6.63E+01	3.13E-02
4.05E+02	2.72E-06	5.96E-04	6.53E+01	3.11E-02
4.10E+02	2.70E-06	5.87E-04	6.42E+01	3.08E-02
4.15E+02	2.68E-06	5.78E-04	6.32E+01	3.06E-02

4.20E+02	2.65E-06	5.69E-04	6.22E+01	3.04E-02
4.25E+02	2.63E-06	5.60E-04	6.11E+01	3.01E-02
4.30E+02	2.61E-06	5.52E-04	6.01E+01	2.99E-02
4.35E+02	2.59E-06	5.43E-04	5.91E+01	2.96E-02
4.40E+02	2.57E-06	5.35E-04	5.81E+01	2.94E-02
4.45E+02	2.55E-06	5.27E-04	5.71E+01	2.92E-02
4.50E+02	2.53E-06	5.19E-04	5.60E+01	2.90E-02
4.55E+02	2.51E-06	5.09E-04	5.48E+01	2.87E-02
4.60E+02	2.48E-06	4.99E-04	5.36E+01	2.84E-02
4.65E+02	2.46E-06	4.90E-04	5.23E+01	2.81E-02
4.70E+02	2.44E-06	4.81E-04	5.11E+01	2.79E-02
4.75E+02	2.41E-06	4.72E-04	4.99E+01	2.76E-02
4.80E+02	2.39E-06	4.63E-04	4.87E+01	2.73E-02
4.85E+02	2.37E-06	4.54E-04	4.75E+01	2.71E-02
4.90E+02	2.34E-06	4.46E-04	4.63E+01	2.68E-02
4.95E+02	2.32E-06	4.37E-04	4.51E+01	2.66E-02
5.00E+02	2.30E-06	4.29E-04	4.39E+01	2.63E-02
5.05E+02	2.28E-06	4.21E-04	4.27E+01	2.61E-02
5.10E+02	2.26E-06	4.14E-04	4.15E+01	2.58E-02
5.15E+02	2.24E-06	4.06E-04	4.03E+01	2.56E-02
5.20E+02	2.21E-06	3.98E-04	3.91E+01	2.53E-02
5.25E+02	2.19E-06	3.91E-04	3.80E+01	2.51E-02
5.30E+02	2.17E-06	3.84E-04	3.68E+01	2.49E-02
5.35E+02	2.15E-06	3.77E-04	3.56E+01	2.46E-02
5.40E+02	2.13E-06	3.70E-04	3.45E+01	2.44E-02
5.45E+02	2.11E-06	3.62E-04	3.32E+01	2.42E-02
5.50E+02	2.09E-06	3.54E-04	3.18E+01	2.39E-02
5.55E+02	2.06E-06	3.47E-04	3.05E+01	2.36E-02
5.60E+02	2.04E-06	3.40E-04	2.92E+01	2.34E-02
5.65E+02	2.02E-06	3.33E-04	2.79E+01	2.31E-02
5.70E+02	2.00E-06	3.26E-04	2.66E+01	2.29E-02
5.75E+02	1.98E-06	3.19E-04	2.53E+01	2.26E-02
5.80E+02	1.96E-06	3.12E-04	2.40E+01	2.24E-02
5.85E+02	1.94E-06	3.06E-04	2.27E+01	2.22E-02
5.90E+02	1.92E-06	2.99E-04	2.14E+01	2.19E-02
5.95E+02	1.89E-06	2.93E-04	2.02E+01	2.17E-02
6.00E+02	1.88E-06	2.87E-04	1.89E+01	2.15E-02
6.05E+02	1.86E-06	2.81E-04	1.76E+01	2.13E-02
6.10E+02	1.84E-06	2.75E-04	1.64E+01	2.10E-02
6.15E+02	1.82E-06	2.70E-04	1.52E+01	2.08E-02
6.20E+02	1.80E-06	2.64E-04	1.39E+01	2.06E-02
6.25E+02	1.78E-06	2.59E-04	1.27E+01	2.04E-02
6.30E+02	1.76E-06	2.54E-04	1.15E+01	2.02E-02
6.35E+02	1.74E-06	2.48E-04	1.03E+01	2.00E-02
6.40E+02	1.73E-06	2.43E-04	9.10E+00	1.98E-02
6.45E+02	1.71E-06	2.38E-04	7.80E+00	1.95E-02
6.50E+02	1.69E-06	2.33E-04	6.40E+00	1.93E-02
6.55E+02	1.67E-06	2.28E-04	5.10E+00	1.91E-02
6.60E+02	1.65E-06	2.22E-04	3.80E+00	1.89E-02
6.65E+02	1.63E-06	2.18E-04	2.50E+00	1.87E-02

6.70E+02	1.61E-06	2.13E-04	1.20E+00	1.85E-02
6.75E+02	1.59E-06	2.08E-04	-1.00E-01	1.83E-02
6.80E+02	1.58E-06	2.04E-04	-1.30E+00	1.81E-02
6.85E+02	1.56E-06	1.99E-04	-2.60E+00	1.79E-02
6.90E+02	1.54E-06	1.95E-04	-3.90E+00	1.77E-02
6.95E+02	1.53E-06	1.91E-04	-5.10E+00	1.75E-02
7.00E+02	1.51E-06	1.87E-04	-6.40E+00	1.73E-02
7.05E+02	1.49E-06	1.83E-04	-7.60E+00	1.71E-02
7.10E+02	1.48E-06	1.79E-04	-8.80E+00	1.69E-02
7.15E+02	1.46E-06	1.75E-04	-1.00E+01	1.67E-02
7.20E+02	1.44E-06	1.71E-04	-1.12E+01	1.66E-02
7.25E+02	1.43E-06	1.68E-04	-1.24E+01	1.64E-02
7.30E+02	1.41E-06	1.64E-04	-1.36E+01	1.62E-02
7.35E+02	1.40E-06	1.61E-04	-1.48E+01	1.60E-02
7.40E+02	1.38E-06	1.58E-04	-1.59E+01	1.59E-02
7.45E+02	1.37E-06	1.54E-04	-1.72E+01	1.57E-02
7.50E+02	1.35E-06	1.51E-04	-1.84E+01	1.55E-02
7.55E+02	1.34E-06	1.48E-04	-1.96E+01	1.54E-02
7.60E+02	1.32E-06	1.44E-04	-2.08E+01	1.52E-02
7.65E+02	1.31E-06	1.41E-04	-2.20E+01	1.50E-02
7.70E+02	1.30E-06	1.38E-04	-2.32E+01	1.49E-02
7.75E+02	1.28E-06	1.35E-04	-2.44E+01	1.47E-02
7.80E+02	1.27E-06	1.33E-04	-2.56E+01	1.45E-02
7.85E+02	1.25E-06	1.30E-04	-2.68E+01	1.44E-02
7.90E+02	1.24E-06	1.27E-04	-2.79E+01	1.42E-02
7.95E+02	1.23E-06	1.25E-04	-2.90E+01	1.41E-02
8.00E+02	1.21E-06	1.22E-04	-3.01E+01	1.39E-02
8.05E+02	1.20E-06	1.20E-04	-3.12E+01	1.38E-02
8.10E+02	1.19E-06	1.17E-04	-3.23E+01	1.37E-02
8.15E+02	1.18E-06	1.15E-04	-3.34E+01	1.35E-02
8.20E+02	1.16E-06	1.13E-04	-3.45E+01	1.34E-02
8.25E+02	1.15E-06	1.11E-04	-3.55E+01	1.33E-02
8.30E+02	1.14E-06	1.09E-04	-3.66E+01	1.31E-02
8.35E+02	1.13E-06	1.06E-04	-3.76E+01	1.30E-02
8.40E+02	1.12E-06	1.04E-04	-3.87E+01	1.29E-02
8.45E+02	1.11E-06	1.02E-04	-3.97E+01	1.27E-02
8.50E+02	1.10E-06	1.01E-04	-4.07E+01	1.26E-02
8.55E+02	1.09E-06	9.88E-05	-4.17E+01	1.25E-02
8.60E+02	1.08E-06	9 70E-05	-4.27E+01	1.24E-02
8.65E+02	1.07E-06	9.52E-05	-4.36E+01	1.23E-02
8.70E+02	1.06E-06	9.35E-05	-4.46E+01	1.22E-02
8.75E+02	1.05E-06	9.18E-05	-4.56E+01	1.20E-02
8.80E+02	1.04E-06	9.02E-05	-4.65E+01	1.19E-02
8.85E+02	1.03E-06	8.87E-05	-4.75E+01	1.18E-02
8.90E+02	1.02E-06	8.71E-05	-4.84E+01	1.17E-02
8.95E+02	1.01E-06	8.55E-05	-4.94E+01	1.16E-02
9.00E+02	9.98E-07	8.39E-05	-5.04E+01	1.15E-02
9.05E+02	9.88E-07	8.24E-05	-5.13E+01	1.14E-02
9.10E+02	9.79E-07	8.10E-05	-5.23E+01	1.13E-02
9.15E+02	9.70E-07	7.95E-05	-5.32E+01	1.12E-02

9.20E+02	9.61E-07	7.81E-05	-5.42E+01	1.11E-02
9.25E+02	9.52E-07	7.67E-05	-5.51E+01	1.10E-02
9.30E+02	9.43E-07	7.53E-05	-5.61E+01	1.09E-02
9.35E+02	9.34E-07	7.41E-05	-5.69E+01	1.08E-02
9.40E+02	9.26E-07	7.28E-05	-5.78E+01	1.07E-02
9.45E+02	9.18E-07	7.16E-05	-5.87E+01	1.06E-02
9.50E+02	9.09E-07	7.04E-05	-5.96E+01	1.05E-02
9.55E+02	9.01E-07	6.91E-05	-6.05E+01	1.04E-02
9.60E+02	8.93E-07	6.80E-05	-6.14E+01	1.03E-02
9.65E+02	8.85E-07	6.69E-05	-6.22E+01	1.02E-02
9.70E+02	8.78E-07	6.58E-05	-6.31E+01	1.01E-02
9.75E+02	8.70E-07	6.47E-05	-6.40E+01	1.00E-02
9.80E+02	8.62E-07	6.37E-05	-6.48E+01	9.95E-03
9.85E+02	8.55E-07	6.26E-05	-6.57E+01	9.87E-03
9.90E+02	8.48E-07	6.17E-05	-6.65E+01	9.79E-03
9.95E+02	8.41E-07	6.07E-05	-6.73E+01	9.70E-03
1.00E+03	8.33E-07	5.97E-05	-6.81E+01	9.62E-03
1.01E+03	8.26E-07	5.88E-05	-6.89E+01	9.54E-03
1.01E+03	8.19E-07	5.79E-05	-6.97E+01	9.46E-03
1.02E+03	8.13E-07	5.70E-05	-7.05E+01	9.39E-03
1.02E+03	8.06E-07	5.61E-05	-7.13E+01	9.31E-03
1.03E+03	8.00E-07	5.53E-05	-7.21E+01	9.24E-03
1.03E+03	7.93E-07	5.44E-05	-7.28E+01	9.17E-03
1.04E+03	7.87E-07	5.36E-05	-7.36E+01	9.09E-03
1.04E+03	7.80E-07	5.28E-05	-7.44E+01	9.02E-03
1.05E+03	7.74E-07	5.20E-05	-7.51E+01	8.95E-03
1.05E+03	7.68E-07	5.13E-05	-7.59E+01	8.88E-03
1.06E+03	7.62E-07	5.05E-05	-7.66E+01	8.82E-03
1.06E+03	7.56E-07	4.98E-05	-7.73E+01	8.75E-03
1.07E+03	7.50E-07	4.91E-05	-7.81E+01	8.68E-03
1.07E+03	7.44E-07	4.84E-05	-7.88E+01	8.61E-03
1.08E+03	7.39E-07	4.77E-05	-7.95E+01	8.55E-03
1.08E+03	7.33E-07	4.70E-05	-8.02E+01	8.49E-03
1.09E+03	7.28E-07	4.64E-05	-8.09E+01	8.42E-03
1.09E+03	7.22E-07	4.57E-05	-8.16E+01	8.36E-03

LIST OF REFERENCES

Alifanov, M. O., Outchvatov, I.V. and Pichkhadze, M. K., 2003, Thermal Protection of Re-entry Vehicles with the Usage of Inflatable Systems. Acta Astronautica, Vol. 53, pp. 541-546.

Andrews, E., Sanders, W. and Gibson L.J., 1999, Compressive and Tensile Behavior of Aluminum Foams. Materials Science and Engineering, Vol. A270, pp. 113-124.

Apetre, N.A., Sankar, B.V. and Venkataraman, S., April 2002, Indentation of a Sandwich Beam with Functionally Graded Core. Proceedings of the 43rd AIAA Structures, Structural Dynamics and Materials Conference, Denver, Colorado, AIAA Paper 2002-1683.

Ashby, M. F., Evans, A., Fleck, N.A., Gibson, L.J., Huchinson, J.W. and Wadley, H.N.G., 2000, Metal Foams: A Design Guide. Butterworth-Heinemann, Boston, MA.

Bankvall, C., May 1973, Heat Transfer in Fibrous Materials, Journal of Testing and Evaluation, JTEVA. Vol. 1, No. 3, pp. 235-243.

Bert, C.W., 1973, Simplified Analysis of Static Shear Correction Factors for Beams of Non-Homogeneous Cross Section. Journal of Composite Materials, Vol. 7, 525-529.

Blosser, M.L., October 1996, Development of Metallic Thermal Protection Systems for the Reusable Launch Vehicle. NASA TM-110296.

Blosser, M. L., May 2000, Advanced Metallic Thermal Protection Systems for Reusable Launch Vehicles. Ph. D. Dissertation, University of Virginia.

Blosser, M. L., 2002, Investigation of Fundamental Modeling and Thermal Protection Issues for a Metallic Thermal Protection System Design. Proceedings of the 40th Aerospace Sciences Meeting and Exhibit, Reno, Nevada, AIAA paper 2002-0503.

Blosser, M. L., Chen, R. R., Schmidt, I. H., Dorsey, J. T., Poteet, C. C. and Bird, R. K., 2002, Advanced Metallic Thermal Protections System Development, Proceedings of the 40th Aerospace Sciences Meeting and Exhibit, Jan 14-17, Reno, Nevada, AIAA 2002-0504.

Bohon, H.L., Sawyer, J.W., Hunt, L.R. and Weistein, I., Dec. 1975, Performance of Thermal Protection Systems in a Mach 7 Environment. Journal of Space and Rockets, Vol. 12, pp. 744-749.

Bohon, H.L., Shildeler, J.L., and Rummler, D.R., October 1977, Radiative Metallic Thermal Protection Systems: A Status report. Journal of Spacecraft and Rockets, Vol. 12, No.10, pp. 626-631.

Budiansky, B., 1965, On the Elastic Moduli of Some Heterogeneous Materials. Journal of Mechanics and Physics of Solids, Vol. 13, pp. 223-227.

Burmeister, L.C., 1983, Convective Heat Transfer. John Wiley & Sons, New York.

Calmidi, V.V. and Mahajan, R.L., May 1999, The Effective Thermal Conductivity of High Porosity Fibrous Metal Foams. ASME Journal of Heat Transfer, Vol. 122, pp. 466-470.

Candler, G. V., Wright, M. J. and McDonald, J. D., 1994, Data-Parallel Lower-Upper Relaxation Method for Reacting Flows. AIAA Journal, Vol. 32, No. 12, pp. 2380-2386.

Cheng, Z.Q. and Batra, R.C., 2000, Three-dimensional Thermoelastic Deformations of a Functionally Graded Elliptic Plate. Composites: Part B, Vol. 31, pp. 97–106.

Chiu, S.A. and Pitts, W.C., Jan 1991, Reusable Surface Insulation for Reentry Spacecraft. Proceedings of 29th Aerospace Sciences Meeting, AIAA Paper 91-0695.

Cho, J.R. and Ha, D.Y., 2001, Averaging and Finite Element Discretization Approaches in the Numerical Analysis of Functionally Graded Materials. Materials Science and Engineering: A, Vol. 302, No. 2, pp. 187–196.

Cho, J.R. and Ha, D.Y., 2002, Optimal Tailoring of 2D Volume-fraction Distributions for Heat-resisting Functionally Graded Materials using FDM. Computer Methods in Applied Mechanics and Engineering, Vol. 191, pp. 3195–3211.

Choi, S., 2002, A Micromechanics Method to Predict the Fracture Toughness of Cellular Materials. Master Thesis, University of Florida, Gainesville, pp. 5.

Chow, T.S., 1971, On the Propagation of Flexural Waves in an Orthotropic Laminated Plate and Its Response to an Impulsive Load. Journal of Composite Materials, Vol. 5, pp. 306-319.

Cooper, P.A and Holloway, P.F., Jan 1981, The Shuttle Tile Story. Aeronautics and Astronautics, pp. 24-36.

Cunnington, G.R. and Tien, C.L., 1970, A Study of Heat Transfer Processes in Multilayer Insulation. In: Bevans JT, editor. Thermophysics: applications to thermal design of spacecraft, AIAA progress in astronautics and aeronautics, Vol. 23, New York: Academic Press, pp. 111.

Daryabeigi, K., January 1999, Analysis and Testing of High Temperature Fibrous Insulation for Reusable Launch Vehicles. 37th AIAA Aerospace Sciences Meeting and Exhibit, Reno, NV, AIAA 99-1044.

Daryabeigi, K., 2002, Thermal Analysis and Design Optimization of Multilayer Insulation for Reentry Aerodynamic Heating. Journal of Spacecraft and Rockets, Vol. 39, No. 4.

Devisikis, W.D., Miserentino, R., Weinstern, I. and Shideler, J.L., 1975, Aerothermal Performance and Structural Integrity of Rene 41 Thermal Protection Systems in a Mach 6.6 Stream. NASA TN D-7943.

Dorsey, J.T., Wu, C., Rivers, K., Martin, C. Jr. and Smith, R., 1999, Airframe Integration Trade Studies for a Reusable Launch Vehicle. NASA Langley Research Center Space Technology and Applications International Forum (STAIF '99), Albuquerque, New Mexico, January 1--February 4.

Dorsey, J.T., Chen, R., and Poteet, C., 2002, Metallic Thermal Protection System Technology Development: Concepts, Requirements and Assessment Overview. 40th AIAA Aerospace Sciences Meeting and Exhibit, Reno, NV, January 14-17.

Eidenoff, H.L. and Rose, L., 1974, Thermal-Structural Evaluation of TD Ni-20Cr Thermal Protection Panels. NASA CR-132487.

Findley, B. and Johnson, W., April 2003, Benefits of Surface Coatings for Impacted Composites to Be Used for Cryogenic Tankage. Proceedings of the 44th AIAA Structures, Structural Dynamics and Materials Conference, Norfolk, Virginia, AIAA 2003-1938

Ford, R.G., Kawasaki, A., Kaysser, W.A., Miyamoto, Y. and Rabin, B.H., September 1999, Functionally Graded Materials Design, Processing and Applications. Kluwer Academic Pub.

Fox, L.R., 1971, Optimization methods for Engineering Design. Massachusetts, Addison-Wesley, pp. 175.

Gibson, L.J. and Ashby, M. F., 1997, Cellular Solids, 2nd edition. Cambridge University Press, Cambridge.

Glass, D.E. and Camrda, C.J., 1992, Preliminary Thermal/Structural Analysis of a Carbon-Carbon/Refractory-Metal Heat-Pipe-Cooled Wing Leading Edge, Thermal Structures and Materials for High Speed Flight, edited by E.A. Thornton, Vol. 140, Progress in Astronautics and Aeronautics, AIAA, Washington, DC, pp. 301-322.

Glicksman, L. R., 1994, Heat Transfer in Foams, in Low Density Cellular Plastics: Physical Basis of Behavior, editors: Hilyard, N. C., and Cunningham, A., Chapman & Hall, London, United Kingdom.

Gnoffo, P.A.; Weilmuenster, K.J. and Hamilton, H.H., January-February 1999, Computational Aerothermodynamic Design Issues for Hypersonic Vehicles. Journal of Spacecraft and Rockets, Vol. 36, No. 1, pp. 21-43.

Haftka, R. T., Gürdal, Z. and Kamat, M. P., 1990, Elements of Structural Optimization. 2nd Edition, Kluwer Publishers, pp. 148.

Hashin, Z. and Shtrikman, S., 1963, A Variational Approach to the Theory of the Elastic Behavior of Multiphase Systems. Journal of Mechanics and Physics of Solids, Vol. 11, pp. 127-140.

Hill, R., 1965, Self-consistent Mechanics of Composite Materials. Journal of Mechanics and Physics of Solids, Vol. 13, pp. 213-222.

Hsueha, C.H. and Lee, S., 2003, Modeling of Elastic Thermal Stresses in Two Materials Ioined by a Graded Layer. Composites: Part B, Vol. 34, pp. 747–752.

Hughes, J.T., Curry, D.M. and Tillian, D.J., 1985, Orbiter Thermal Protection System. Space Shuttle Technology Conference Proceedings: Part 2, pp. 1062-1081.

Jackson, L.R. and Dixon, S.C., April 1980, A Design Assessment of Multiwall, Metallic Stand-off, and RSI Reusable Thermal Protection Systems Including Space Shuttle Application. NASA TM 81780.

Keller, K., Blumenberg, J., and Tomsik, J., 1988, Fibre Orientation and the Conduction of Heat by a Gas Enclosed in Ceramic Layers. Z. Flugwiss, Weltraumforsch, Vol. 12, pp. 258-260.

Keller, K., Hoffmann, M., Zorner, W., and Blumenberg, J., 1992, Application of High Temperature Multilayer Insulations. Acta Astronautica, Vol. 26, No. 6, pp. 451-458.

Kelly, H.N. and Blosser, M.L., July 1994, Active Cooling From the Sixties to NASP. NASA TM 109079.

Kim, K.S. and Noda, N., 2001. Green's Function Approach to Three-dimensional Heat Conduction Equation of Functionally Graded Materials. Journal of Thermal Stresses Vol. 24, pp. 457–477.

Kollar, P.L. and Springer, G.S., 2002, Mechanics of Composite Structures. Cambridge University press, Cambridge, UK.

Krishnaprakas, C.K., Narayana, B. and Dutta, P., 2000, Heat Transfer Correlations for Multilayer Insulation Systems .Cryogenics, Vol. 40, No. 7, pp. 431-435.

Lee, S.C. and Cunningtont, G.R., July– September 1998, Heat Transfer in Fibrous Insulations: Comparison of Theory and Experiment. Journal of Thermalphysics and Heat Transfer, Vol. 12, No. 3.

Lee, S.C., and Cunnington, G.R., April-June 2000, Conduction and Radiation Heat Transfer in High Porosity Fiber Thermal Insulation. Journal of Thermophysics and Heat Transfer, Vol. 14, No. 2, pp.121-136.

Lo, K.H, Christensen, R.M. and Wu, E.M., 1977a, A High-order Theory of Plate Deformation Part 1: Homogeneous Plates. Journal of Applied Mechanics, Vol. 44, No. 4, pp. 663-668.

Lo, K.H, Christensen, R.M., Wu, E.M., 1977b, A high-order Theory of Plate Deformation part 2: Laminated Plates. Journal of Applied Mechanics, Vol. 44, No. 4, pp. 669-676.

Mori, T. and Tanaka, K., 1973, Average Stress in Matrix and Average Elastic Energy of Materials with Misfitting Inclusions. Acta Metallurgica, Vol. 21, 571-574.

Myers, D.E., Martin, C.J. Jr. and Blosser, M.L., June 2000, Parametric Weight Comparison of Advanced Metallic, Ceramic Tile, and Ceramic Blanket Thermal Protection Systems. NASA/TM-2000-210289, pp. 49.

NASA, August 1968, Entry Thermal Protection, NASA SP-8014

Olynick, D. R., and Henline,W. D., 1995, Comparison of Coupled Radiative Flow Solutions with Project Fire II Flight Data. Journal of Spacecraft and Rockets, Vol. 9, No. 4, pp. 586-594.

Ootao, Y. and Tanigawa, Y., 1999. Three-dimensional Transient Thermal Stresses of Functionally Graded Rectangular Plate due to Partial Heating. Journal of Thermal Stresses, Vol. 22, pp. 35–55.

Pai, P.F. and Nayfeh, A.N., 1995, Nonlinear Displacement-based Finite Element Analyses of Composite Shells - a New Total Lagrangian Formulation. International Journal of Solids Structure, Vol.32, pp. 3047-3073.

Phanikumar, M.S. and Mahajan, R.L., 2002, Non-Darcy Natural Convection in High Porosity Metal Foams. International Journal of Heat and Mass Transfer, Vol. 45, pp. 3781.

Powell, R.W., Lockwood, M.K. and Cook, S.A., 1998, The Road From the NASA Access-to-Space Study to a Reusable Launch Vehicle. 49th International Astronautical Congress, Melbourne, Australia, September 28th--October 2nd, pp. 10.

Purse, P.E., Faget, M. A. and Smith, N.F., 1964, Manned Spacecraft: Engineering Design and Operation. Fairchild Publications, Inc., New York, pp. 497.

Ravichandran, K.S., 1994, Elastic Properties of Two-phase Composites. Journal of the American Ceramic Society, Vol. 77, No. 5, pp. 1178-1184.

Reddy, J.N., 1984a, A Refined Nonlinear Theory of Plates with Transverse Shear Deformation. International Journal of Solids Structure, Vol. 20, No. 9–10, pp.881-906.

Reddy, J.N., 1984b, A Simple Higher-order Theory for Laminated Composite Plates. Journal of Applied Mechanics, Vol. 51, pp. 745-52.

Reddy, J.N., 1996, Mechanics of Laminated Composite: Plates Theory and Analysis. CRC press, Boca Raton, FL.

Reddy J.N., 1999, Theory and Analysis of Elastic Plates. Philadelphia (PA): Taylor & Francis.

Reissner, E., 1975, On Transverse Bending of Plates, including the Effects of Transverse Shear Deformation. International Journal of Solids Structure, Vol. 11, pp. 569-573.

Reissner, E., 1985, Reflection on the Theory of Elastic plates. Applied Mechanics Review, Vol. 38, pp.1453-1464.

Reusable Launch Vehicle: Technology Development and Test Program, 1995, Committee on Reusable Launch Vehicle Technology and Test Program, National Research Council, National Academy Press, Washington, D.C., pp. 50-52.

Roe, P. L., Oct. 1981, Approximate Riemann Solvers, Parameter Vectors, and Difference Schemes. Journal of Computational Physics, Vol. 43, pp. 357-372.

Rummler, D.R. and Black, W.E., April 1975, Evaluation of Coated Columbium for Thermal Protection Systems Application. Denver, CO, AIAA paper 75-187.

Sankar, B.V., 2001, An Elasticity Solution for Functionally Graded Beams. Composites Science & Technology, Vol. 61, pp. 689-696.

Sankar, B.V. and Tzeng, J.T., 2001, Thermal Stress Analysis of Functionally Graded Beams. AIAA Structures, Structural Dynamics & Materials Conference, Seattle, Washington, April 2001, AIAA Paper 2001-1513.

Sankar, B.V. and Tzeng, J.T., 2002, Thermal Stresses in Functionally Graded Beams. AIAA Journal, Vol. 40, No. 6, pp. 1228-1232.

Savoia, M. and Reddy, J.N., 1992, A Variational Approach to Three-dimensional Elasticity Solutions of Laminated Composite Plates. Journal of Applied mechanics, Vol. 59, pp. 166-175.

Shideler, J.L., Kelly, H.N., Avery, D.E., Blosser, M.L. and Adelman, H.M., July-August 1982, Multiwall TPS- An Emerging Concept. Journal of Spacecraft and Rockets, Vol. 19, No. 4, pp. 358-36.

Smeltzer, S.S. and Waters, A.W., 2003, Nonlinear Thermal Analyses of a Liquid Hydrogen Tank Wall, JANNAF 39th CS/27th APS/21st PSHS/3rd MSS Joint Subcommittee Meeting, Colorado Springs, Colorado, December 1-5, 2003

Spinnler, M, Winter, E. and Viskanta, R., 2002, Studies on High-temperature Multilayer Thermal Insulations. International Journal of Heat and Mass Transfer, Vol. 47, pp. 1305-1312.

Stanley, D.O. and Piland, W.M., October 1993, Technology Requirements for Affordable Single-Stage Rocket Launch Vehicles. IAF Paper 93-627.

Sullins, A.D. and Daryabeigi K., June 2001, Effective Thermal Conductivity of High Porosity Open Cell Nickel Foam. 35th AIAA Thermophysics Conference, Anaheim, California, AIAA 2001-2819.

Tarn, J.Q. and Wang, Y.M., 1995, Asymptotic Thermoelastic Analysis of Anisotropic Inhomogeneous and Laminated Plates. Journal of Thermal Stresses, Vol. 18, pp. 35–58.

Tomota, Y., Kuroki, K., Mori, T. and Tamura, I., 1976, Tensile Deformation of Two-ductile-phase Alloys: Flow Curves of α-γ Fe-Cr-Ni alloys. Materials Science and Engineering, Vol. 24, pp. 85-94.

Vel, S.S. and Batra, R.C., 2002, Exact Solution for Thermoelastic Deformations of Functionally Graded Thick Rectangular Plates. AIAA Journal, Vol. 40, pp. 1421–1433.

Vel, S.S. and Batra, R.C., 2003a. Three-dimensional Exact Solution for the Vibration of Functionally Graded Rectangular Plates. Journal of Sound and Vibrations (in press).

Vel, S.S. and Batra, R.C., 2003b. Exact thermoelasticity Solution for Cylindrical Bending Deformations of Functionally Graded Plates. Proceedings of the IUTAM Symposium on Dynamics of Advanced Materials and Smart Structures, Yonezawa, Japan, May 20–24.

Vel, S.S. and Batra, R.C., 2003c, Three-dimensional Analysis of Transient Thermal Stresses in Functionally Graded Plates. International Journal of Solids and Structures, Vol. 40, pp. 7181–7196.

Venkataraman, S. and Sankar, B.V., April 2001, Analysis of Sandwich Beams with Functionally Graded Core. Proceedings of the 42nd AIAA Structures, Structural Dynamics and Materials Conference, Seattle, Washington, AIAA Paper 2001-1281.

Venkataraman, S., Zhu, H., Sankar, B.V., Haftka, R.T., and Blosser; M., September 2001, Optimum Design of a Functionally Graded Metallic Foam Thermal Insulation. 16th American Society for Composites Technical Meeting, Blacksburg, VA.

Vinson, J.R. and Sierakowski, R.L., 1986, The Behavior of Structures Composed of Composite Materials. Martinus Nijhoff Publishers, Dordrecht, The Netherlands.

Wakashima, K. and Tsukamoto, H., 1991, Mean-Field Micromechanics Model and Its Application to the Analysis of Thermo-mechanical Behavior of Composite Materials. Materials Science and Engineering A, Vol. 146, pp. 291-316.

Wakashima, K. and Tsukamoto, H., 1992, A Unified Micromechanical Approach toward Thermomechanical Tailoring of Metal Matrix Composites. The Iron and Steel Institute of Japan International, Vol. 32, No. 8, pp. 883-892.

Walpole, L.J., 1966, On the Bounds for the Overall Elastic Moduli of Inhomogeneous Systems. Journal of Mechanics and Physics of Solids, Vol. 14, pp. 151-162.

Whitney, J.M., 1973, Shear Correction Factors for Orthotropic Laminates Under Static Load. Journal of Applied Mechanics, Vol. 40, No. 1, pp. 302-304.

Whitney, M. J., 1987, Structural Analysis of Laminated Anisotropic Plates. CRC Press.

Wittrick, W.H., 1987, Analytical Three-Dimensional Elastic Solutions to Some Plate Problems and Some Observations on Mindlin's Plate Theory. International Journal of Solids and Structures, Vol. 23, pp. 441-464

Yang, P.C., Norris, C.H. and Stavsky, Y., 1966, Elastic Wave Propagation in Heterogeneous Plates, International Journal of Solids and Structures. Vol. 2, pp. 665-684.

Yang, J. and Shen, H.S., 2002, Vibration Characteristics and Transient Response of Shear-Deformable Functionally Graded Plates in Thermal Environment. Journal of Sound and Vibration, Vol. 255, pp. 579–602.

Zenkert, D., 1997, The handbook of Sandwich Construction. EMAS,West Midlands, UK.

Zenkour, A.M., 2003, Exact Mixed-classical Solutions for the Bending Analysis of Shear Deformable Rectangular Plates. Applied Mathematical Modeling, Vol. 27, pp. 515-534

Zhu, H., Sankar, B.V., Haftka, R.T. and Venkataraman, S., 2002, Minimum Mass Design of Insulation Made of Functionally Graded Material. Proceedings of the 43rd AIAA Structures, Structural Dynamics and Materials Conference, Denver, Colorado, AIAA Paper 2002-1425.

Zhu, H. and Sankar, B.V., April 2004, Analysis of TPS Sandwich Panel with Foam Core. Proceedings of the 45th AIAA Structures, Structural Dynamics and Materials Conference, Palm Springs, California, AIAA Paper 2004-1935.

BIOGRAPHICAL SKETCH

Huadong Zhu was born in Pingyi, Shandong Province, China, in 1975. He received his B.S. degree in mechanical engineering from the Shandong University of Technology, China, in July 1996. Then he completed his graduate study for the M.S. degree in engineering mechanics at Northwestern Polytechnic University, China, 1999. In 2000, he joined the Advanced Composites Center at the Department of Mechanical and Aerospace Engineering, University of Florida, for his Ph. D. degree.

I certify that I have read this study and that in my opinion it conforms to acceptable standards of scholarly presentation and is fully adequate, in scope and quality, as a dissertation for the degree of Doctor of Philosophy.

Bhavani V. Sankar, Chairman
Professor of Mechanical and Aerospace Engineering

I certify that I have read this study and that in my opinion it conforms to acceptable standards of scholarly presentation and is fully adequate, in scope and quality, as a dissertation for the degree of Doctor of Philosophy.

Raphael T. Haftka, Cochairman
Distinguished Professor of Mechanical and Aerospace Engineering

I certify that I have read this study and that in my opinion it conforms to acceptable standards of scholarly presentation and is fully adequate, in scope and quality, as a dissertation for the degree of Doctor of Philosophy.

Malisa Sarntinoranont
Assistant Professor of Mechanical and Aerospace Engineering

I certify that I have read this study and that in my opinion it conforms to acceptable standards of scholarly presentation and is fully adequate, in scope and quality, as a dissertation for the degree of Doctor of Philosophy.

William Hager
Professor of Mathematics

This dissertation was submitted to the Graduate Faculty of the College of Engineering and to the Graduate School and was accepted as partial fulfillment of the requirements for the degree of Doctor of Philosophy.

December 2004

Pramod P. Khargonekar
Dean, College of Engineering

Kenneth Gerhardt
Interim Dean, Graduate School